Finite Element Methods with local Trefftz trial functions

Dissertation

zur Erlangung des Grades des
Doktors der Naturwissenschaften (Dr. rer. nat.)
der Naturwissenschaftlich-Technischen Fakultäten
der Universität des Saarlandes

eingereicht von

Dipl.-Math. Steffen Weißer

Saarbrücken
2012

Tag des Kolloquiums:	27. September 2012
Dekan der Fakultät:	Prof. Dr. Mark Groves
Vorsitzender:	Prof. Dr. Ernst Albrecht
1. Berichterstatter:	Prof. Dr. Sergej Rjasanow
2. Berichterstatter:	Prof. Dipl.-Ing. Dr. Ulrich Langer
3. Berichterstatter:	Prof. Dr. Raytcho Lazarov
akademischer Beisitzer:	Dr. Richards Grzibovskis

Dedicated to my parents, Cornelia and German,
my wife, Anna, and my sister, Simone.

Abstract

In the development of numerical methods for boundary value problems, the requirement of flexible mesh handling gains more and more importance. The available work deals with a new kind of conforming finite element methods on polygonal/polyhedral meshes. The idea is to use basis functions which are defined implicitly as local solutions of the underlying homogeneous problem with constant coefficients. They are referred to local Trefftz functions. These local problems are treated by means of boundary integral equations and are approximated by the use of the boundary element method in the numerics.

The method is applied to the stationary diffusion equation, where lower as well as higher order basis functions are introduced in two space dimensions. The convergence is analysed with respect to the H^1- as well as the L_2-norm and rates of convergence are proven. In case of non-constant diffusion coefficients, a special approximation is proposed. Beside the uniform refinement, an adaptive strategy is given which makes use of the residual error estimator and an introduced refinement procedure. The reliability of the residual error estimate is proven on polygonal meshes. Finally, the generalization to arbitrary polyhedral meshes with polygonal faces is discussed. All theoretical results and considerations are confirmed by numerical experiments.

Zusammenfassung

In der Entwicklung numerischer Verfahren zur Approximation von Randwertaufgaben werden flexible Vernetzungen der zugrunde liegenden Gebiete immer wichtiger. Die vorliegende Arbeit beschäftigt sich mit neuartigen Finiten Element Methoden, die zu konformen Approximationen auf polygonalen und polyhedralen Gittern führen. Der Gedanke dieser Vorgehensweise liegt darin, die Ansatzfunktionen implizit als Lösungen von lokalen Randwertaufgaben zu definieren, wie dies auch schon E. Trefftz vorgeschlagen hat. Hierbei wird die Differentialgleichung des Ursprungsproblems mit konstanten Koeffizienten und homogener rechter Seite verwendet. Die lokalen Probleme werden mit Randintegralgleichungen und in der Realisierung mit Randelementmethoden behandelt.

Das Verfahren wird auf die stationäre Diffusionsgleichung angewendet, wofür Ansatzfunktionen niedriger als auch höherer Ordnung eingeführt werden. Konvergenzraten bezüglich der H^1- sowie der L_2-Norm werden untersucht und bewiesen. Im Falle eines nicht konstanten Diffusionskoeffizienten wird eine spezielle Vorgehensweise vorgeschlagen. Neben der gleichmäßigen Verfeinerung der Netze wird ebenso eine adaptive Strategie angegeben, die von dem residualen Fehlerschätzer und einer eingeführten Verfeinerung Gebrauch macht. Die Zuverlässigkeit des Fehlerschätzers auf polygonalen Netzen wird bewiesen und schließlich wird das Verfahren erweitert, so dass es auf polyhedralen Gittern mit polygonalen Elementflächen angewendet werden kann. Alle theoretischen Resultate und Überlegungen werden durch numerische Experimente bestätigt.

Acknowledgements

This dissertation could not have been written without the support of varies persons which helped in many different ways.

I thank Sergej Rjasanow, my supervisor, for giving me the opportunity to do all the research which was necessary to write down this thesis. With his encouragement and support, it was possible to make the acquaintance of several researchers in the scientific community. He was always available for any kind of questions and helped when it was necessary.

Additionally, I thank some professors which crossed my academic career. Ulrich Langer awakened my ambition to publish results already in the beginning of my doctoral studies and he put life into several discussions. Yalchin Efendiev and Raytcho Lazarov made a research visit possible at the Texas A&M University in College Station, USA, where we had uncountable discussions on topics far beyond this dissertation.

I also thank the members of the research group of Sergej Rjasanow. Their open-mindedness and helpfulness created a great working atmosphere and enabled a pleasant time.

Not negligible was the support of my family and friends. They contributed to my leisure time that was essential for recovery and to find new inspiration.

My deepest gratitude, however, is reserved for my wife, Anna Benz-Weißer, whose logical mind, sound and thoughtful advice, sympathetic ear and unselfish support are of indispensable value for me.

Contents

Introduction

On Tuesday, 21st February, 1888, Erich Trefftz was born in Leipzig, Germany. In 1908, he began his studies in mechanical engineering and soon changed to mathematics. His most important teachers were Carl Runge, David Hilbert and Ludwig Prandtl. Under the guidance of Richard von Mises, Trefftz started his academic career with his doctoral thesis in Strasbourg in 1913. He was a soldier in the First Word War and managed to get his habilitation already in 1919. Trefftz became a full professor in Aachen and moved after three years to the Technical University of Dresden, where he worked until he died in consequence of a malicious disease on 21st January, 1937.

Figure 1: Erich Trefftz (1888–1937), see [59]

One of his famous publications is [72], 'Ein Gegenstück zum Ritzschen Verfahren' (a counterpart to Ritz' method) lectured in Zürich on the 2nd International Congress of Technical Mechanics in 1926. Instead of approximating the solution of a Dirichlet boundary value problem, according to Ritz, by a function

$$v(x) = g(x) + \sum_{j=1}^{n} c_j q_j(x),$$

where g fulfils the boundary condition and q_j vanishes on the boundary, Trefftz

proposed an approximation of the form

$$w(x) = \sum_{j=1}^{n} c_j p_j(x),$$

where p_j fulfils the differential equation. In both cases the coefficients c_j are computed such that the approximations are somehow optimal. Thus, the Trefftz method yields a function which fulfils the differential equation and approximates the boundary data. Additionally, Trefftz proposed in his publication to decompose the domain and to prescribe certain conditions for the approximation across the interfaces of the subdomains.

Years later, the original idea of Trefftz was further developed. Here, we mention the direct methods of Jirousek and the indirect methods of Herrera which were also studied by Ziliñski. For an overview see [38] and the references therein as well as the book [60]. But there are also other methods that base on these ideas. For example, the method of fundamental solutions, see [46, 67], and also domain decomposition methods can be traced back to the work of Trefftz.

In 1990, Hsiao and Wendland proposed the first domain decomposition approach in boundary element methods [42]. Already in this publication, we can find the basic idea of the finite element method with local Trefftz trial functions. The approximation of the solution of the boundary value problem is defined to fulfil the differential equation locally in each part of the decomposed domain. In 2009, Copeland, Langer and Pusch interpreted the subdomains of the decomposition as elements and began to study the boundary element domain decomposition approach in the framework of a finite element method in [20]. A more detailed description was published in [21]. Thus, the BEM-based FEM was born. Since that time, the method was the topic of several developments which include the work of Hofreither et. al. [39, 40, 41] as well as the present dissertation containing [77]. But there is still ongoing research in different directions.

The advantageous of this new approach are for example that it is applicable on general polygonal meshes in two dimensions and on general polyhedral meshes in the three dimensional case. Therefore, the BEM-based FEM is very flexible with respect to the discretization of the domain and can handle locally refined meshes as well as meshes with non-matching interfaces. Although the meshes are not regular in the classical sense, the method still yields conforming approximations. Since the trial functions are defined implicitly to fulfil the underlying differential equation locally, the obtained approximation already captures some properties of the exact solution.

The scope of the present dissertation goes from the introduction of lower as well as higher order basis functions and proofs of convergence rates over an adaptive strategy with the residual error estimate to a generalization to polyhedral elements. All these topics and the advantageous described above are also the subject of recent research in other areas.

The discontinuous Galerkin method is very flexible with respect to the meshes due to the discontinuous approximations across element boundaries, see [25]. For

the same reason, the method yields non-conforming approximations which are easily extended with higher order basis functions. In [9, 48], a posteriori error estimates were introduced. For the more recent developments of the discontinuous Petrov-Galerkin method, a *hp*-strategy can be found in [23].

In multiscale finite element methods, the basis functions are defined implicitly as local solutions of the underlying differential equation, see [31] and the references therein. Here, the local problems are dealt with additional local finite element methods whereas in the BEM-based FEM a local boundary element method is utilized. This local boundary element method in the BEM-based FEM allows to reformulate the variational formulation and to reduce the dimension of the local problems. For the multiscale methods an adaptive approach was proposed in [1] and there are the first attempts to get higher order convergence with the help of local spectral basis functions, see [30].

Another area of increasing interest is the mimetic finite difference method. Convergence results were proven in [14] for diffusion problems on polyhedral meshes. A residual based error estimator was introduced in [10] and recent results yield arbitrary order of convergence for a nodal mimetic discretization on polygonal meshes, see [11].

Beside the alternative strategies to handle boundary value problems, also in the finite element developments the use of polygonal and polyhedral elements has begun. Already in 1975, Wachspress [76] proposed the construction of conforming rational basis functions on convex polygons with any number of sides. In recent years, several improved basis functions on polygonal elements have been introduced and applied in linear elasticity for example, see [70, 71]. They are often referred to generalized barycentric coordinates. The harmonic coordinates are one example and we will recover them in the BEM-based FEM for the diffusion equation. These coordinates are applied in computer graphics, see [43, 49, 64]. An analysis can be found in [35]. There are even the first attempts which seek to introduce quadratic finite elements on polygons [61].

The outline of the present dissertation is as follows. In Chapter 1, we introduce the model problem which is considered throughout the dissertation and we discuss the basics as well as some regularity statements. Additionally, we give a definition of regular and stable polygonal meshes and prove some properties of them. Chapter 2 deals with the introduction of lower as well as higher order basis functions. We show convergence estimates and discuss the numerical realization in case of an advanced approximation of the diffusion coefficient. An adaptive BEM-based finite element method is proposed in Chapter 3. Therefore, the residual error estimate is introduced and its reliability is proven on regular and stable polygonal meshes. In Chapter 4, the lower order method is generalized to three space dimensions such that the BEM-based FEM is applicable on polyhedral elements with polygonal faces. Finally, we give a conclusion.

Chapter 1

Preliminaries

Throughout this preliminary chapter, the basic notation is introduced. We state the model problem and give the definitions of several function spaces. For these definitions, classical books like [2] and [34] are used, but also [50] for function spaces on the boundary of the domain. Afterwards, the variational formulation of the model problem is introduced and an abstract approximation idea is given. In Section 1.4, various regularity results for the solution of the model problem are summarised from [34, 36, 44], for example. The regularity depends on the shape of the domain as well as on the given data. A special focus lies on jumping coefficients in the material parameters.

Afterwards, we discuss the discretization of the domain. The BEM-based FEM is applicable on general polygonal meshes, thus we give a proper definition of the admitted discretizations and prove some properties. These results are important throughout the forthcoming proofs in later chapters. Additionally, we discuss a new strategy to refine the polygonal meshes in the two dimensional case.

Finally, the boundary integral formulation for the Laplace equation with Dirichlet boundary conditions is reviewed and analysed according to [50, 68]. This formulation is needed in local problems while reformulating the variational equation of the modal problem for the global finite element strategy. The local boundary integral equations are treated with boundary element methods as in [68]. They are presented in the last section of this chapter.

1.1 Model problem

In the whole dissertation, theory, numerics and the key ideas are carried out on a model problem. As it is usual in introductory books on new numerical schemes which approximate the solution of boundary value problems, we deal with the Laplace problem with Dirichlet boundary condition. But moreover, the generalized Poisson problem with mixed boundary conditions is considered to capture the whole extend of the underlying scheme.

Let Ω be a bounded polygonal domain in $\mathbb{R}^2$ or a bounded polyhedral domain

in $\mathbb{R}^3$. Its boundary $\Gamma = \overline{\Gamma}_D \cup \overline{\Gamma}_N$ is split into two parts, where Dirichlet and Neumann boundary conditions are prescribed, respectively. Here, the closure of a set is marked with an overline. The Dirichlet part Γ_D of the boundary is assumed to have a strictly positive $d-1$ dimensional measure $|\Gamma_D| > 0$. For given data $f \in L_2(\Omega)$, $g_D \in H^{1/2}(\Gamma_D)$ and $g_N \in L_2(\Gamma_N)$, the model problem reads

$$\begin{aligned} -\mathrm{div}(a\nabla u) &= f \quad && \text{in } \Omega, \\ u &= g_D && \text{on } \Gamma_D, \\ a\nabla u \cdot n &= g_N && \text{on } \Gamma_N, \end{aligned} \tag{1.1}$$

where n denotes the unit outer normal vector of Ω and $a \in L_\infty(\Omega)$ is a scalar function with

$$0 < a_{\min} \le a(x) \le a_{\max} \quad \text{for } x \in \overline{\Omega}.$$

The Lebesgue and Sobolev spaces are defined more precisely in the next section. The assumption on the coefficient function a guarantees the ellipticity of the differential equation. Together with the other ingredients, the boundary value problem is well posed and admits a unique solution in a weak sense as we will see later.

Beside the simple structure of the model problem, it already captures some difficulties and finds applications in real life problems. One could think about high oscillating coefficients or the case when $a_{\min}$ tends to zero such that the ratio $a_{\max}/a_{\min}$ gets unbounded. In models for heat transport, electro magnetism and elastic membranes the considered model equation can be found. Another application of increasing interest is the model of flow in porous media which is used in simulations of ground water flow and oil reservoirs, for example.

1.2 Function spaces and trace operators

In the studies of boundary value problems, the solutions have to be specified in proper function spaces. In the following, we give definitions of several spaces. For this reason, let Ω be any measurable subset of $\mathbb{R}^d$, $d \in \mathbb{N}$ with strictly positive Lebesgue measure. The Banach spaces $L_1(\Omega)$ and $L_2(\Omega)$ are defined in the usual way with the corresponding norms

$$\|u\|_{L_1(\Omega)} = \int_\Omega |u| \quad \text{and} \quad \|u\|_{L_2(\Omega)} = \left(\int_\Omega |u|^2 \right)^{1/2},$$

respectively. Here, the symbol $|\cdot|$ denotes the absolute value. But in other contexts, it might denote the Euclidean norm, the d or $d-1$ dimensional measure or even the cardinality of a discrete set. Furthermore, let the space of locally integrable functions be labeled by

$$L_1^{loc}(\Omega) = \{u : u \in L_1(K) \text{ for any compact } K \subset \Omega\}.$$

The space $L_2(\Omega)$ together with the scalar product

$$(u,v)_{L_2(\Omega)} = \int_\Omega uv,$$

which is often abbreviated to $(\cdot,\cdot)$, becomes a Hilbert space. Additionally, we denote by $L_\infty(\Omega)$ the space of measurable and almost everywhere bounded functions. It is equipped with the norm

$$\|u\|_{L_\infty(\Omega)} = \operatorname{ess\,sup}_{x\in\Omega} |u(x)| = \inf_{K\subset\Omega,|K|=0} \sup_{x\in\Omega\setminus K} |u(x)|,$$

where $|K|$ is the d dimensional Lebesgue measure of K. For a $d-1$ dimensional manifold Γ, the space $L_2(\Gamma)$ is defined in an analog way. Here, the surface measure is used instead of the volume measure.

The space of continuous functions over Ω is denoted by $C^0(\Omega)$ and equipped with the supremum norm

$$\|u\|_{C^0(\Omega)} = \sup_{x\in\Omega} |u(x)|.$$

Let $\alpha = (\alpha_1,\dots,\alpha_d) \in \mathbb{N}_0^d$ be a multi-index, i.e. a d-tuple with non-negative entries, and set

$$|\alpha| = \alpha_1 + \cdots + \alpha_d \quad \text{as well as} \quad \partial^\alpha = \left(\frac{\partial}{\partial x_1}\right)^{\alpha_1} \cdots \left(\frac{\partial}{\partial x_d}\right)^{\alpha_d}.$$

The order of the partial derivative ∂^α is the number $|\alpha|$. For any integer $k \geq 0$ and Ω open, we define

$$C^k(\Omega) = \{u : \partial^\alpha u \text{ exists and is continuous on } \Omega \text{ for } |\alpha| \leq k\}.$$

In the special case that $k = 0$, the space of continuous functions over Ω is recovered. Furthermore, we define

$$C_0^k(\Omega) = \{u \in C^k(\Omega) : \operatorname{supp} u \subset \Omega\},$$

where

$$\operatorname{supp} u = \overline{\{x \in \Omega : u(x) \neq 0\}},$$

and set

$$C^\infty(\Omega) = \bigcap_{k\geq 0} C^k(\Omega) \quad \text{as well as} \quad C_0^\infty(\Omega) = \bigcap_{k\geq 0} C_0^k(\Omega).$$

Finally, we review the space of Lipschitz functions

$$C^{0,1}(\Omega) = \{u \in C^0(\Omega) : \exists L > 0 : |u(x) - u(y)| \leq L|x-y| \text{ for } x,y \in \Omega\}$$

and

$$C^{k,1}(\Omega) = \{u \in C^k(\Omega) : \partial^\alpha u \in C^{0,1}(\Omega) \text{ for } |\alpha| = k\}$$

for $k \in \mathbb{N}$. The space of Hölder continuous functions is a straightforward generalization. For $\kappa \in (0, 1]$, it is

$$C^{0,\kappa}(\Omega) = \{u \in C^0(\Omega) : \exists C > 0 : |u(x) - u(y)| \leq C|x - y|^\kappa \text{ for } x, y \in \Omega\}$$

and

$$C^{k,\kappa}(\Omega) = \{u \in C^k(\Omega) : \partial^\alpha u \in C^{0,\kappa}(\Omega) \text{ for } |\alpha| = k\}$$

for $k \in \mathbb{N}$.

1.2.1 Sobolev spaces

Let Ω be a non-empty open subset of $\mathbb{R}^d$, $d \in \mathbb{N}$. The Sobolev space $H^k(\Omega)$ of order $k \in \mathbb{N}_0$ is defined by

$$H^k(\Omega) = \{u \in L_2(\Omega) : \partial^\alpha u \in L_2(\Omega) \text{ for } |\alpha| \leq k\} \tag{1.2}$$

with the norm $\|\cdot\|_{H^k(\Omega)}$ and the semi norm $|\cdot|_{H^k(\Omega)}$, where

$$\|u\|_{H^k(\Omega)} = \Bigg(\sum_{|\alpha| \leq k} \|\partial^\alpha u\|^2_{L_2(\Omega)} \Bigg)^{1/2} \quad \text{and} \quad |u|_{H^k(\Omega)} = \Bigg(\sum_{|\alpha| = k} \|\partial^\alpha u\|^2_{L_2(\Omega)} \Bigg)^{1/2}.$$

Here, the partial derivative $\partial^\alpha u$ has to be understood in the weak sense. More precisely, let the functional $g_\alpha : C_0^\infty(\Omega) \to \mathbb{R}$ be the distributional derivative of u with index α, i.e. g_α fulfils

$$(u, \partial^\alpha \varphi)_{L_2(\Omega)} = (-1)^{|\alpha|} g_\alpha(\varphi)$$

for all $\varphi \in C_0^\infty(\Omega)$. Furthermore, let g_α have the representation

$$g_\alpha(\varphi) = \int_\Omega \varphi \, \partial^\alpha u$$

for all $\varphi \in C_0^\infty(\Omega)$ with some function $\partial^\alpha u \in L_1^{loc}(\Omega)$ which is defined uniquely up to an equivalence class. Then, $\partial^\alpha u$ is called the weak derivative of u with index α. The additional condition $\partial^\alpha u \in L_2(\Omega)$ in (1.2) ensures that the weak derivative can be chosen such that it is square integrable.

For the definition of Sobolev spaces with fractional order $s \geq 0$, we write $s = k + \mu$ with $k \in \mathbb{N}_0$ and $\mu \in [0, 1)$. The Sobolev-Slobodekii norm is given by

$$\|u\|_{H^s(\Omega)} = \Bigg(\|u\|^2_{H^k(\Omega)} + \sum_{|\alpha| = k} |\partial^\alpha u|^2_{H^\mu(\Omega)} \Bigg)^{1/2},$$

where

$$|u|_{H^\mu(\Omega)} = \Bigg(\int_\Omega \int_\Omega \frac{|u(x) - u(y)|^2}{|x - y|^{d+2\mu}} \, dx dy \Bigg)^{1/2}.$$

Therefore, we define

$$H^s(\Omega) = \{u \in H^k(\Omega) : |\partial^\alpha u|_{H^\mu(\Omega)} < \infty \text{ for } |\alpha| = k\}.$$

The Sobolev norm $\|\cdot\|_{H^s(\Omega)}$ for arbitrary real $s \geq 0$ is induced by the scalar product

$$(u,v)_{H^s(\Omega)} = (u,v)_{H^k(\Omega)} + \sum_{|\alpha|=k} (\partial^\alpha u, \partial^\alpha v)_{H^\mu(\Omega)}$$

with

$$(u,v)_{H^k(\Omega)} = \sum_{|\alpha|\leq k} (\partial^\alpha u, \partial^\alpha v)_{L_2(\Omega)}$$

and

$$(u,v)_{H^\mu(\Omega)} = \int_\Omega \int_\Omega \frac{\big(u(x)-u(y)\big)\big(v(x)-v(y)\big)}{|x-y|^{d+2\mu}}\, dxdy.$$

Thus, $H^s(\Omega)$ is a Hilbert space for all $s \geq 0$.

1.2.2 Sobolev spaces on the boundary

For the definition of Sobolev spaces on the boundary of a domain, we have to restrict the class of admitted domains. Therefore, let $\Omega \subset \mathbb{R}^d$, $d \in \mathbb{N}$ be a bounded open set with boundary Γ. Additionally, we assume that Γ is non-empty and can be parametrised in the way

$$\Gamma = \bigcup_{i=1}^p \overline{\Gamma}_i, \quad \Gamma_i = \left\{x \in \mathbb{R}^d : x = \chi_i(\xi) \text{ for } \xi \in K_i \subset \mathbb{R}^{d-1}\right\}. \tag{1.3}$$

With regard to the decomposition of Γ, let $\{\varphi_i\}_{i=1}^p$ be a partition of unity with non-negative cut off functions $\varphi_i \in C_0^\infty(\mathbb{R}^d)$ such that

$$\sum_{i=1}^p \varphi_i(x) = 1 \quad \text{for } x \in \Gamma, \qquad \varphi_i(x) = 0 \quad \text{for } x \in \Gamma \setminus \Gamma_i.$$

For a function u defined on Γ, we write

$$u(x) = \sum_{i=1}^p u(x)\varphi_i(x) = \sum_{i=1}^p u_i(x) \quad \text{for } x \in \Gamma,$$

where $u_i(x) = u(x)\varphi_i(x)$. In the next step, x is replaced by the parametrisation from (1.3) and we obtain

$$u_i(x) = u(x)\varphi_i(x) = u(\chi_i(\xi))\varphi_i(\chi_i(\xi)) \quad \text{for } \xi \in K_i \subset \mathbb{R}^{d-1}, i = 1, \ldots, p.$$

The last expression is abbreviated to $\widetilde{u}_i(\xi)$. These functions are defined on bounded subsets of $\mathbb{R}^{d-1}$, and thus the Sobolev spaces from Section 1.2.1 can

be used. To fulfil $u_i \in H^s(K_i)$ for $s \geq 0$, the corresponding derivatives of the parametrisation χ_i have to exist. For the definition of these derivatives of order up to $s \leq k$, we have to assume $\chi_i \in C^{k-1,1}(K_i)$.

For $0 \leq s \leq k$, the Sobolev norm

$$\|u\|_{H^s(\Gamma),\chi} = \left(\sum_{i=1}^{p} \|u_i\|^2_{H^s(K_i)} \right)^{1/2},$$

which depends on the parametrisation of Γ, is defined. By the use of this norm the Sobolev spaces $H^s(\Gamma)$ can be introduced. For a Lipschitz domain Ω and $s \in (0,1)$, the Sobolev-Slobodekii norm

$$\|u\|_{H^s(\Gamma)} = \left(\|u\|^2_{L_2(\Gamma)} + \int_\Gamma \int_\Gamma \frac{|u(x)-u(y)|^2}{|x-y|^{d-1+2s}} \, ds_x ds_y \right)^{1/2}$$

is equivalent to $\|\cdot\|_{H^s(\Gamma),\chi}$, and thus the space $H^s(\Gamma)$ is independent of the parametrisation chosen in (1.3).

For $s < 0$, we define $H^s(\Gamma)$ as the dual space of $H^{-s}(\Gamma)$ and equip it with the norm

$$\|u\|_{H^s(\Gamma)} = \sup_{0 \neq v \in H^{-s}(\Gamma)} \frac{u(v)}{\|v\|_{H^{-s}(\Gamma)}}.$$

Additionally, we need some spaces which are only defined on a part of the boundary. Let Γ_0 be an open subset of the sufficiently smooth boundary Γ. For $s \geq 0$, we set the Sobolev space

$$H^s(\Gamma_0) = \{u = \widetilde{u}|_{\Gamma_0} : \widetilde{u} \in H^s(\Gamma)\}$$

with the norm

$$\|u\|_{H^s(\Gamma_0)} = \inf_{\widetilde{u} \in H^s(\Gamma) : \widetilde{u}|_{\Gamma_0} = u} \|\widetilde{u}\|_{H^s(\Gamma)}.$$

Furthermore, let

$$\widetilde{H}^s(\Gamma_0) = \{u = \widetilde{u}|_{\Gamma_0} : \widetilde{u} \in H^s(\Gamma), \operatorname{supp} \widetilde{u} \subset \Gamma_0\},$$

and for $s < 0$, we set $H^s(\Gamma_0)$ as the dual space of $\widetilde{H}^s(\Gamma_0)$.

Finally, we define a Sobolev space over the boundary with piecewise regularity

$$H^s_{\mathrm{pw}}(\Gamma) = \{u \in L_2(\Gamma) : u|_{\Gamma_i} \in H^s(\Gamma_i), i = 1, \ldots, p\},$$

and we equip it with the norm

$$\|u\|_{H^s_{\mathrm{pw}}(\Gamma)} = \left(\sum_{i=1}^{p} \|u|_{\Gamma_i}\|^2_{H^s(\Gamma_i)} \right)^{1/2}.$$

1.2.3 Properties of Sobolev spaces

To state some properties of Sobolev spaces, we have to guaranty certain regularities of the domain Ω and its boundary Γ. Therefore, we take from [36]

Definition 1. Let Ω be an open subset of $\mathbb{R}^d$. We say that its boundary Γ is continuous (respectively Lipschitz, continuously differentiable, of class $C^{k,1}$, k times differentiable) if for every $x \in \Gamma$ there exists a neighbourhood U of x in $\mathbb{R}^d$ and new orthogonal coordinates $\{\xi_1, \ldots, \xi_d\}$ such that

1. U is an hypercube in the new coordinates:
$$U = \{(\xi_1, \ldots, \xi_d) : -c_i < \xi_i < c_i, i = 1, \ldots, d\}$$
2. there exists a continuous (respectively Lipschitz, continuous differentiable, of class $C^{k,1}$, k times continuously differentiable) function f, defined in
$$U' = \{(\xi_1, \ldots, \xi_{d-1}) : -c_i < \xi_i < c_i, i = 1, \ldots, d-1\}$$
and such that
$$\begin{aligned} |f(\xi')| \leq c_d/2 \quad &\text{for every } \xi' = (\xi_1, \ldots, \xi_{d-1}) \in U', \\ \Omega \cap U &= \{\xi = (\xi', \xi_d) \in U : \xi_d < f(\xi')\}, \\ \Gamma \cap U &= \{\xi = (\xi', \xi_d) \in U : \xi_d = f(\xi')\}. \end{aligned}$$

From now on, we restrict ourselves to bounded domains Ω. So, the boundary Γ is compact, and thus we can find a finite cover of Γ which can be used to construct a parametrisation as given in (1.3). We state the famous Sobolev embedding theorem which can be found in [2, 15], for example.

Theorem 1. (Sobolev embedding) *Let $\Omega \subset \mathbb{R}^d$, $d \in \mathbb{N}$ be a bounded domain with Lipschitz boundary and let $2k > d$ with $k \in \mathbb{N}$. For $u \in H^k(\Omega)$, it is $u \in C^0(\overline{\Omega})$ and there exists a constant $C_S > 0$ such that*
$$\|u\|_{C^0(\overline{\Omega})} \leq C_S \|u\|_{H^k(\Omega)}$$
for all $u \in H^k(\Omega)$.

Remark 1. In [15], it is shown that for convex domains Ω with diameter smaller or equal to one, the constant in Theorem 1 has the form
$$C_S = c\,|\Omega|^{-1/2}$$
with a constant $c > 0$ which only depends on d and k.

Next, we give some results for traces of functions in Sobolev spaces. For sufficiently smooth functions u over $\overline{\Omega}$, we set the trace operator γ_0 as restriction of u to the boundary Γ, i.e.
$$\gamma_0 u = u\big|_\Gamma.$$
This operator has continuous extensions such that the following theorems taken from [2] and [50] are valid.

Theorem 2. *If the bounded subset Ω of $\mathbb{R}^d$ has a boundary Γ of class $C^{k-1,1}$ and if $1/2 < s \leq k$ then*

$$\gamma_0 : H^s(\Omega) \to H^{s-1/2}(\Gamma)$$

is a bounded linear operator, i.e.

$$\|\gamma_0 u\|_{H^{s-1/2}(\Gamma)} \leq c_T \|u\|_{H^s(\Omega)} \quad \text{for } u \in H^s(\Omega).$$

This operator has a continuous right inverse

$$\mathcal{E} : H^{s-1/2}(\Gamma) \to H^s(\Omega)$$

with $\gamma_0 \mathcal{E} v = v$ for all $v \in H^{s-1/2}(\Gamma)$ and

$$\|\mathcal{E} v\|_{H^s(\Omega)} \leq c_{IT} \|v\|_{H^{s-1/2}(\Gamma)} \quad \text{for } v \in H^{s-1}(\Gamma).$$

Theorem 3. *Let $\Omega \subset \mathbb{R}^d$ be a bounded domain with Lipschitz boundary Γ. Then, there exists a bounded linear operator*

$$\gamma : H^1(\Omega) \to L_2(\Gamma)$$

with

$$\|\gamma u\|_{L_2(\Gamma)} \leq c_{LT} \|u\|_{H^1(\Omega)} \quad \text{for } u \in H^1(\Omega).$$

1.3 Variational formulation

For the finite element method, the model problem (1.1) has to be understood in a week sense. To obtain a variational formulation, the differential equation in the model problem is multiplied by an arbitrary smooth test function v which vanishes on the Dirichlet boundary Γ_D. Afterwards, the equation is integrated by parts and the Neumann boundary conditions are incorporated. This procedure yields the equality

$$\int_\Omega a \nabla u \cdot \nabla v = \int_\Omega f v + \int_{\Gamma_N} g_N \, v,$$

which is the basis for the variational formulation. The reduced regularity of the test function

$$v \in V = H^1_D(\Omega) = \{v \in H^1(\Omega) : \gamma_0 v = 0 \text{ on } \Gamma_D\}$$

is sufficient. The integrals can be interpreted as duality products and consequently the equation remains valid for given data $g_N \in H^{-1/2}(\Gamma_N)$ and f in the dual of $H^1_D(\Omega)$. The Hilbert space V is equipped with the norm $\|\cdot\|_V = \|\cdot\|_{H^1(\Omega)}$. To handle the inhomogeneous Dirichlet datum, an extension $u_D \in H^1(\Omega)$ of g_D is used. This extension exists since $g_D \in H^{1/2}(\Gamma_D)$. We seek the unknown solution $u \in H^1(\Omega)$ in the form $u = u_0 + u_D$ with $u_0 \in H^1_D(\Omega)$. This yields the variational formulation

$$\text{Find } u_0 \in V : \quad a_\Omega(u_0, v) = \ell(v), \quad \forall v \in V, \tag{1.4}$$

with the bilinear form

$$a_\Omega(u,v) = \int_\Omega a\nabla u \cdot \nabla v,$$

and

$$\ell(v) = (f,v) + (g_N,v)_{\Gamma_N} - a_\Omega(u_D,v).$$

Here, $(\cdot,\cdot)$ and $(\cdot,\cdot)_{\Gamma_N}$ denote the L_2-scalar products over Ω and Γ_N, respectively. In the case of $g_N \notin L_2(\Gamma_N)$ and $f \notin L_2(\Omega)$, the L_2-scalar products are interpreted again as duality products.

Due to the properties of the coefficient function $a \in L_\infty(\Omega)$, the bilinear form is continuous on V, i.e. there is a constant $M > 0$ such that

$$|a_\Omega(u,v)| \le M\|u\|_V\|v\|_V \quad \text{for } u,v \in V.$$

This is a consequence of the Cauchy-Schwarz inequality as we see easily

$$|a_\Omega(u,v)| \le a_{\max}\int_\Omega |\nabla u\cdot\nabla v| \le a_{\max}\|\nabla u\|_{L_2(\Omega)}\|\nabla v\|_{L_2(\Omega)} \le a_{\max}\|u\|_{H^1(\Omega)}\|v\|_{H^1(\Omega)}.$$

Furthermore, the bilinear form $a_\Omega(\cdot,\cdot)$ is V-elliptic, i.e. there is a constant $m > 0$ such that

$$a_\Omega(v,v) \ge m\|v\|_V^2 \quad \text{for } v \in V.$$

To prove this inequality, we need the lower bound of the coefficient function as well as the following result, which is proven even for more general norms in [33].

Lemma 1. *Let $\Omega \subset \mathbb{R}^d$, $d \in \mathbb{N}$ be a bounded Lipschitz domain with boundary Γ and let $\Gamma_D \subset \Gamma$ with $|\Gamma_D| > 0$. Then, there exists a constant $c_{PF} > 0$ such that*

$$\|u\|_{L_2(\Omega)}^2 \le c_{PF}\left\{|u|_{H^1(\Omega)}^2 + \left(\int_{\Gamma_D} u\right)^2\right\}$$

for $u \in H^1(\Omega)$.

For $v \in V$, we obtain

$$\begin{aligned} a_\Omega(v,v) &\ge a_{\min}|v|_{H^1(\Omega)}^2 = \frac{a_{\min}}{2}\left(|v|_{H^1(\Omega)}^2 + |v|_{H^1(\Omega)}^2 + \left(\int_{\Gamma_D} v\right)^2\right) \\ &\ge \frac{a_{\min}}{2}\min\left\{1,\frac{1}{c_{PF}}\right\}\|v\|_{H^1(\Omega)}^2. \end{aligned}$$

Another possibility to prove the V-ellipticity is to use the equivalence of the norm $\|\cdot\|_{H^1(\Omega)}$ and the semi norm $|\cdot|_{H^1(\Omega)}$ on V. This equivalence can be seen easily from Lemma 1, but there is also a direct proof available, see [18].

In analogy to the continuity of the bilinear form, we recognize the linearity and the continuity of the right hand side ℓ of (1.4) on V, i.e. there is a constant $c_\ell > 0$ such that

$$|\ell(v)| \leq c_\ell \|v\|_V \quad \text{for } v \in V.$$

A well known result in variational calculus is

Theorem 4. (Lax-Milgram lemma) *Let V be a Hilbert space, $a(\cdot,\cdot) : V \times V \to \mathbb{R}$ a continuous V-elliptic bilinear form, and let $\ell : V \to \mathbb{R}$ be a continuous linear form. Then the abstract variational problem:*

$$\textit{Find } u \in V: \quad a(u,v) = \ell(v), \quad \forall v \in V$$

has one and only one solution.

In the proof of the Lax-Milgram lemma, the Riesz representation theorem is utilized, see for example [18] or the original work [47]. It is

Theorem 5. (Riesz representation theorem) *Let V be a Hilbert space with scalar product $(\cdot,\cdot)_V$ and corresponding induced norm $\|\cdot\|_V = \sqrt{(\cdot,\cdot)_V}$. Furthermore, let V' be the dual of V equipped with the norm*

$$\|\ell\|_{V'} = \sup_{0 \neq v \in V} \frac{|\ell(v)|}{\|v\|_V}.$$

For each $\ell \in V'$, there exists a unique $u \in V$ such that

$$(u,v)_V = \ell(v) \quad \textit{for } v \in V$$

and

$$\|u\|_V = \|\ell\|_{V'}.$$

The variational formulation (1.4) fulfils all ingredients of the Lax-Milgram lemma and has therefore a unique solution $u_0 \in V$. Consequently, we obtain $u = u_0 + u_D$ as unique solution of the week formulation of our model problem.

Remark 2. Since $a_\Omega(\cdot,\cdot)$ is symmetric in the model problem, the unique solvability can also be proven directly by applying the Riesz representation theorem. Due to the properties of the bilinear form, $a_\Omega(\cdot,\cdot)$ is a scalar product on V. The right hand side $\ell(\cdot)$ of (1.4) belongs to the dual of V. Thus, Theorem 5 guaranties a unique function $u_0 \in V$ such that

$$a_\Omega(u_0, v) = \ell(v) \quad \text{for } v \in V.$$

The induced norm

$$\|v\|_E = \sqrt{a_\Omega(v,v)}$$

is called energy norm and as a consequence of the continuity and the ellipticity of the bilinear form on V, the energy norm is equivalent to the H^1-norm.

In the numerics, it is not possible to work with the space V directly. Therefore, a finite dimensional subspace V_h of V is introduced and the discrete variational formulation

$$\text{Find } u_{0h} \in V_h : \quad a_\Omega(u_{0h}, v_h) = \ell(v_h), \quad \forall v_h \in V_h \tag{1.5}$$

is considered. This approach is also called discrete Galerkin formulation. Since $V_h \subset V$, the method is said to be conforming. Due to the finite dimension of V_h, we can introduce a basis Ψ with $V_h = \operatorname{span} \Psi$ and $\dim V_h = n$ for some $n \in \mathbb{N}$. Next, we express u_{0h} as linear combination of basis functions

$$u_{0h} = \sum_{\psi \in \Psi} \beta_\psi \psi,$$

and we have to test (1.5) only with $v_h = \phi$ for all $\phi \in \Psi$. Consequently, we end up with a system of linear equations to compute the unknown coefficients β_ψ of u_{0h}. More precisely, let $\underline{\beta}$ be the vector with components β_ψ. We obtain

$$A\underline{\beta} = b$$

with

$$A = (a_\Omega(\psi, \phi))_{\phi,\psi \in \Psi} \in \mathbb{R}^{n \times n} \quad \text{and} \quad b = (\ell(\phi))_{\phi \in \Psi} \in \mathbb{R}^n.$$

The system matrix A is symmetric and positive definite because of the symmetry and the V-ellipticity of the bilinear form $a_\Omega(\cdot, \cdot)$. Therefore, the $n \times n$ system of linear equations admits a unique solution.

Nevertheless, the question remains how the variational formulations (1.4) and (1.5) are related to each other. Céa's lemma gives the answer. The discrete Galerkin formulation (1.5) yields the best approximation of the solution of (1.4).

Lemma 2. (Céa's lemma) *Let V be a Hilbert space and $V_h \subset V$ a finite dimensional subspace of V, let $a(\cdot, \cdot) : V \times V \to \mathbb{R}$ be a continuous V-elliptic bilinear form, and let $\ell : V \to \mathbb{R}$ be a continuous linear form. Furthermore, let $u \in V$ be the solution of*

$$\textit{Find } u \in V : \quad a(u, v) = \ell(v), \quad \forall v \in V$$

and $u_h \in V_h$ the solution of

$$\textit{Find } u_h \in V_h : \quad a(u_h, v_h) = \ell(v_h), \quad \forall v_h \in V_h.$$

Then, the abstract error estimate

$$\|u - u_h\|_V \leq \frac{M}{m} \min_{v_h \in V_h} \|u - v_h\|_V$$

holds.

Proof. By the use of the V-ellipticity, the Galerkin orthogonality

$$a(u - u_h, v_h) = 0 \quad \text{for } v_h \in V_h, \tag{1.6}$$

as well as the continuity of the bilinear form, we obtain

$$\begin{aligned} m \|u - u_h\|_V^2 &\leq a(u - u_h, u - u_h) \\ &= a(u - u_h, u - v_h) \\ &\leq M \|u - u_h\|_V \|u - v_h\|_V \end{aligned}$$

for arbitrary $v_h \in V_h$. Taking the minimum with respect to v_h and dividing by m and $\|u - u_h\|_V$ finishes the proof. □

In Chapter 2, we discuss a possible choice of basis functions and the approximation properties of the corresponding discrete space V_h in two dimensions. These ideas are extended to three dimensions in Chapter 4. Whereas the theory in this section is valid for arbitrary data $g_N \in H^{-1/2}(\Gamma_N)$ and f in the dual of $H_D^1(\Omega)$, we restrict ourselves to the case $g_N \in L_2(\Gamma_N)$ and $f \in L_2(\Omega)$ which is more suitable for the numerics.

1.4 Regularity statements

In the previous section, we have seen that the weak solution of the model problem (1.1) which is obtained by solving the corresponding variational formulation fulfils $u \in H^1(\Omega)$. This regularity statement is the worst case. In general, one would expect that the solution of the model problem is two times differentiable in the classical or at least in the weak sense such that its second derivatives are square integrable. Under certain assumptions on the domain Ω and on the regularity of the boundary data, it is possible to prove higher regularity of the solution. In this section, we summarize several regularity results from the literature. We restrict ourselves to the case of pure Dirichlet boundary conditions, but in the cited literature one can also find similar results for more general boundary conditions.

First, we state some results taken from [34]. Here, the derivatives are understood in the classical sense, and we seek a solution which is two times differentiable. A bounded domain $\Omega \subset \mathbb{R}^d$ for $d \in \mathbb{N}$ is said to fulfil the exterior sphere condition if for every point $x \in \partial\Omega$ there exists a d-dimensional ball B satisfying $\overline{B} \cap \overline{\Omega} = x$. This holds for example if the boundary of Ω is of class C^2 or if Ω is a convex d-dimensional polygon. For $\kappa \in (0, 1)$, we have

Theorem 6. *Let $\Omega \subset \mathbb{R}^d$, $d \in \mathbb{N}$ be a bounded domain, and let $a \in C^{1,\kappa}(\Omega)$ be such that*

$$0 < a_{\min} \leq a(x) \leq a_{\max} \quad \textit{for } x \in \overline{\Omega}.$$

Furthermore, let f be bounded and belong to $C^{0,\kappa}(\Omega)$. Suppose that Ω satisfies an exterior sphere condition. Then, if g is continuous on Γ, the Dirichlet problem

$$\begin{aligned} -\mathrm{div}(a\nabla u) &= f \quad \text{in } \Omega, \\ u &= g \quad \text{on } \Gamma, \end{aligned}$$

has a unique solution $u \in C^0(\overline{\Omega}) \cap C^{2,\kappa}(\Omega)$.

Several properties are known for the solution of such a Dirichlet problem. Let L denote the differential operator defined by

$$Lu = \mathrm{div}(a\nabla u).$$

We say that L is elliptic if the condition

$$0 < a_{\min} \leq a(x) \leq a_{\max} \quad \text{for } x \in \overline{\Omega}$$

holds. In the theory of partial differential equations of second order, the maximum principle is an important tool. It is sometimes also called minimum-maximum principle.

Theorem 7. (Weak maximum principle) *Let L be elliptic in the bounded domain Ω. Suppose that*

$$Lu \geq 0 \quad (Lu \leq 0) \qquad \text{in } \Omega$$

with $u \in C^2(\Omega) \cap C^0(\overline{\Omega})$. Then the maximum (minimum) of u in $\overline{\Omega}$ is achieved on $\partial\Omega$, that is,

$$\sup_{\Omega} u = \sup_{\partial\Omega} u \quad (\inf_{\Omega} u = \inf_{\partial\Omega} u).$$

The last two results also include the Dirichlet problem for the Poisson equation which is important in the definition of basis functions in Chapter 2. For this case ($a \equiv 1$), we additionally state the strong form of the maximum principle.

Theorem 8. (Strong maximum principle) *Let Ω be a domain (not necessarily bounded) and let $u \in C^2(\Omega)$ such that*

$$\Delta u \geq 0 \quad (\Delta u \leq 0) \qquad \text{in } \Omega.$$

Suppose there exists a point $y \in \Omega$ for which

$$u(y) = \sup_{\Omega} u \quad (u(y) = \inf_{\Omega} u).$$

Then u is constant. Consequently a harmonic function cannot assume an interior maximum or minimum value unless it is constant.

The monograph [36] deals with problems in non-smooth domains and analyses the existents and uniqueness of solutions of (1.1) in Sobolev spaces. This means that the derivatives in the partial differential equation are understood in the weak sense.

Theorem 9. *Let Ω be a bounded open subset of $\mathbb{R}^d$ with a $C^{1,1}$ boundary. Let $a \in C^{0,1}(\Omega)$ be such that*

$$0 < a_{\min} \leq a(x) \quad \text{for almost every } x \in \overline{\Omega}.$$

Then for every $f \in L_2(\Omega)$ and every $g \in H^{3/2}(\Gamma)$, there exists a unique solution of

$$\begin{aligned} -\operatorname{div}(a\nabla u) &= f \quad \text{in } \Omega, \\ \gamma_0 u &= g \quad \text{on } \Gamma, \end{aligned}$$

with $u \in H^2(\Omega)$.

The condition on the boundary can be relaxed under the assumption that Ω is convex. For this case, we restrict ourselves to homogeneous Dirichlet boundary conditions.

Theorem 10. *Let Ω be a convex, bounded and open subset of $\mathbb{R}^d$ and $a \in C^{0,1}(\Omega)$ such that*

$$0 < a_{\min} \leq a(x) \leq a_{\max} \quad \text{for } x \in \overline{\Omega}.$$

Then for each $f \in L_2(\Omega)$, there exists a unique solution of

$$\begin{aligned} -\operatorname{div}(a\nabla u) &= f \quad \text{in } \Omega, \\ \gamma_0 u &= 0 \quad \text{on } \Gamma, \end{aligned} \tag{1.7}$$

with $u \in H^2(\Omega)$.

Next, we focus on the two dimensional setting ($d = 2$) and assume that Ω is a polygonal bounded domain. We decompose the boundary Γ into straight line segments Γ_i such that

$$\Gamma = \bigcup_{i=1}^{p} \overline{\Gamma}_i, \qquad x_i = \overline{\Gamma}_i \cap \overline{\Gamma}_{i+1} \quad \text{for } i = 1, \ldots, p \text{ where } \Gamma_{p+1} = \Gamma_1,$$

and the angle between two consecutive segments Γ_i and Γ_{i+1} is smaller than π. The segments are ordered counterclockwise and x_i denotes the vertex between them. For convex Ω of this kind, the trace operator for smooth functions, considered at the end of Section 1.2, can be extended continuously to a bounded linear operator

$$\gamma_{\mathrm{pw}} : H^k(\Omega) \to H^{k-1/2}_{\mathrm{pw}}(\Gamma)$$

for $k \in \mathbb{N}$, see [36]. Now, we are interested in the boundary value problem

$$\begin{aligned} -\Delta u &= f \quad \text{in } \Omega, \\ \gamma_{\mathrm{pw}} u &= g \quad \text{on } \Gamma, \end{aligned} \tag{1.8}$$

for $f \in L_2(\Omega)$ and $g \in H^{3/2}_{\mathrm{pw}}(\Gamma)$. For convex domains Ω, like the elements of regular meshes defined in the next section, we already know from Theorem 10 that

the problem admits a unique solution in $H^2(\Omega)$ for homogeneous boundary data. To find similar results for inhomogeneous Dirichlet data, we reduce the problem to the previous case. Therefore, the question arises if a function $u_g \in H^2(\Omega)$ exists such that

$$\gamma_{\mathrm{pw}} u_g = g. \tag{1.9}$$

In [36], the author demands additional regularity on

$$\Delta u_g - f \in L_2(\Omega),$$

but this is not necessary due to the equivalence of two different definitions of Sobolev spaces which has been shown in [51].

Theorem 11. *Let $f \in L_2(\Omega)$, $g \in H^{3/2}_{\mathrm{pw}}(\Gamma)$ and let g be continuous in the vertices x_i, $i = 1, \ldots, p$ of the boundary Γ. Then there exists a function $u_g \in H^2(\Omega)$ such that* (1.9) *holds true. Consequently, problem* (1.8) *admits a unique solution $u \in H^2(\Omega)$.*

If we allow non-convex polygonal domains, the smoothness of the solution decreases. Assume, we have a polygonal domain Ω with one reentrant corner. So all interior angles between the boundary segments are smaller than π beside at one vertex x_s. This vertex is called a singular point and the interior angle at this point exceeds π. The Dirichlet problem for the Laplace equation is now studied again in the variational framework. By the use of localization techniques, it is possible to show that the solution of (1.8) for homogeneous boundary data can be decomposed into

$$u = w + \rho.$$

Here, $w \in H^2(\Omega)$ is the regular part of the solution. But the remainder fulfils $\rho \notin H^2(\Omega)$ and its singularity depends on the interior angle at x_s. Consequently, the solution of the problem gets singular and it is $u \notin H^2(\Omega)$. Nevertheless, it is known that the Laplace problem with homogeneous Dirichlet datum on polygonal domains with reentrant corners admits unique solutions which are at least in $H^{3/2}(\Omega)$, see [37]. This result is proven by the help of decomposition theorems. Such a theorem is given in [44] even for more general cases, namely for interface problems.

In the special case that the diffusion coefficient is piecewise constant, we call (1.7) an interface problem. From now on, we assume that the domains, where $a(\cdot)$ is constant, are polygonal bounded. The union of the boundaries of these domains is called the interface, and the vertices of them are called singular points. Considering the domain $\Omega = [-1, 1]^2$, we define with the help of polar coordinates (r, φ) the function

$$g(x) = r^{\lambda} \begin{cases} \cos(\lambda(\pi/2 - b_2)) \cos(\lambda(\varphi - \pi/2 + b_1)) & \text{for } 0 \le \varphi < \pi/2, \\ \cos(\lambda b_1) \cos(\lambda(\varphi - \pi + b_2)) & \text{for } \pi/2 \le \varphi < \pi, \\ \cos(\lambda b_2) \cos(\lambda(\varphi - \pi - b_1)) & \text{for } \pi \le \varphi < 3\pi/2, \\ \cos(\lambda(\pi/2 - b_1)) \cos(\lambda(\varphi - 3\pi/2 - b_2)) & \text{for } 3\pi/2 \le \varphi < 2\pi, \end{cases}$$

see [45]. With a given diffusion coefficient

$$a(x) = \begin{cases} a_1 & \text{for } 0 \le \varphi < \pi/2, \\ a_2 & \text{for } \pi/2 \le \varphi < \pi, \\ a_3 & \text{for } \pi \le \varphi < 3\pi/2, \\ a_4 & \text{for } 3\pi/2 \le \varphi < 2\pi, \end{cases}$$

it is possible to choose the parameters $\lambda > 0$, b_1, b_2 in such a way that $u = g$ is the weak solution of the interface problem

$$\begin{aligned} -\mathrm{div}(a\nabla u) &= f \quad \text{in } \Omega, \\ u &= g \quad \text{on } \Gamma. \end{aligned}$$

Vice versa, it is also possible to choose a_i, $i = 1, \ldots, 4$ for given $\lambda > 0$, b_1 and b_2 such that $u = g$ solves the boundary value problem. In both cases, the solution fulfils $u \in H^{1+s}(\Omega)$ for $0 < s \le \lambda$ if $\lambda < 1$. Analysing this example, it is possible to find data and parameters such that $u \in H^{1+\varepsilon}(\Omega)$ for arbitrary small $\varepsilon \in (0, 1)$ as well as $u \in H^{2-\varepsilon}(\Omega)$, see [57]. For example, if we choose $a_1 = a_3 = 1$ and $a_2 = a_4 = \widetilde{a}$, the regularity of the solution gets arbitrarily low for $\widetilde{a} \to \infty$. Consequently, the distribution of the piecewise constant material coefficient function $a(\cdot)$ has a big influence on the regularity of the solution.

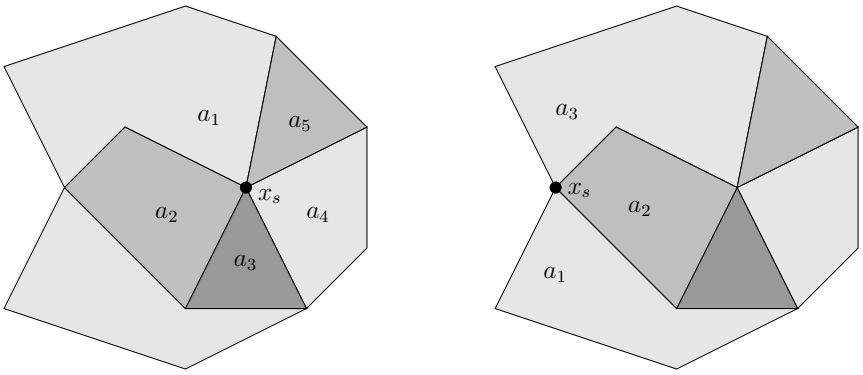

Figure 1.1: Local distribution a_i for $x_s \in \Omega$ (left) and $x_s \in \Gamma$ (right)

If we pick a singular point x_s and order the domains counterclockwise which border on x_s and where $a(\cdot)$ is constant, see Figure 1.1, we get a local distribution a_i, $i = 1, \ldots, n$ of the piecewise constant material coefficient function. Here, n denotes the number of neighbouring domains to x_s. If $x_s \in \Gamma$, we start the numbering next to the boundary and if $x_s \in \Omega$, we set $a_{n+1} = a_1$. In both cases, we assume that $a_i \neq a_{i+1}$ for $i = 1, \ldots, n-1$ and $i = 1, \ldots, n$, respectively. Otherwise, two domains are merged. The material coefficient is called quasi-monotone with respect to $x_s \in \Omega$ if there exists only one index i with

$$a_i > a_{i-1} \quad \text{and} \quad a_i > a_{i+1},$$

see Figure 1.2. So, there is no local maxima beside the one at index i. For $x_s \in \Gamma$, the material coefficient is called quasi-monotone with respect to x_s if there exists an index i such that

$$a_1 > \ldots > a_i < \ldots < a_n,$$

where a_1 and a_n are next to Γ. The quasi-monotonicity condition is always valid with respect to interior singular points if at most three domains meet there. For singular points on the boundary, it is always valid if at most two domains meet. Under the assumption that the material coefficient is quasi-monotone with respect to each singular point, there are further regularity statements for the interface problem. In [57], the author has shown that under this assumption the solution of the boundary value problem belongs at least to $H^{5/4}(\Omega)$.

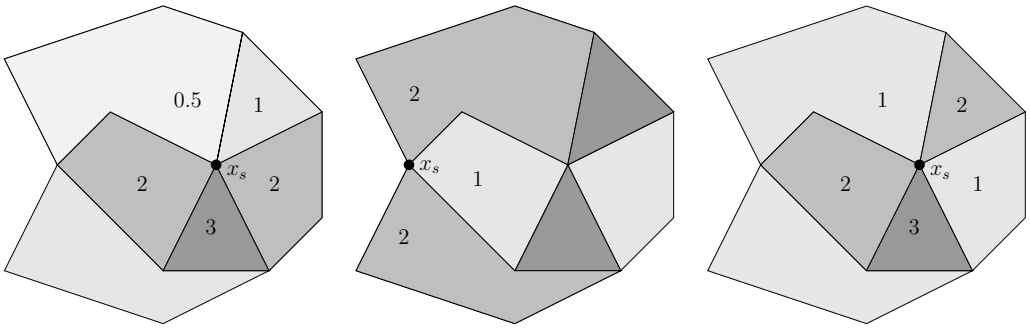

Figure 1.2: Quasi-monotone coefficient with respect to $x_s \in \Omega$ (left), $x_s \in \Gamma$ (middle) and non-quasi-monotone coefficient with respect to $x_s \in \Omega$ (right)

1.5 Properties and refinement of regular meshes

For the finite element method, we have to introduce a discretization $\mathcal{K}_h$ of Ω. In this section, we restrict ourselves to the two dimensional case $\Omega \subset \mathbb{R}^2$. In contrast to classical conforming finite element methods, we allow meshes with arbitrary convex polygonal elements which are bounded. Examples of such meshes are given in Figure 1.3. The elements $K \in \mathcal{K}_h$ are non-overlapping open sets such that

$$\overline{\Omega} = \bigcup_{K \in \mathcal{K}_h} \overline{K}.$$

The elements consist of nodes and edges. An edge E is always located between two nodes, the start and the end point, which are also the only nodes on E. In each corner of an element K, a node is located, but there could also be some nodes on straight lines of the boundary ∂K, compare the left picture in Figure 1.4. We stress this fact more carefully. If we have a triangle with three nodes and we add some nodes on the boundary, this triangle turns formally into a polygon. These additional nodes enrich the approximation space in the finite element method in Chapter 2. In this context, nodes on straight lines are natural since they are just

classical nodes for polygons. In triangular or quadrilateral meshes these nodes appear as hanging nodes which are undesirable and do not influence the accuracy of the approximation. In classical finite element implementations, such hanging nodes have to be treated in a special way whereas methods working on polygonal meshes include them naturally.

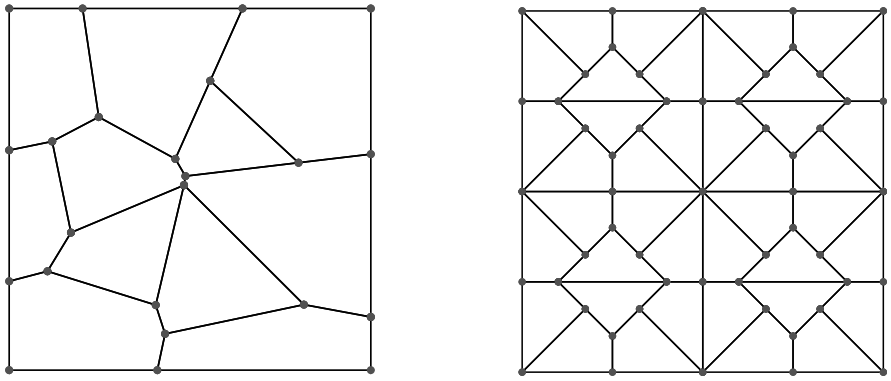

Figure 1.3: Two examples for meshes with polygonal elements

The length of an edge E and the diameter of an element K are denoted by h_E and $h_K = \sup\{|x-y| : x, y \in \partial K\}$, respectively. We introduce the diameter ρ_K of the largest circle inscribed in K with center z_K, see Figure 1.4. If z_K is not unique an arbitrary but fixed one is chosen.

Definition 2. The mesh $\mathcal{K}_h$ is called regular if it fulfils:

1. The aspect ratio is uniformly bounded from above by σ, i.e. $h_K/\rho_K < \sigma \quad \forall K \in \mathcal{K}_h$.

2. All elements $K \in \mathcal{K}_h$ are convex polygons.

Additionally, we assume that $h_K < 1$ for all elements $K \in \mathcal{K}_h$. This condition is no grievous restriction on the mesh since $h_K < 1$ can always be satisfied by scaling Ω. Nevertheless, it is necessary in the forthcoming local boundary integral formulations.

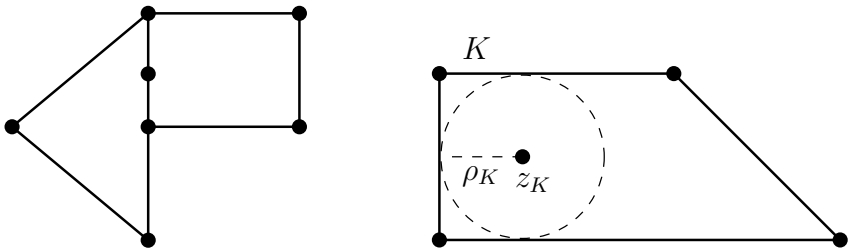

Figure 1.4: Elements with additional nodes on the straight boundary (left) and element K with inscribed circle (right)

For the later analysis, we need some notation. $\mathcal{N}_h$ denotes the set of all nodes in the mesh $\mathcal{K}_h$. It is $\mathcal{N}_h = \mathcal{N}_{h,\Omega} \cup \mathcal{N}_{h,D} \cup \mathcal{N}_{h,N}$, where $\mathcal{N}_{h,\Omega}$, $\mathcal{N}_{h,D}$, $\mathcal{N}_{h,N}$ contain the nodes in the interior of Ω, on the Dirichlet boundary Γ_D and on the interior of the Neumann boundary Γ_N, respectively. The transition points between Γ_D and Γ_N belong to $\mathcal{N}_{h,D}$. We label the set of all edges of the mesh with $\mathcal{E}_h$. In analogy to the set of nodes, we decompose $\mathcal{E}_h = \mathcal{E}_{h,\Omega} \cup \mathcal{E}_{h,D} \cup \mathcal{E}_{h,N}$, where $\mathcal{E}_{h,\Omega}$, $\mathcal{E}_{h,D}$ and $\mathcal{E}_{h,N}$ contain all edges in the interior of Ω, on the Dirichlet boundary Γ_D and on the Neumann boundary Γ_N, respectively. Moreover, the sets $\mathcal{N}(K)$ and $\mathcal{N}(E)$ contain all nodes which belong to the element $K \in \mathcal{K}_h$ and the edge $E \in \mathcal{E}_h$, respectively. Finally, we denote the set of edges which belong to the element K by $\mathcal{E}(K)$.

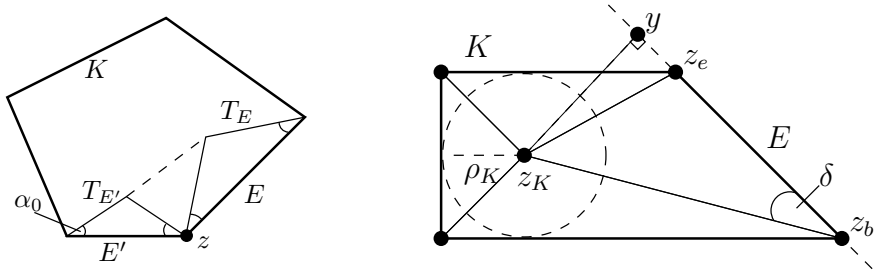

Figure 1.5: Element with two isosceles triangles adjacent to the node z (left) and element with inscribed circle, auxiliary triangulation and projection y of z_K onto the straight line through E (right)

Lemma 3. *Let $\mathcal{K}_h$ be a regular mesh according to Definition 2. Then, there is an angle α_0 with $0 < \alpha_0 \leq \pi/3$ such that for all elements $K \in \mathcal{K}_h$ and all its edges $E \in \mathcal{E}(K)$ the isosceles triangle T_E with longest side E and two interior angles α_0 lies inside the element K, see Figure 1.5. The angle α_0 only depends on σ.*

Proof. For arbitrary $K \in \mathcal{K}_h$, we construct a triangulation by connecting all vertices $z \in \mathcal{N}(K)$ with z_K. Next, we bound the angles between the new introduced edges and the previous ones $E = \overline{z_b z_e} \in \mathcal{E}(K)$ from below, see Figure 1.5. Without loss of generality, we assume that the angle δ is smaller than $\pi/2$. Using the projection y of z_K onto the straight line through the edge E, we recognize

$$\sin \delta = \frac{|y - z_K|}{|z_b - z_K|} \geq \frac{\rho_K}{h_K} \geq \frac{1}{\sigma}.$$

Consequently, it is $\delta \geq \arcsin \sigma^{-1}$. Since this estimate is valid for all angles next to ∂K of the auxiliary triangulation, the isosceles triangles with common angle $\alpha_0 = \min\{\pi/3, \arcsin \sigma^{-1}\}$ lie inside the auxiliary triangles and therefore inside K. □

Remark 3. The upper bound of α_0 is chosen in such a way that the longest side of the isosceles triangle T_E is always the edge E. This fact is not important in the previous lemma, but it simplifies forthcoming proofs.

Corollary 1. *Let $\mathcal{K}_h$ be a regular mesh. Every node belongs to finitely many elements, i.e. $|\{K \in \mathcal{K}_h : z \in \mathcal{N}(K)\}| \leq c \ \forall z \in \mathcal{N}_h$. The constant $c > 0$ only depends on σ.*

Proof. Due to the regularity of $\mathcal{K}_h$, every interior angle of an element is bounded from below by α_0 as we have seen in Lemma 3. This angle only depends on σ. Therefore, we have

$$|\{K \in \mathcal{K}_h : z \in \mathcal{N}(K)\}| \leq \left\lfloor \frac{2\pi}{\alpha_0} \right\rfloor,$$

where the term on the right hand side denotes the biggest integer smaller than or equal to $2\pi/\alpha_0$. □

The isosceles triangles and the auxiliary triangulation introduced in Lemma 3 and its proof play an important role. They are used in later proofs to handle the polygonal elements. In [35], the following proposition is proven with similar considerations as in the proof of Lemma 3.

Proposition 1. *For a regular mesh $\mathcal{K}_h$, all angles of all triangles in the auxiliary triangulation defined in the proof of Lemma 3 are less than $\pi - \arcsin(1/\sigma)$.*

One consequence of this proposition is that the auxiliary triangulation fulfils a maximum angle condition. Therefore, the standard approximation properties of finite element interpolation for linear as well as for higher order basis functions are valid on this discretization, see [4]. The constants appearing in the estimates depend only on the maximal aspect ratio σ of the mesh $\mathcal{K}_h$ since the maximal angle in Proposition 1 only depends on this regularity parameter.

For the analysis of local boundary element methods used in the BEM-based FEM and some proofs in Chapter 3, the regularity of a mesh is not enough. Another important property is that the diameter of an element is comparable to the length of its shortest edge. This is ensured by the following definition.

Definition 3. The regular mesh $\mathcal{K}_h$ is called stable if there is a constant $c_1 > 0$ such that for all elements $K \in \mathcal{K}_h$ and all its edges $E \in \mathcal{E}(K)$ it holds

$$h_K \leq c_1 h_E.$$

In Section 3.2, we have to consider neighbourhoods of nodes, edges and elements for a proper definition of a quasi-interpolation operator. At the current point, we want to give a preview and prove some properties. These neighbourhoods are open sets and they are defined as element patches by

$$\overline{\omega}_z = \bigcup_{z \in \mathcal{N}(K')} \overline{K'}, \qquad \overline{\omega}_E = \bigcup_{E \in \mathcal{E}(K')} \overline{K'}, \qquad \overline{\omega}_K = \bigcup_{\overline{K} \cap \overline{K'} \neq \varnothing} \overline{K'}$$

for $z \in \mathcal{N}_h$, $E \in \mathcal{E}_h$ and $K \in \mathcal{K}_h$, see Figure 1.6. An important role plays the neighbourhood ω_z of a node z. Its diameter is denoted by h_{ω_z} and it is of comparable size to $K \subset \omega_z$ as shown in

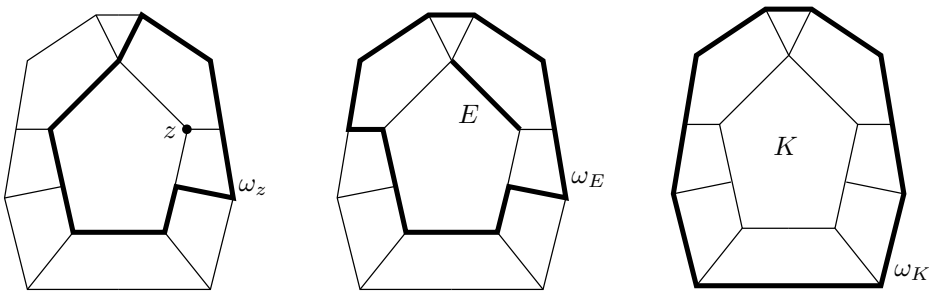

Figure 1.6: Examples for neighbourhoods of nodes, edges and elements

Lemma 4. *Let $\mathcal{K}_h$ be regular and stable. Then, the mesh fulfils:*

1. *The number of nodes per element is uniformly bounded, i.e. $|\mathcal{N}(K)| \leq c, \quad \forall K \in \mathcal{K}_h$.*

2. *Each element is covered by a uniformly bounded number of neighbourhoods of elements, i.e. $|\{K' \in \mathcal{K}_h : K \subset \omega_{K'}\}| \leq c, \quad \forall K \in \mathcal{K}_h$.*

3. *For all $z \in \mathcal{N}_h$ and $K \subset \omega_z$, it is $h_{\omega_z} \leq c h_K$.*

The generic constant $c > 0$ only depends on σ and c_1 from Definitions 2 and 3.

Proof. 1. Let $K \in \mathcal{K}_h$. In two dimensions, the number of nodes $|\mathcal{N}(K)|$ and the number of edges of the element K are identical. Since K is convex and since it lies in a square with side length h_K, the circumference $|\partial K|$ can be estimated in terms of h_K. Namely, it is $|\partial K| \leq 4h_K$. Additionally, we have $h_K \leq c_1 h_E$ for every edge E of K because of the stability of $\mathcal{K}_h$. These facts yield

$$|\mathcal{N}(K)| h_K \leq c_1 \sum_{E \in \mathcal{E}(K)} h_E = c_1 |\partial K| \leq 4 c_1 h_K$$

and prove the first part.

2. Let $K \in \mathcal{K}_h$. Obviously, the neighbourhood of an element $K' \in \mathcal{K}_h$ can be reformulated to

$$\overline{\omega}_{K'} = \bigcup_{z \in \mathcal{N}(K')} \overline{\omega}_z.$$

Consequently, K is covered by all $\omega_{K'}$ which contain at least one $\omega_z \subset \omega_{K'}$ with $z \in \mathcal{N}(K)$ since $K \subset \omega_z$. For each $z \in \mathcal{N}(K)$, the patch ω_z covers itself at most $\lfloor \frac{2\pi}{\alpha_0} \rfloor$ elements, where α_0 only depends on σ, see Corollary 1. Therefore, ω_z is contained in at most $\lfloor \frac{2\pi}{\alpha_0} \rfloor$ neighbourhoods $\omega_{K''}$. So, K is covered by at most

$$|\mathcal{N}(K)| \cdot \left\lfloor \frac{2\pi}{\alpha_0} \right\rfloor \leq c$$

neighbourhoods of elements $\omega_{K'}$.

3. We first recognize, that we have $h_{K'} \leq c_1 h_E \leq c_1 h_K$ for $K, K' \in \mathcal{K}_h$ with $E \in \mathcal{E}(K) \cap \mathcal{E}(K')$. If we apply this inequality successively in the neighbourhood ω_z of the node $z \in \mathcal{N}_h$, we obtain with Corollary 1

$$h_{K'} \leq c_1^{\lfloor 2\pi/\alpha_0 \rfloor - 1} h_K \qquad \text{for arbitrary } K, K' \subset \omega_z.$$

This yields

$$h_{\omega_z} \leq 2 \max_{K' \subset \omega_z} h_{K'} \leq 2 c_1^{\lfloor 2\pi/\alpha_0 \rfloor - 1} h_K \quad \text{for } K \subset \omega_z$$

and concludes the proof since α_0 only depends on σ.

□

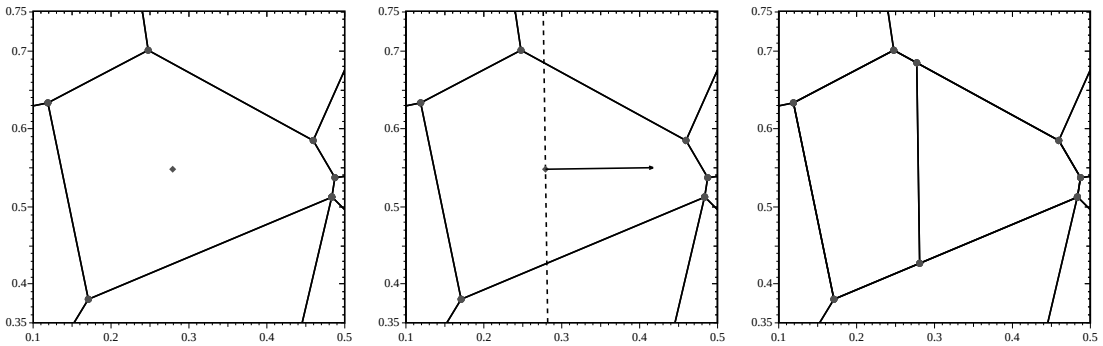

Figure 1.7: Refinement of an element: element with centre $\bar{x}$ (left), element with eigenvector (middle), two new elements (right)

The use of polygonal meshes is quite interesting for practical applications. In some real life problems, the materials already show polygonal structures like in crystals or different soil layers in ground water simulations. Furthermore, in the discretization of complex domains and interfaces between different meshes, polygonal elements are more flexible and advantageous over triangulations. Nevertheless, only a few commercial mesh generators are able to create and refine such meshes. To perform numerical convergence tests which confirm the theoretical results, a new procedure has been implemented to refine the polygonal meshes locally and globally. In a first step, some elements, or in the case of uniform refinement, all elements are marked. Afterwards, the procedure divides the marked elements. For the decision how to split an element K into two new ones, we first compute the matrix

$$M_{\text{Cov}} = \int_K (x - \bar{x})(x - \bar{x})^\top dx,$$

where

$$\bar{x} = \frac{1}{|K|} \int_K x \, dx$$

is the barycentre of the element. The two by two matrix M_{Cov} is symmetric and positive definite due to construction. So, we compute its eigenvalues and the corresponding eigenvectors. The eigenvector which belongs to the biggest eigenvalue points into the direction of the longest extend of the element K. Consequently, we split the element orthogonal to this eigenvector through the barycentre $\bar{x}$ of K. After these steps have been carried out, two new elements are obtained, see Figure 1.7. The regularity and stability of the mesh have to be ensured by the implementation of the algorithm. Similar ideas are used in [63] to cluster point clouds which are used for matrix approximation in fast boundary element methods.

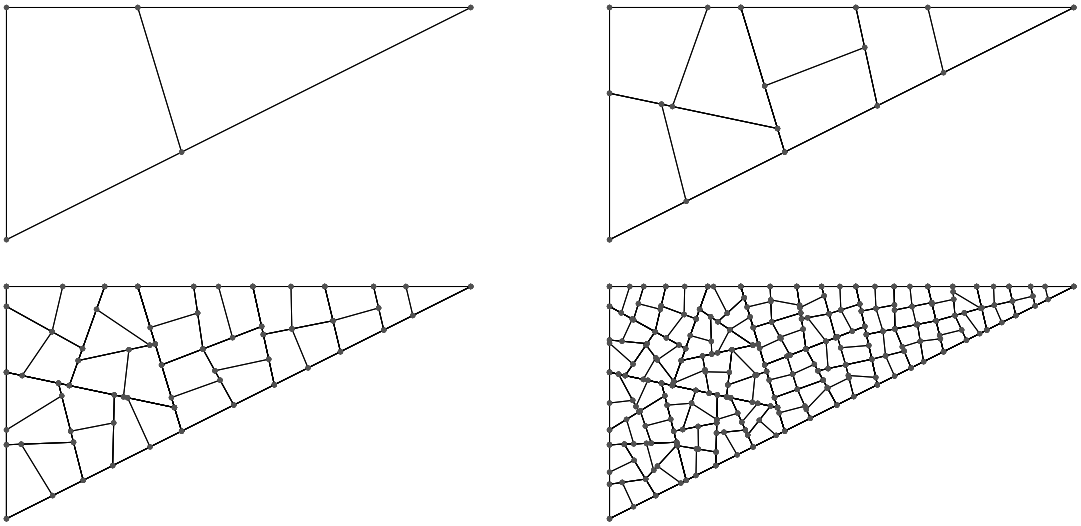

Figure 1.8: Uniform refinement of a triangle after one, three, five and seven refinement steps

Figures 1.8 shows a uniform refinement starting from a triangle. The meshes are obtained after one, three, five and seven refinement steps. We recognize that even a refinement of a triangle results in an unstructured polygonal mesh. Nevertheless, the resulting sequence of meshes has a uniform character. A big advantage of the introduced strategy can be seen in an adaptive context. It is possible to perform local refinements within a few elements. Classical mesh refinement techniques for triangular meshes, for example, suffer from the fact that local refinement propagates in neighbouring regions. This behaviour is necessary since the resulting meshes have to be admissible and thus the use of hanging nodes is very restricted or even avoided.

1.6 Boundary element method

As already mentioned in Section 1.3, we have to introduce some basis functions for the finite element method. These functions are defined over polygonal and polyhedral convex elements as solutions of local boundary value problems in Chapter 2

and 4. To handle the implicitly defined functions, the boundary integral formulation is used. In the numerics, this formulation is realized by the use of boundary element methods. For this reason, we review the theory and the numerics of the Dirichlet problem for the Laplace equation presented in [50, 68].

1.6.1 Boundary integral formulation

Let $K \subset \mathbb{R}^d$, $d = 2, 3$ be a bounded open domain with polygonal or polyhedral boundary. In the later application, we think of $K \in \mathcal{K}_h$ for some polygonal or polyhedral mesh $\mathcal{K}_h$, but in general K can be an arbitrary non-convex domain. Consider the problem

$$\begin{aligned} -\Delta u &= 0 \quad \text{in } K, \\ u &= g \quad \text{on } \partial K \end{aligned} \tag{1.10}$$

with some given function $g \in H^{1/2}(\partial K)$. For the following theory of boundary integral formulations, we need the usual trace operator $\gamma_0^K : H^1(K) \to H^{1/2}(\partial K)$ introduced in Theorem 2. Here, the index indicates that the trace is taken with respect to the domain K. Let $v \in H^1(K)$ with Δv in the dual of $H^1(K)$. Due to Green's first identity [50], there exists a unique function $\gamma_1^K v \in H^{-1/2}(\partial K)$ such that

$$\int_K \nabla v(y) \cdot \nabla w(y)\, dy = \int_{\partial K} \gamma_1^K v(y) \gamma_0^K w(y)\, ds_y - \int_K w(y) \Delta v(y)\, dy \tag{1.11}$$

for $w \in H^1(K)$. We call $\gamma_1^K v$ the conormal derivative of v. If v is smooth, e.g. $v \in H^2(K)$, we have

$$(\gamma_1^K v)(x) = n_K(x) \cdot (\gamma_0^K \nabla v)(x) \quad \text{for } x \in \partial K,$$

where $n_K(x)$ denotes the outer normal vector of the domain K at x. The trace and the conormal derivative are also called Dirichlet and Neumann trace for the Laplace equation.

Additionally, we need the fundamental solution of the Laplacian. This singular function is given as

$$U^*(x,y) = \begin{cases} -\dfrac{1}{2\pi} \ln|x-y|, & \text{for } x, y \in \mathbb{R}^2 \\ \dfrac{1}{4\pi\,|x-y|}, & \text{for } x, y \in \mathbb{R}^3 \end{cases}.$$

The fundamental solution fulfils the equation

$$-\Delta_y U^*(x,y) = \delta_0(y-x),$$

where δ_0 is the Dirac delta distribution. If we substitute $v(y) = U^*(x,y)$ in Green's second identity

$$\int_K (v(y)\Delta u(y) - u(y)\Delta v(y))\, dy = \int_{\partial K} \left(\gamma_0^K v(y) \gamma_1^K u(y) - \gamma_0^K u(y) \gamma_1^K v(y)\right) ds_y,$$

see [50], we obtain a representation formula for the solution u in every point $x \in K$. It reads

$$u(x) = \int_{\partial K} U^*(x,y)\gamma_1^K u(y)\, ds_y - \int_{\partial K} \gamma_{1,y}^K U^*(x,y)\gamma_0^K u(y)\, ds_y. \tag{1.12}$$

Consequently, if the data $\gamma_0^K u$ and $\gamma_1^K u$ is known, it is possible to evaluate the function u everywhere in the domain K. Furthermore, it is possible to calculate the Neumann datum if the Dirichlet datum is known as in (1.10). We apply the trace operator and the conormal derivative operator to the representation formula. This yields the system of equations

$$\begin{pmatrix} \gamma_0^K u \\ \gamma_1^K u \end{pmatrix} = \begin{pmatrix} \frac{1}{2}\mathbf{I} - \mathbf{K}_K & \mathbf{V}_K \\ \mathbf{D}_K & \frac{1}{2}\mathbf{I} + \mathbf{K}'_K \end{pmatrix} \begin{pmatrix} \gamma_0^K u \\ \gamma_1^K u \end{pmatrix}. \tag{1.13}$$

This system contains the standard boundary integral operators which are well studied, see e.g. [50, 65, 68]. For $x \in \partial K$, we have the single-layer potential operator

$$(\mathbf{V}_K \zeta)(x) = \gamma_0^K \int_{\partial K} U^*(x,y)\zeta(y)\, ds_y \quad \text{for } \zeta \in H^{-1/2}(\partial K),$$

the double-layer potential operator

$$(\mathbf{K}_K \xi)(x) = \lim_{\varepsilon \to 0} \int_{y \in \partial K : |y-x| \geq \varepsilon} \gamma_{1,y}^K U^*(x,y)\xi(y)\, ds_y \quad \text{for } \xi \in H^{1/2}(\partial K),$$

and the adjoint double-layer potential operator

$$(\mathbf{K}'_K \zeta)(x) = \lim_{\varepsilon \to 0} \int_{y \in \partial K : |y-x| \geq \varepsilon} \gamma_{1,x}^K U^*(x,y)\zeta(y)\, ds_y \quad \text{for } \zeta \in H^{-1/2}(\partial K),$$

as well as the hypersingular integral operator

$$(\mathbf{D}_K \xi)(x) = -\gamma_1^K \int_{\partial K} \gamma_{1,y}^K U^*(x,y)\xi(y)\, ds_y \quad \text{for } \xi \in H^{1/2}(\partial K).$$

These integral operators

$$\begin{aligned} \mathbf{V}_K &: H^{-1/2}(\partial K) \to H^{1/2}(\partial K), \\ \mathbf{K}_K &: H^{1/2}(\partial K) \to H^{1/2}(\partial K), \\ \mathbf{K}'_K &: H^{-1/2}(\partial K) \to H^{-1/2}(\partial K), \\ \mathbf{D}_K &: H^{1/2}(\partial K) \to H^{-1/2}(\partial K) \end{aligned}$$

are linear and continuous. For $K \subset \mathbb{R}^2$ with $h_K < 1$ or $K \subset \mathbb{R}^3$, the single-layer potential operator induces a bilinear form $(\mathbf{V}_K \cdot, \cdot)_{L_2(\partial K)}$, which is $H^{1/2}(\partial K)$-elliptic and continuous on $H^{1/2}(\partial K)$, see [50, 68]. Here, the L_2-scalar product

has to be interpreted as duality pairing. According to the Lax-Milgram lemma, see Theorem 4, the single-layer potential operator is invertible. Therefore, the first equation of system (1.13) yields a connection between the Dirichlet and the Neumann trace

$$\gamma_1^K u = \mathbf{S}_K \gamma_0^K u \quad \text{with} \quad \mathbf{S}_K = \mathbf{V}_K^{-1} \left(\tfrac{1}{2}\mathbf{I} + \mathbf{K}_K\right). \tag{1.14}$$

The operator

$$\mathbf{S}_K : H^{1/2}(\partial K) \to H^{-1/2}(\partial K)$$

is called Steklov-Poincaré operator and it is linear and continuous due to its definition. Using the second equation of system (1.13), we find the symmetric representation

$$\mathbf{S}_K = \mathbf{D}_K + \left(\tfrac{1}{2}\mathbf{I} + \mathbf{K}_K'\right) \mathbf{V}_K^{-1} \left(\tfrac{1}{2}\mathbf{I} + \mathbf{K}_K\right). \tag{1.15}$$

The inversion of the single-layer potential operator in the evaluation of the Steklov-Poincaré operator is not desirable. To compute the unknown Neumann datum $t = \gamma_1^K u \in H^{-1/2}(\partial K)$ from given Dirichlet datum $g = \gamma_0^K u \in H^{1/2}(\partial K)$, it is more convenient to use the variational formulation

$$\text{Find } t \in H^{-1/2}(\partial K) : \; (\mathbf{V}_K t, \xi)_{L_2(\partial K)} = \left(\left(\tfrac{1}{2}\mathbf{I} + \mathbf{K}_K\right) g, \xi\right)_{L_2(\partial K)} \; \forall \xi \in H^{1/2}(\partial K).$$

This formulation admits a unique solution according to the Lax-Milgram lemma and is consequently equivalent to the evaluation of $\mathbf{S}_K$.

Finally, we are able to solve the Laplace problem (1.10) at least theoretically. First, we compute the Neumann datum from the Dirichlet datum with the use of the Steklov-Poincaré operator and then we insert it into the representation formula (1.12) which solves the problem. The solution obtained this way fulfils $u \in H^1(K)$, see [50, 68].

1.6.2 Discretization

In most cases, the boundary integral operators mentioned in Subsection 1.6.1 cannot be realized analytically in simulations. Therefore, numerical approximations are needed. In the following, we review the boundary element method which is used for the discretization of the boundary integral equations.

Let $K \subset \mathbb{R}^d$, $d = 2, 3$ be a polygonal domain with $h_K < 1$ or a polyhedral domain. The first step in solving (1.10) with the help of the boundary integral formulation is to discretize the boundary of K and to introduce a boundary mesh, see Figure 1.9. In the two dimensional case, we decompose the polygonal boundary into line segments. The coarsest discretization is obtained if each line segment coincides with an edge of K. The three dimensional case is more complicated. Here, we have to introduce a triangulation of the surface. This triangulation has to be admissible in the sense of classical finite element methods, i.e. two neighbouring triangles share either a common node or a common edge. Furthermore, we have to ensure some form regularity such that the ratio between the diameter of the triangle and the diameter of the largest inscribed circle of the

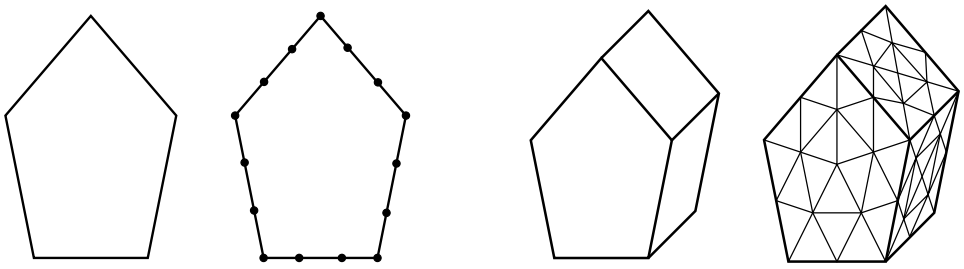

Figure 1.9: A domain and its boundary mesh for $d = 2$ (left) and $d = 3$ (right)

triangle is uniformly bounded for all elements of the surface mesh, see [65, 68]. The boundary mesh is denoted by $\mathcal{B}_h$ and its elements by T, where T is either a line segment ($d = 2$) or a triangle ($d = 3$). The set of nodes is labeled $\mathcal{M}_h$.

For each $T \in \mathcal{B}_h$, we define a function

$$\tau_T^0 = \begin{cases} 1, & \text{in } T \\ 0, & \text{else} \end{cases} \qquad \text{and set} \qquad \Phi_N = \{\tau_T^0 : T \in \mathcal{B}_h\},$$

which is a basis of the space of piecewise constant functions over the mesh $\mathcal{B}_h$. It is $\operatorname{span} \Phi_N \subset H^{-1/2}(\partial K)$, and thus we use this discrete space for the approximation of the Neumann trace. Additionally, we define for $z \in \mathcal{M}_h$ a function

$$\varphi_z = \begin{cases} 1, & \text{at } z \\ \text{linear}, & \text{on } T \in \mathcal{B}_h \\ 0, & \text{at } x \in \mathcal{M}_h \setminus \{z\} \end{cases} \qquad \text{and set} \qquad \Phi_D = \{\varphi_z : z \in \mathcal{M}_h\}.$$

These functions form a basis of the space of piecewise linear and globally continuous functions over the boundary ∂K. Therefore, it is $\operatorname{span} \Psi_D \subset H^{1/2}(\partial K)$ and we use this discrete space for the approximation of the Dirichlet trace.

In the boundary value problem (1.10) the Dirichlet datum $g \in H^{1/2}(\partial K)$ is given. We carry out the L_2-projection onto the space of piecewise linear and globally continuous functions to get an approximation $g_h \in \operatorname{span} \Phi_D$. This projected datum is used in a discrete Galerkin formulation

$$\text{Find } t_h \in \operatorname{span} \Phi_N : \quad (\mathbf{V}_K t_h, \vartheta)_{L_2(\partial K)} = \left(\left(\tfrac{1}{2}\mathbf{I} + \mathbf{K}_K\right) g_h, \vartheta\right)_{L_2(\partial K)} \quad \forall \vartheta \in \Phi_N$$

to approximate the unknown Neumann datum $t = \gamma_1^K u \in H^{-1/2}(\partial K)$. Due to the properties of the boundary integral operators, the variational formulation has a unique solution. The representations

$$t_h = \sum_{\tau \in \Phi_N} t_\tau \tau \qquad \text{and} \qquad g_h = \sum_{\varphi \in \Phi_D} g_\varphi \varphi$$

yield the system of linear equations

$$\mathbf{V}_{K,h} \underline{t}_h = \left(\tfrac{1}{2}\mathbf{M}_{K,h} + \mathbf{K}_{K,h}\right) \underline{g}_h,$$

where the underline refers to the coefficient vector, e.g. $\underline{t}_h = (t_\tau)_{\tau\in\Phi_N}$. The matrices are defined as

$$\mathbf{V}_{K,h} = \Big((\mathbf{V}_K\tau,\vartheta)_{L_2(\partial K)}\Big)_{\vartheta\in\Phi_N,\tau\in\Phi_N}$$

and

$$\mathbf{M}_{K,h} = \Big((\varphi,\vartheta)_{L_2(\partial K)}\Big)_{\vartheta\in\Phi_N,\varphi\in\Phi_D}, \quad \mathbf{K}_{K,h} = \Big((\mathbf{K}_K\varphi,\vartheta)_{L_2(\partial K)}\Big)_{\vartheta\in\Phi_N,\varphi\in\Phi_D}.$$

After the computation of $\underline{t}_h$, we use the approximations $g_h \in \operatorname{span}\Phi_D$ of the Dirichlet datum and $t_h \in \operatorname{span}\Phi_N$ of the Neumann datum in the representation formula (1.12) to obtain an approximation

$$u_h(x) = \int_{\partial K} U^*(x,y)t_h(y)\,ds_y - \int_{\partial K} \gamma_{1,y}^K U^*(x,y)g_h(y)\,ds_y \tag{1.16}$$

of the exact solution u in K. The approximation fulfils $u_h \in H^1(K)$.

The boundary element method presented here is well studied and several approximation properties are proven, see [65, 68]. For illustration, some results are stated below. In the case that g_h is replaced by the exact Dirichlet datum g in the considerations of this subsection, there are the estimates

$$\|t - t_h\|_{L_2(\partial K)} \le ch\,|t|_{H^1_{\mathrm{pw}}(\partial K)}$$

and

$$|u(x) - u_h(x)| \le c(x)h^3\,|t|_{H^1_{\mathrm{pw}}(\partial K)} \quad \text{for } x \in K$$

as well as

$$\|u - u_h\|_{H^1(K)} \le ch^{3/2}\,|t|_{H^1_{\mathrm{pw}}(\partial K)}$$

for an exact solution $u \in H^{5/2}(K)$. In these estimates, h denotes the biggest diameter of the mesh elements $T \in \mathcal{B}_h$. Additionally, it is assumed in the derivation of these estimates, see [68], that the mesh is globally quasi-uniform, i.e. the ratio between the biggest and smallest element diameter is bounded uniformly.

Till now, we have seen how to approximate the Neumann trace by the use of the Steklov-Poincaré operator. Next, we want to discretize the symmetric representation (1.15) of the operator. For this reason, we set

$$\widetilde{\mathbf{S}}_K g_h = \mathbf{D}_K g_h + \left(\tfrac{1}{2}\mathbf{I} + \mathbf{K}_K'\right) t_h$$

and choose an arbitrary function

$$q_h = \sum_{\xi\in\Phi_D} q_\xi \xi \in \operatorname{span}\Phi_D.$$

It is

$$\begin{aligned}\left(\widetilde{\mathbf{S}}_K g_h, q_h\right)_{L_2(\partial K)} &= \left(\mathbf{D}_K g_h + \left(\tfrac{1}{2}\mathbf{I} + \mathbf{K}'_K\right) t_h, q_h\right)_{L_2(\partial K)} \\ &= \left(\mathbf{D}_K g_h, q_h\right)_{L_2(\partial K)} + \tfrac{1}{2}\left(q_h, t_h\right)_{L_2(\partial K)} + \left(\mathbf{K}_K q_h, t_h\right)_{L_2(\partial K)} \\ &= \underline{q}_h^\top \mathbf{D}_{K,h} \underline{g}_h + \underline{q}_h^\top \left(\tfrac{1}{2}\left(\mathbf{M}_{K,h}\right)^\top + \left(\mathbf{K}_{K,h}\right)^\top\right) \underline{t}_h \\ &= \underline{q}_h^\top \mathbf{D}_{K,h} \underline{g}_h + \underline{q}_h^\top \left(\tfrac{1}{2}\left(\mathbf{M}_{K,h}\right)^\top + \left(\mathbf{K}_{K,h}\right)^\top\right) \mathbf{V}_{K,h}^{-1} \left(\tfrac{1}{2}\mathbf{M}_{K,h} + \mathbf{K}_{K,h}\right) \underline{g}_h \\ &= \underline{q}_h^\top \mathbf{S}_{K,h} \underline{g}_h,\end{aligned}$$

where

$$\mathbf{S}_{K,h} = \mathbf{D}_{K,h} + \left(\tfrac{1}{2}\left(\mathbf{M}_{K,h}\right)^\top + \left(\mathbf{K}_{K,h}\right)^\top\right) \mathbf{V}_{K,h}^{-1} \left(\tfrac{1}{2}\mathbf{M}_{K,h} + \mathbf{K}_{K,h}\right)$$

with

$$\mathbf{D}_{K,h} = \left(\left(\mathbf{D}_K \varphi, \xi\right)_{L_2(\partial K)}\right)_{\xi \in \Phi_D, \varphi \in \Phi_D}.$$

Consequently, we can use the approximation

$$\left(\mathbf{S}_K g_h, q_h\right)_{L_2(\partial K)} \approx \left(\widetilde{\mathbf{S}}_K g_h, q_h\right)_{L_2(\partial K)} = \underline{q}_h^\top \mathbf{S}_{K,h} \underline{g}_h \tag{1.17}$$

for the bilinear form induced by the Steklov-Poincaré operator.

Finally, the question arises how to set up all the boundary integral matrices in the implementation. The mass matrix $\mathbf{M}_{K,h}$ can be computed analytically, whereas numerical integration is used to compile $\mathbf{V}_{K,h}$ and $\mathbf{K}_{K,h}$. There are several possibilities for this integration. Either a fully numerical or a semi analytical scheme can be chosen. The latter one uses Gaussian quadrature for the outer integral and evaluates the integral operator analytically in the Gaussian points. At the end, the matrix entries of $\mathbf{D}_{K,h}$ are computed as linear combinations of matrix entries from $\mathbf{V}_{K,h}$. For a detailed description see [68].

The strategies reviewed in this subsection are for lower order approximation. But it is not difficult to extend the ideas to a higher order boundary element method. Here, $H^{-1/2}(\partial K)$ is discretized with piecewise linear functions and $H^{1/2}(\partial K)$ with piecewise quadratic and globally continuous functions, for example. In the two dimensional case, this means, that we extend the basis Φ_N with functions

$$\tau_T^1 = \begin{cases} 1, & \text{at } z_e \\ \text{linear}, & \text{on } T \\ 0, & \text{else} \end{cases}$$

for all $T \in \mathcal{B}_h$, where z_e is the node at the end of the line segment T. The basis Φ_D is equipped with additional bubble functions

$$\varphi_T = 4\varphi_{z_b}\varphi_{z_e}$$

for all $T \in \mathcal{B}_h$, where z_e is as before and z_b is the node at the beginning of the line segment T. We obtain directly a higher order method using these extended bases in the formulation of the discrete Galerkin scheme above.

Chapter 2

BEM-based FEM in 2D

The purpose of the following pages is to introduce the BEM-based FEM for the model problem in two dimensions. The ideas how to define the first order trial functions are taken from [20] and are based on the symmetric boundary element domain decomposition method presented in [42]. The trial functions are defined implicitly as solutions of local boundary value problems. These problems are solved approximately by the boundary element method. Therefore, the global strategy is called BEM-based finite element method. In contrast to the publications [20, 21, 40], where the method is analysed in the domain decomposition framework, we favour the viewpoint of a finite element method, and we deal with mixed boundary conditions as well as with non-vanishing right hand side in the differential equation.

After the discussion of the first order trial functions, we introduce higher order trial functions over polygonal meshes based on new ideas. Interpolation operators are declared and approximation properties are proven by the use of recent results from [35] and extending them to the situation of higher order approximation. This strategy yields convergence estimates for the finite element method with exact trial functions where numerical errors in their approximation are neglected.

In previous realizations, the diffusion coefficient has been approximated by a piecewise constant function such that the numerical realization is straightforward as we see in the first section. But this restriction deteriorates the convergence of the higher order method with non-constant coefficient. For this reason, we propose a new kind of approximation which overcomes the difficulties, and we discuss how to realize the advanced strategy numerically.

Throughout the chapter, we present several numerical examples which illustrate the addressed problems and confirm the theoretical results.

2.1 Lower order method

As the name of the method already indicates, we are dealing with a finite element method. Therefore, the basis of the further considerations is the discrete varia-

tional formulation (1.5) of the model problem (1.1). The aim is to define a proper space V_h such that we can use it in the discrete Galerkin formulation and set up the corresponding system of linear equations as stated in Section 1.3. In classical finite element methods, piecewise linear and globally continuous functions over a mesh are used for the definition of V_h. But this is only possible for triangulations. One advantage of the BEM-based FEM is that it works on arbitrary polygonal meshes which are regular according to Definition 2. Let $\mathcal{K}_h$ be such a regular mesh which serves as discretization of the domain Ω. The idea is to define a basis Ψ and to set V_h as the linear hull of Ψ.

The functions in Ψ are defined in the spirit of Trefftz such that they fulfil the partial differential equation of the boundary value problem in some sense. In contrast to the original idea of Trefftz where the basis functions satisfy the equation globally, we only force them to fulfil it locally, on each element of the discretization $\mathcal{K}_h$. Additionally, we simplify the differential equation for the basis functions and prescribe zero right hand side as well as constant material coefficients. For our model problem, we end up with the Laplace equation. To get a unique definition, we have to state boundary values on the boundary of the elements for the local problems. Since we are interested in a lower order method, we prescribe linear data. To get a nodal basis, we set the functions equal to one at one node and equal to zero at every other node of the mesh. More precisely, we define for every $z \in \mathcal{N}_h$, the function ψ_z as unique solution of

$$\begin{aligned} -\Delta\psi_z &= 0 \quad \text{in } K \quad \text{for all } K \in \mathcal{K}_h, \\ \psi_z(x) &= \begin{cases} 1 & \text{for } x = z \\ 0 & \text{for } x \in \mathcal{N}_h \setminus \{z\} \end{cases}, \\ &\psi_z \text{ is linear on each edge of the mesh.} \end{aligned} \tag{2.1}$$

Obviously, the basis functions ψ_z are defined as solutions of local boundary value problems (in K). The support of these functions ψ_z is small since they vanish on all elements $K \in \mathcal{K}_h$ with $z \notin \mathcal{N}(K)$. Due to the nature of the Dirichlet problem for the Laplace equation on convex domains, it is well known that ψ_z is arbitrary smooth in the interior of K and continuous on the closure of K for $K \in \mathcal{K}_h$, see [34]. Consequently, the basis functions are globally continuous on Ω and thus belong to the space $H^1(\Omega)$. In Figure 2.1, some basis functions are illustrated over one element.

The minimum-maximum principle for harmonic functions says that ψ_z reaches its minimal and maximal value at the boundary of K, see Section 1.4. Therefore, we have

$$0 < \psi_z < 1 \quad \text{in } K$$

for $z \in \mathcal{N}(K)$. Additionally, we recognize that ψ_z has no strict local minima or maxima inside of K. Otherwise, there would be a contradiction to the minimum-maximum principle since ψ_z is harmonic in every small neighbourhood of the extremum and thus reaches its extremal values on the boundary of the neighbourhood.

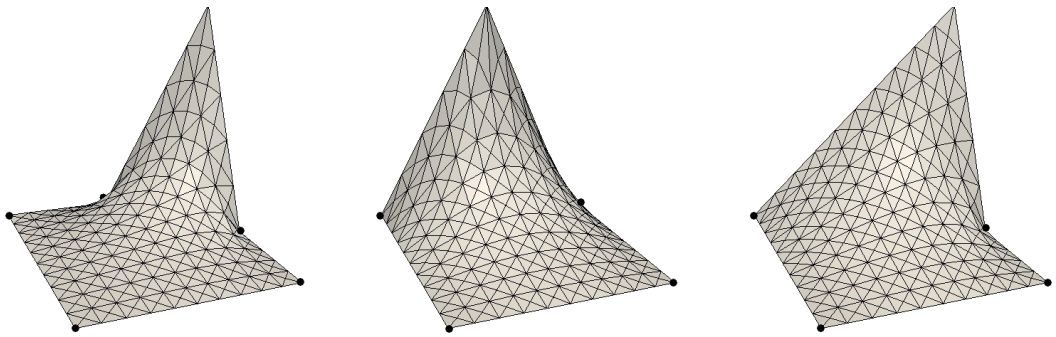

Figure 2.1: Visualisation of lower order trial functions on quadrangle elements, nodes are marked with black dots

In the case that $\mathcal{K}_h$ is an admissible triangulation without hanging nodes, the basis functions turn out to be the standard hat functions of classical finite element methods. This relation is quite obvious since the lowest order linear basis functions fulfil the data on the boundary of each element and they are harmonic because of their linearity. According to the unique solvability of the Dirichlet problem for the Laplace equation the hat functions coincide with the basis functions defined here. In this sense, the BEM-based FEM can be seen as a generalization of standard finite element methods.

If $\mathcal{K}_h$ is a polygonal mesh, another connection can be recognized. For the model problem, we rediscover the so called harmonic coordinates mentioned in several articles like [32, 35, 43, 49]. These harmonic coordinates restricted to one element $K \in \mathcal{K}_h$ are a special type of barycentric coordinates, i.e. they satisfy

$$\psi_z(x) \geq 0 \quad \text{on } \overline{K} \tag{2.2}$$

for $z \in \mathcal{N}(K)$ and it is

$$v = \sum_{z \in \mathcal{N}(K)} v(z)\psi_z \tag{2.3}$$

for any linear function v on $\overline{K}$ according to [35]. Condition (2.2) follows directly from the minimum-maximum principle. To verify (2.3), we observe that both sides of the equation are harmonic and coincide on the boundary of K. Therefore, the difference of both sides is harmonic and identical to zero on the boundary. Using the minimum-maximal principle again shows that equation (2.3) is valid in the whole element.

In [32], the authors have proven for any set of barycentric coordinates and especially for the harmonic coordinates, which are considered in this section, that they satisfy the estimate

$$0 \leq L_z^{\text{low}} \leq \psi_z \leq L_z^{\text{up}} \leq 1 \quad \text{on } \overline{K}$$

for $z \in \mathcal{N}(K)$. Here, L_z^{low} and L_z^{up} are piecewise linear functions defined as follows. Both functions are equal to one at the node z and they are equal to zero

at every other node on the boundary of K. Additionally, L_z^{low} is linear on the triangle constructed by connecting the node before and after z on the boundary, and zero else, see Figure 2.2. The function L_z^{up} is linear on each triangle that is obtained by connecting z with all other nodes on the boundary of K.

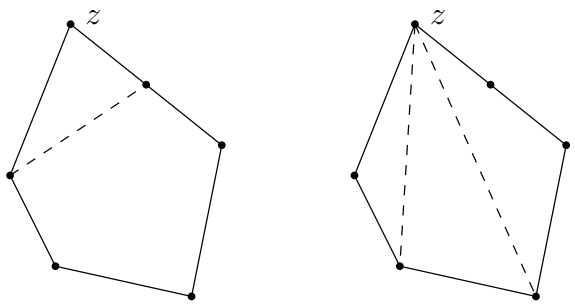

Figure 2.2: Triangles for construction of L_z^{low} (left) and L_z^{up} (right)

We come back to the discrete Galerkin formulation and set

$$\Psi^{(1)} = \{\psi_z : z \in \mathcal{N}_h\} \quad \text{and} \quad \Psi_D = \{\psi_z : z \in \mathcal{N}_{h,D}\}.$$

Using these sets of functions, we introduce the finite dimensional space

$$V_h = \operatorname{span} \Psi \quad \text{with} \quad \Psi = \Psi^{(1)} \setminus \Psi_D$$

which is conforming, i.e. $V_h \subset V$. A discrete extension u_{Dh} of the Dirichlet boundary datum is needed. For simplicity, we choose the interpolation of g_D with trial functions $\psi_z \in \Psi_D$ as extension u_{Dh}. The Galerkin formulation (1.5) yields together with

$$u_{0h} = \sum_{\psi \in \Psi} \beta_\psi \psi \quad \text{and} \quad u_{Dh} = \sum_{\psi \in \Psi_D} \beta_\psi \psi$$

the system of linear equations

$$\sum_{\psi \in \Psi} \beta_\psi \, a_\Omega(\psi, \phi) = (f, \phi) + (g_N, \phi)_{\Gamma_N} - \sum_{\psi \in \Psi_D} \beta_\psi \, a_\Omega(\psi, \phi) \quad \text{for } \phi \in \Psi.$$

In the approximation of u_{0h} and u_{Dh}, we use the same symbol β_ψ for the coefficients but there should be no confusion since $\Psi \cap \Psi_D = \varnothing$. We see that the main topic is to evaluate the bilinear form $a_\Omega(\cdot, \cdot)$ applied to trial functions in the set up of the system. The boundary integral $(g_N, \phi)_{\Gamma_N}$ can be computed quite easily since the function ϕ is a piecewise linear polynomial over Γ_N. To handle (f, ϕ), we can split the volume integral over Ω into integrals over elements and use numerical integration over each polygonal region. For this quadrature, it is possible to split the polygon even further into triangles or to use appropriate quadrature rules for polygonal elements, see [54]. After solving the system of equations, the

approximation of the unknown function u in the model problem (1.1) is given by $u_h = u_{0h} + u_{Dh}$.

Lets address the computation of the bilinear form applied to trial functions. The drawback of the actual formulation is that one has to integrate the gradient of the implicitly defined trial functions over the interior of the elements. Under the restriction that the material coefficient $a(\cdot)$ is constant on each element $K \in \mathcal{K}_h$, i.e.

$$a(x) = a_K \quad \text{for } x \in K \text{ and } K \in \mathcal{K}_h,$$

or it is approximated by a piecewise constant one, it is possible to rewrite this formulation. With the help of Green's first identity (1.11), we observe

$$a_\Omega(\psi, \phi) = \sum_{K \in \mathcal{K}_h} a_K \int_K \nabla\psi \cdot \nabla\phi = \sum_{K \in \mathcal{K}_h} a_K \int_{\partial K} \gamma_1^K \psi \gamma_0^K \phi.$$

So, we can reduce the volume integral to integrals over the boundary of the elements. Here, we have to integrate the product of the Dirichlet and the Neumann traces of trial functions where the first one is known by definition (2.1) and the other one can be expressed by the use of the Steklov-Poincaré operator. Since the traces of these trial functions lie in the discrete space $\operatorname{span} \Phi_D$ used in Section 1.6 for the boundary element method, we obtain

$$\int_{\partial K} \gamma_1^K \psi \gamma_0^K \phi = \int_{\partial K} \gamma_0^K \phi \, \mathbf{S}_K \gamma_0^K \psi \approx \underline{\gamma_0^K \phi} \, \mathbf{S}_{K,h} \, \underline{\gamma_0^K \psi}$$

according to (1.17). Here, the underline refers to the coefficient vector of the discrete representation. A closer look at the traces shows that

$$\gamma_0^K \psi_z = \varphi_z \in \Phi_D$$

for a trial function $\psi_z \in \Psi$. This means, that the trace of a trial function ψ_z coincides with a basis function used in the local boundary element method. Therefore, the vectors $\underline{\gamma_0^K \phi}$ and $\underline{\gamma_0^K \psi}$ contain only zeros and a single one. Consequently, the boundary integral is approximated by one entry of the matrix of the symmetric discretization of the local Steklov-Poincaré operator.

We set up the global finite element matrix using local stiffness matrices which belong to elements. These matrices are the symmetric discretizations of the local Steklov-Poincaré operators weighted with the elementwise constant coefficient. For the model problem, the global system matrix is symmetric and positive definite as it has been mentioned already in Section 1.3. Additionally, we obtain a sparse matrix since the trial functions have local support. Therefore, an appropriate iterative solver can be used to find the solution of the system of linear equations. In the realization for the later examples, we utilize a conjugate gradient method.

The finite element method on polygonal meshes with lowest order harmonic trial functions yields linear convergence in the H^1-norm as well as quadratic convergence in the L_2-norm. This behaviour is observed in our first example and is analysed later.

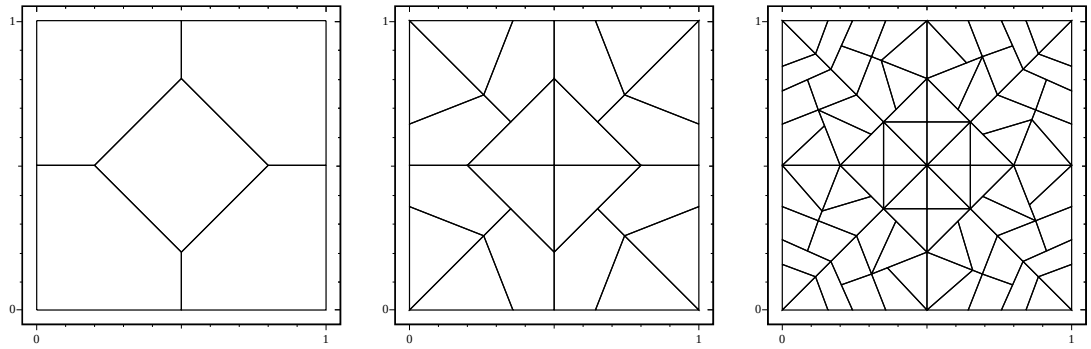

Figure 2.3: Initial mesh (left), refined mesh after two steps (middle), refined mesh after four steps (right)

Example 1. The function $u(x) = \exp(2\pi(x_1 - 0.3))\cos(2\pi(x_2 - 0.3))$, $x \in \mathbb{R}^2$ fulfils

$$\begin{aligned} -\Delta u &= 0 \quad \text{in } \Omega = (0,1)^2, \\ u &= g_D \quad \text{on } \Gamma \end{aligned}$$

with $g_D = \gamma_0 u$. The error is analysed with respect to $h = \max\{h_K : K \in \mathcal{K}_h\}$. The convergence can be seen in Figure 2.4 for the finite element method on a sequence of uniform refined meshes, compare Figure 2.3.

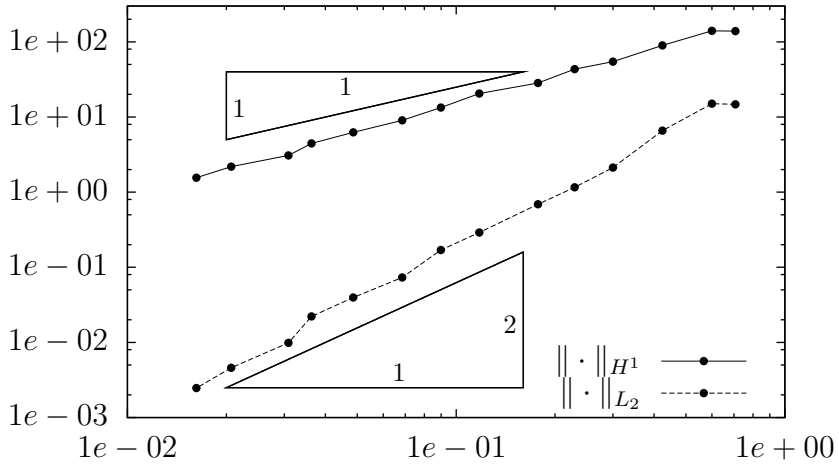

Figure 2.4: Absolute error with respect to h for Example 1 and triangles with slope one and two

2.2 Extensions to higher order

The lowest order harmonic trial functions are understood quite well and thus the question for higher order approximations arises. A straightforward generalization is to add harmonic trial functions which have quadratic boundary data.

We define for each edge $E \in \mathcal{E}_h$ a function ψ_E. Let $z_b, z_e \in \mathcal{N}(E)$ be the nodes at the beginning and at the end of the edge $E = \overline{z_b z_e}$. Then, ψ_E is the unique solution of

$$\begin{aligned} -\Delta\psi_E &= 0 && \text{in } K \quad \text{for all } K \in \mathcal{K}_h, \\ \psi_E &= 4\,\psi_{z_b}\psi_{z_e} && \text{on } \widetilde{E} \quad \text{for all } \widetilde{E} \in \mathcal{E}_h. \end{aligned}$$

Due to the definition of ψ_E, it vanishes in all nodes and on all edges of the mesh apart from E. For an illustration of such a trial function, see Figure 2.5. The restriction of ψ_E onto E is the well known quadratic bubble function which is zero in the corner points and one at the midpoint of the edge. For $E \in \mathcal{E}_{h,\Omega}$, we have $\operatorname{supp}\psi_E = \overline{K_1 \cup K_2}$, where $K_1, K_2 \in \mathcal{K}_h$ are the neighbouring elements of E with $E \in \mathcal{E}(K_1) \cap \mathcal{E}(K_2)$. If $E \in \mathcal{E}_{h,D} \cup \mathcal{E}_{h,N}$ belongs to the boundary of the domain Ω, it has just one neighbouring element of course. Since the trial function is harmonic in the interior of each element, ψ_E is arbitrary smooth in K and continuous on the closure of K for all $K \in \mathcal{K}_h$, see [34]. As in the case of lower order trial functions the minimum-maximum principle is applicable. We conclude that ψ_E has no strict local extrema inside an element and fulfils the estimate

$$0 < \psi_E < 1 \quad \text{in } K$$

for $E \in \mathcal{E}(K)$ as the nodal basis functions.

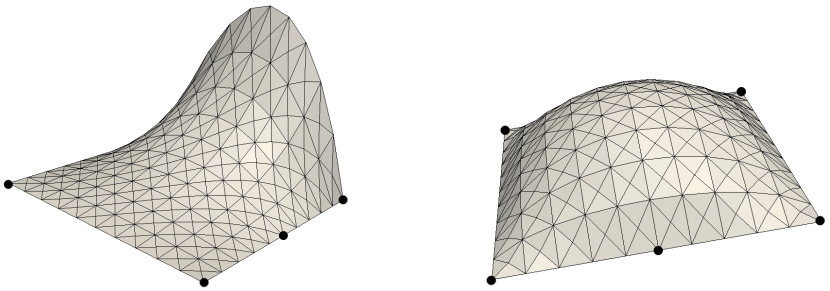

Figure 2.5: Visualisation of higher order trial functions ψ_E (left) and ψ_K (right) on quadrangle elements, nodes are marked with black dots

To obtain higher order convergence, we enrich the trial space $V_h = \operatorname{span}\Psi$ by adding the edge trial functions ψ_E to the basis Ψ. Therefore, we set

$$\Psi = \Psi^{(2)} \setminus \Psi_D$$

with

$$\Psi^{(2)} = \Psi^{(1)} \cup \{\psi_E : E \in \mathcal{E}_h\},$$

where we also have to enrich Ψ_D to

$$\Psi_D = \{\psi_z, \psi_E : z \in \mathcal{N}_{h,D}, E \in \mathcal{E}_{h,D}\}.$$

The discrete space V_h is now equipped with harmonic functions of higher polynomial order over the edges of the mesh. This space seems to suit to approximate

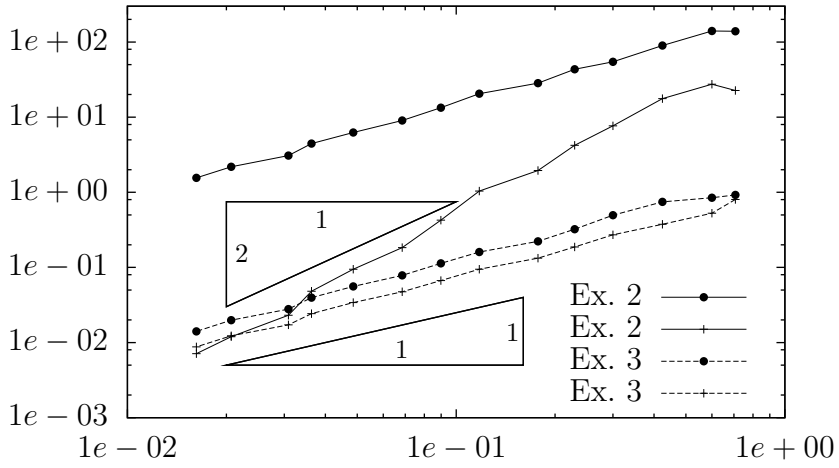

Figure 2.6: Absolute error in H^1-norm with respect to h for Example 2 and Example 3 with $\Psi = \Psi^{(1)} \setminus \Psi_D$ ($\bullet$) and $\Psi = \Psi^{(2)} \setminus \Psi_D$ ($+$), respectively, and triangles with slope two and one

harmonic functions with higher order. Consequently, we can use the enriched V_h in the Galerkin formulation which has been stated in Section 1.3. The boundary datum g_D is now approximated by piecewise quadratic polynomials over Γ_D and the extension u_{Dh} is chosen as linear combination of trial functions $\psi \in \Psi_D$. Under the restriction of a piecewise constant diffusion coefficient the numerical realization can be done in a similar way as before. We just have to use higher order trial functions in the local boundary element method.

Example 2. We solve again the Laplace problem mentioned in Example 1 for the harmonic function $u(x) = \exp(2\pi(x_1 - 0.3))\cos(2\pi(x_2 - 0.3))$ and plot the convergence in Figure 2.6.

Example 3. Consider the Dirichlet boundary value problem

$$\begin{aligned} -\Delta u &= f \quad \text{in } \Omega = (0,1)^2, \\ u &= 0 \quad \text{on } \Gamma, \end{aligned}$$

where $f \in L_2(\Omega)$ is chosen in such a way that $u(x) = \sin(\pi x_1)\sin(\pi x_2)$ for $x \in \Omega$ is the exact solution. The convergence results can be found in Figure 2.6.

In the last two examples, we have seen that the trial space V_h fits quite well for problems with vanishing right hand side f but lacks in the general case. This behaviour is not surprising since an approximation $u_h \in V_h$ always satisfy $-\Delta u_h = 0$ in all $K \in \mathcal{K}_h$. It is necessary to enrich the trial space V_h even further.

For each element $K \in \mathcal{K}_h$, we introduce a so called element bubble function ψ_K, see Figure 2.5, which fulfils

$$\begin{aligned} -\Delta \psi_K &= 1 \quad \text{in } K, \\ \psi_K &= 0 \quad \text{else} \end{aligned}$$

and is therefore uniquely defined. This function ψ_K is arbitrary smooth in K and continuous on the closure of K, see [34]. According to the weak maximum principle, ψ_K reaches at least one minimum on the boundary of K and thus we have

$$\psi_K \geq 0 \quad \text{in } K.$$

Adding these bubble functions to the basis

$$\Psi = \Psi^{(3)} \setminus \Psi_D$$

with

$$\Psi^{(3)} = \Psi^{(2)} \cup \{\psi_K : K \in \mathcal{K}_h\},$$

we obtain an improved trial space which is still conforming, i.e.

$$V_h = \operatorname{span} \Psi \subset V.$$

Using this final space V_h in the Galerkin formulation to solve the Poisson problem in Example 3, we get the desired rates of convergence. For the numerical realization, we refer to Section 2.5.

Example 4. We solve again the problem mentioned in Example 3 for the function $u(x) = \sin(\pi x_1)\sin(\pi x_2)$ and plot the convergence in Figure 2.7. Due to the enriched trial space, we get quadratic convergence in the H^1-norm and cubic convergence in the L_2-norm.

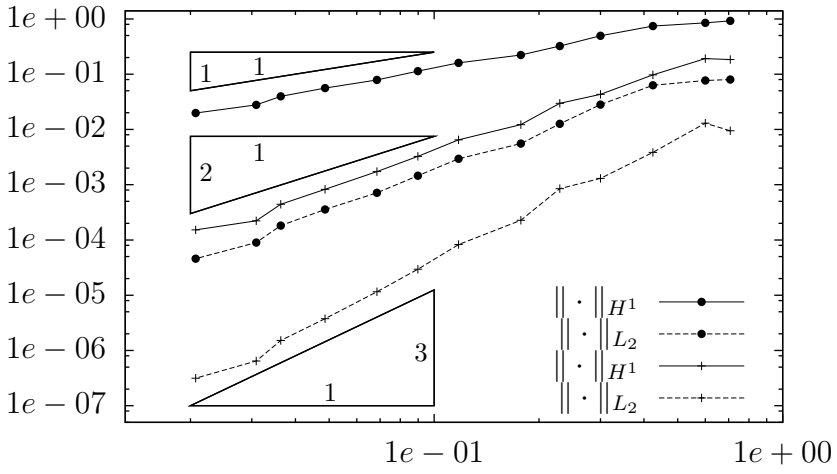

Figure 2.7: Absolute error in H^1- and L_2-norm with respect to h for Example 4 with $\Psi = \Psi^{(1)} \setminus \Psi_D$ ($\bullet$) and $\Psi = \Psi^{(3)} \setminus \Psi_D$ ($+$), respectively, and triangles with slope one, two and three

2.3 Interpolation error and FEM convergence

The common way to find convergence estimates for finite element methods is to use Céa's lemma, see Lemma 2, and replace the function in the argument of the minimum by an interpolation. If we have an appropriate interpolation operator $\mathfrak{I} : H^2(\Omega) \to V_h$, we get

$$\|u - u_h\|_{H^1(\Omega)} \leq \frac{M}{m} \min_{v_h \in V_h} \|u - v_h\|_{H^1(\Omega)} \leq \frac{M}{m} \|u - \mathfrak{I}u\|_{H^1(\Omega)}.$$

Obviously, the problem to find convergence estimates for finite element methods reduces to find a good interpolation operator and to study its properties.

In the following, we introduce three interpolation operators. The first one interpolates a given function $u \in H^2(\Omega)$ using lower order trial functions. This operator has already been studied in [35] and some interpolation estimates have been shown. Additionally, we introduce two higher order interpolation operators and prove new estimates with similar but extended ideas. For $v \in H^2(\Omega)$, we define the operators $\mathfrak{I}^{(i)} : H^2(\Omega) \to H^1(\Omega)$, $i = 1, 2, 3$ as follows

$$\mathfrak{I}^{(i)} v = \sum_{\psi \in \Psi^{(i)}} \alpha_\psi \psi, \quad i = 1, 2, 3,$$

where

$$\alpha_{\psi_z} = v(z) \quad \text{for } z \in \mathcal{N}_h,$$

$$\alpha_{\psi_E} = v\left(\frac{z_b + z_e}{2}\right) - \left(\mathfrak{I}^{(1)} v\right)\left(\frac{z_b + z_e}{2}\right) \quad \text{for } E \in \mathcal{E}_h \text{ with } E = \overline{z_b z_e}$$

and

$$\alpha_{\psi_K} = \frac{1}{\psi_K(z_K)} \left(v(z_K) - \left(\mathfrak{I}^{(2)} v\right)(z_K)\right) \quad \text{for } K \in \mathcal{K}_h.$$

These operators use pointwise interpolation. Evaluations of functions $v \in H^2(\Omega)$ in one point are well defined because of the fact that $H^2(\Omega) \subset C^0(\overline{\Omega})$ in two dimensions according to the Sobolev embedding theorem, see for example Subsection 1.2.3, Theorem 1.

Since we can decompose the square of the $H^1(\Omega)$-norm into a sum of squares of $H^1(K)$-norms over elements, it is enough to examine the interpolation properties over a single element. Let $\mathcal{P}^k(K)$ denote the space of polynomials over K with degree k.

Lemma 5. *The restrictions of the interpolation operators $\mathfrak{I}^{(i)}$, $i = 1, 2, 3$ to each element $K \in \mathcal{K}_h$ fulfil*

1. *$\mathfrak{I}^{(1)} p = p$ for $p \in \mathcal{P}^1(K)$,*
2. *$\mathfrak{I}^{(2)} p = p$ for $p \in \mathcal{P}^2(K)$ with $\Delta p = 0$, and*
3. *$\mathfrak{I}^{(3)} p = p$ for $p \in \mathcal{P}^2(K)$.*

Proof. Let $p \in \mathcal{P}^k(K)$ with $\Delta p = 0$ for $k = 1, 2$. Obviously, the trace of p on the boundary of K is a polynomial of degree k. Therefore, we can express this trace exactly with the trial functions out of $\Psi^{(k)}$ restricted to ∂K. It is

$$p\big|_{\partial K} = \mathfrak{I}^{(k)} p\big|_{\partial K}, \tag{2.4}$$

and both p as well as $\mathfrak{I}^{(k)} p$ fulfil the Dirichlet problem

$$\begin{aligned} \Delta u &= 0 \quad \text{in } K, \\ u &= p \quad \text{on } \partial K. \end{aligned}$$

Since this problem has a unique solution, it follows that $\mathfrak{I}^{(k)} p = p$.

Next, we show $\mathcal{P}^2(K) \subset \operatorname{span} \Psi^{(3)}$. Let $p \in \mathcal{P}^2(K)$. As before, we can express the trace of p by (2.4) with $k = 2$. Furthermore, we set $\alpha = \Delta p \in \mathbb{R}$ and

$$\widetilde{p} = \alpha \psi_K + \mathfrak{I}^{(2)} p \in \operatorname{span} \Psi^{(3)}. \tag{2.5}$$

Both functions p and $\widetilde{p}$ fulfil the boundary value problem

$$\begin{aligned} \Delta u &= \alpha \quad \text{in } K, \\ u &= p \quad \text{on } \partial K. \end{aligned}$$

Therefore, they are equal, i.e. $p = \widetilde{p}$. Solving (2.5) for α yields

$$\alpha = \frac{1}{\psi_K(x)} \left(p(x) - \mathfrak{I}^{(2)} p(x) \right) \quad \text{for } x \in K$$

which means $\alpha = \alpha_{\psi_K}$ and proves $\mathfrak{I}^{(3)} p = p$. □

Another property of the interpolation operator is the continuity. This has been shown for $\mathfrak{I}^{(1)}$ in [35]. In the subsequent lemma, we prove the corresponding estimate for the interpolation operators $\mathfrak{I}^{(k)}$, $k = 2, 3$ in a similar way. Lets assume that the diameter h_K of the element $K \in \mathcal{K}_h$ is one. This can be ensured by scaling. In the following, c denotes a generic constant that only depends on the maximal aspect ratio σ of the mesh given in Definition 2.

Lemma 6. *Let $\mathcal{K}_h$ be a regular mesh and $K \in \mathcal{K}_h$ with $h_K = 1$. For $i = 1, 2, 3$, there exists a constant $c = c(\sigma)$ independent of K such that*

$$\|\mathfrak{I}^{(i)} v\|_{H^1(K)} \leq c \, \|v\|_{H^2(K)} \quad \textit{for } v \in H^2(K).$$

Proof. In this proof, we make use of the minimum-maximum principle, see Section 1.4. Let $v \in H^2(K)$ and $i = 3$. The interpolation $\mathfrak{I}^{(3)} v$ fulfils the Dirichlet problem

$$\begin{aligned} \Delta \widetilde{v} &= \alpha_K \quad \text{in } K, \\ \widetilde{v} &= g_v \quad \text{on } \partial K \end{aligned} \tag{2.6}$$

in the classical sense with a piecewise quadratic function $g_v = \mathfrak{I}^{(3)} v\big|_{\partial K}$ on the boundary. Consequently, it also satisfies the weak formulation

$$\text{Find } \widetilde{v} \in H^1(K): \quad \gamma_0^K \widetilde{v} = g_v \quad \text{and} \quad \int_K \nabla \widetilde{v} \cdot \nabla w = (\alpha_K, w)_{L_2(K)}, \quad \forall w \in H_0^1(K).$$

To obtain homogeneous boundary data, we decompose $\widetilde{v} = \widetilde{v}_0 + \widetilde{v}_g$, where $\widetilde{v}_0 \in H_0^1(K)$ and $\widetilde{v}_g \in H^1(K)$ with $\gamma_0^K \widetilde{v}_g = g_v$. According to Proposition 1, the auxiliary triangulation of K which is obtained by connecting $z_K \in K$ with all vertices of K fulfils a maximum angle condition. Therefore, we can use the standard interpolation operator on triangular meshes for quadratic trial functions to get some $\widetilde{v}_g$. Due to this choice and since $h_K = 1$, it is

$$\|v - \widetilde{v}_g\|_{H^1(K)} \leq C_1 \, |v|_{H^2(K)},$$

see [4], where the constant C_1 only depends on the maximum angle and thus on the maximal aspect ratio σ. The reverse triangular inequality yields

$$\|\widetilde{v}_g\|_{H^1(K)} \leq C_1 \, |v|_{H^2(K)} + \|v\|_{H^1(K)} \leq \max\{1, C_1\} \, \|v\|_{H^2(K)}.$$

The function $\widetilde{v}_0$ fulfils

$$\text{Find } \widetilde{v}_0 \in H_0^1(K): \quad \int_K \nabla \widetilde{v}_0 \cdot \nabla w = (\alpha_K, w)_{L_2(K)} - \int_K \nabla \widetilde{v}_g \cdot \nabla w, \quad \forall w \in H_0^1(K).$$

In [34], the Poincaré inequality is stated as

$$\|w\|_{L_2(K)} \leq \left(\frac{1}{\pi} |K| \right)^{1/2} |w|_{H^1(K)} \quad \text{for } w \in H_0^1(K).$$

According to this inequality and since $|K| \leq h_K^2 = 1$, it is

$$\|\widetilde{v}_0\|_{H_1(K)}^2 = \|\widetilde{v}_0\|_{L_2(K)}^2 + |\widetilde{v}_0|_{H_1(K)}^2 \leq \left(1 + \pi^{-1}\right) |\widetilde{v}_0|_{H_1(K)}^2.$$

Due to the variational formulation for $\widetilde{v}_0$, we find with the help of the Cauchy-Schwarz inequality as well as the Poincaré inequality that

$$\begin{aligned} |\widetilde{v}_0|_{H^1(K)}^2 &= \left| (\alpha_K, \widetilde{v}_0)_{L_2(K)} - \int_K \nabla \widetilde{v}_g \cdot \nabla \widetilde{v}_0 \right| \\ &\leq |\alpha_K| |K|^{1/2} \|\widetilde{v}_0\|_{L_2(K)} + |\widetilde{v}_g|_{H^1(K)} |\widetilde{v}_0|_{H^1(K)} \\ &\leq \pi^{-1/2} |\alpha_K| |K| |\widetilde{v}_0|_{H^1(K)} + |\widetilde{v}_g|_{H^1(K)} |\widetilde{v}_0|_{H^1(K)} \end{aligned}$$

which yields

$$|\widetilde{v}_0|_{H^1(K)} \leq \pi^{-1/2} |\alpha_K| |K| + |\widetilde{v}_g|_{H^1(K)}. \tag{2.7}$$

In the next step, the term $|\alpha_K|$ is estimated. We make use of Theorem 1 which states $H^2(K) \subset C^0(\overline{K})$ and

$$\|w\|_{C^0(\overline{K})} \leq C_S \|w\|_{H^2(K)} \quad \text{for } w \in H^2(K).$$

Therefore, we have

$$\begin{aligned} |\alpha_K| &\leq \frac{1}{|\psi_K(z_K)|} \left(|v(z_K)| + \sum_{z \in \mathcal{N}(K)} |\alpha_{\psi_z}| \psi_z(z_K) + \sum_{E \in \mathcal{E}(K)} |\alpha_{\psi_E}| \psi_E(z_K) \right) \\ &\leq \frac{1}{|\psi_K(z_K)|} \left(1 + \sum_{z \in \mathcal{N}(K)} \psi_z(z_K) + \sum_{E \in \mathcal{E}(K)} 2\psi_E(z_K) \right) \|v\|_{C^0(\overline{K})}. \end{aligned}$$

The whole term in big brackets is harmonic as a function of z_K in K. It reaches its maximum on the boundary ∂K because of the maximum principle and is therefore smaller or equal four. We get

$$|\alpha_K| \leq \frac{4C_S}{|\psi_K(z_K)|} \|v\|_{H^2(K)}$$

and have to estimate $\psi_K(z_K)$. Let

$$p(x) = \frac{1}{4} \left(\rho_K^2 - |x - z_K|^2 \right) \quad \text{for } x \in K,$$

and let $B_{\rho_K}(z_K) \subset K$ be the circle with radius ρ_K and center z_K. Because of the weak maximum principle, we know that $\psi_K \geq 0$ in K. It is

$$\begin{aligned} \Delta (\psi_K - p) = 0 \quad &\text{in } B_{\rho_K}(z_K) \text{ and} \\ \psi_K - p \geq 0 \quad &\text{on } \partial B_{\rho_K}(z_K). \end{aligned}$$

The strong maximum principle yields $\psi_K(x) \geq p(x)$ for $x \in B_{\rho_K}(z_K)$ and especially $\psi_K(z_K) \geq \rho_K^2/4$. Finally, we obtain

$$|\alpha_K| \leq \frac{8C_S}{\rho_K^2} \|v\|_{H^2(K)}$$

which gives together with (2.7)

$$\begin{aligned} |\widetilde{v}_0|_{H^1(K)} &\leq 8\pi^{-1/2} C_S \frac{|K|}{\rho_K^2} \|v\|_{H^2(K)} + |\widetilde{v}_g|_{H^1(K)} \\ &\leq C_2 \|v\|_{H^2(K)} + \|\widetilde{v}_g\|_{H^1(K)}. \end{aligned}$$

The constant C_2 only depends on σ. This is seen by the following considerations. We have the bound $|K| \leq h_K^2$ as well as $h_K^2/\rho_K^2 \leq \sigma^2$, and we can estimate C_S uniformly according to Remark 1 since

$$|K| \geq \pi \rho_K^2 \geq \pi \sigma^{-2} h_K^2 = \pi \sigma^{-2}$$

is uniformly bounded for all $K \in \mathcal{K}_h$ with $h_K = 1$ due to Definition 2.

The final step in the proof is to combine all estimates.

$$\begin{aligned}
\|\mathfrak{I}^{(3)} v\|_{H^1(K)} &\leq \|\widetilde{v}_0\|_{H^1(K)} + \|\widetilde{v}_g\|_{H^1(K)} \\
&\leq \sqrt{1+\pi^{-1/2}}\, |\widetilde{v}_0|_{H^1(K)} + \|\widetilde{v}_g\|_{H^1(K)} \\
&\leq \sqrt{1+\pi^{-1/2}}\, \left(C_2 \|v\|_{H^2(K)} + \|\widetilde{v}_g\|_{H^1(K)}\right) + \|\widetilde{v}_g\|_{H^1(K)} \\
&\leq C_2 \sqrt{1+\pi^{-1/2}}\, \|v\|_{H^2(K)} + \max\{1, C_1\} \left(1 + \sqrt{1+\pi^{-1/2}}\right) \|v\|_{H^2(K)} \\
&= c\, \|v\|_{H^2(K)}.
\end{aligned}$$

The cases $i = 1, 2$ are proven in the same way. Here, the proof is even shorter since α_K vanishes in the auxiliary problem (2.6). □

The polynomial approximations of functions in Sobolev spaces and their properties are important. Especially, the following lemma is of interest.

Lemma 7. *Let $\Omega \subset \mathbb{R}^d$, $d = 2, 3$ be a bounded convex domain with diameter h_Ω and let $v \in H^{k+1}(\Omega)$ for $k \in \mathbb{N}$. Then, there exists a polynomial $p \in \mathcal{P}^k(\Omega)$ and a constant $C = C(j, k, d)$ with*

$$|v - p|_{H^j(\Omega)} \leq C\, h_\Omega^{k+1-j}\, |v|_{H^{k+1}(\Omega)} \quad \text{for } j = 0, 1, \ldots, k+1.$$

For a proof see [22, 75]. A simple consequence of this lemma is the estimate

$$\|v - p\|_{H^2(K)} \leq C\, |v|_{H^2(K)}$$

for a function $v \in H^2(K)$ with corresponding $p \in \mathcal{P}^1(K)$ and the estimate

$$\|v - p\|_{H^2(K)} \leq C h_K |v|_{H^3(K)} \tag{2.8}$$

for a function $v \in H^3(K)$ with corresponding $p \in \mathcal{P}^2(K)$. The constant C is independent of the element K.

With the help of the previous considerations, we can state the main results for the interpolation error.

Theorem 12. *For a regular mesh $\mathcal{K}_h$ of a bounded polygonal domain $\Omega \subset \mathbb{R}^2$, the interpolation operators $\mathfrak{I}^{(i)} : H^2(\Omega) \to \operatorname{span} \Psi^{(i)}$, $i = 1, 3$ fulfil*

$$\|v - \mathfrak{I}^{(1)} v\|_{H^1(\Omega)} \leq c\, h\, |v|_{H^2(\Omega)} \quad \text{for } v \in H^2(\Omega)$$

and

$$\|v - \mathfrak{I}^{(3)} v\|_{H^1(\Omega)} \leq c\, h^2\, |v|_{H^3(\Omega)} \quad \text{for } v \in H^3(\Omega),$$

where $h = \max\{h_K : K \in \mathcal{K}_h\}$ and the constant c only depends on the maximal aspect ratio σ of the mesh.

Proof. The first inequality has already been proven in [35] and thus we restrict ourselves to the second estimate. Let us start to examine the error over one element $K \in \mathcal{K}_h$. We have to scale this element in such a way that its diameter becomes one. The scaled element is denoted by $\widehat{K}$ and we define the affine map

$$\widehat{x} \in \widehat{K} \mapsto x = F(\widehat{x}) = B\widehat{x}$$

with the matrix $B = h_K I$. We have $F : \widehat{K} \to K$ and $\det B = h_K^2$, $\|B\|_2 = h_K$ as well as $\|B^{-1}\|_2 = h_K^{-1}$. Let $v \in H^k(K)$, then it is $\widehat{v} = v \circ F \in H^k(\widehat{K})$ with

$$|\widehat{v}|_{H^k(\widehat{K})} \leq c\|B\|_2^k |\det B|^{-1/2} |v|_{H^k(K)}$$

and

$$|v|_{H^k(K)} \leq c\|B^{-1}\|_2^k |\det B|^{1/2} |\widehat{v}|_{H^k(\widehat{K})},$$

where the constant c only depends on $k \in \mathbb{N}_0$, see [18].

Let $\widehat{\mathfrak{I}}^{(3)}$ be the interpolation operator with respect to $\widehat{K}$. Due to the pointwise interpolation, it does not matter if v is first transformed into $\widehat{v}$ and then interpolated or if v is first interpolated $\mathfrak{I}^{(3)}v$ and then transformed. This means

$$\widehat{\mathfrak{I}}^{(3)}\widehat{v} = \widehat{\mathfrak{I}^{(3)}v}.$$

Consequently, we obtain

$$\begin{aligned} \|v - \mathfrak{I}^{(3)}v\|_{H^1(K)}^2 &= \|v - \mathfrak{I}^{(3)}v\|_{L_2(K)}^2 + |v - \mathfrak{I}^{(3)}v|_{H^1(K)}^2 \\ &\leq ch_K^2 \|\widehat{v} - \widehat{\mathfrak{I}}^{(3)}\widehat{v}\|_{L_2(\widehat{K})}^2 + c\,|\widehat{v} - \widehat{\mathfrak{I}}^{(3)}\widehat{v}|_{H^1(\widehat{K})}^2 \\ &\leq c\,\|\widehat{v} - \widehat{\mathfrak{I}}^{(3)}\widehat{v}\|_{H^1(\widehat{K})}^2 \end{aligned}$$

since $h_K \leq 1$. Let $\widehat{p} \in \mathcal{P}^2(\widehat{K})$ be the polynomial of Lemma 7 which closely approximates $\widehat{v}$. Applying Lemma 5 and Lemma 6, we obtain

$$\begin{aligned} \|\widehat{v} - \widehat{\mathfrak{I}}^{(3)}\widehat{v}\|_{H^1(\widehat{K})} &\leq \|\widehat{v} - \widehat{p}\|_{H^1(\widehat{K})} + \|\widehat{\mathfrak{I}}^{(3)}(\widehat{v} - \widehat{p})\|_{H^1(\widehat{K})} \\ &\leq (1+c)\,\|\widehat{v} - \widehat{p}\|_{H^2(\widehat{K})} \\ &\leq (1+c)C\,|\widehat{v}|_{H^3(\widehat{K})}, \end{aligned} \tag{2.9}$$

where we also have used (2.8). Comparing the last two estimates and transforming back to the element K yields

$$\|v - \mathfrak{I}^{(3)}v\|_{H^1(K)}^2 \leq ch_K^4\,|v|_{H^3(K)}^2.$$

In the last step of the proof, we have to sum up this inequality over all elements of the mesh and apply the square root to it. This gives

$$\|v - \mathfrak{I}^{(3)}v\|_{H^1(\Omega)} \leq c\left(\sum_{K\in\mathcal{K}_h} h_K^4\,|v|_{H^3(K)}^2\right)^{1/2} \leq c\,h^2\,|v|_{H^3(K)}$$

and finishes the proof. □

Instead of measuring the interpolation error in the H^1-norm, we can use the L_2-norm. As we see in the next lemma, one power of h is gained by this change of norms.

Lemma 8. *For a regular mesh $\mathcal{K}_h$ of a bounded polygonal domain $\Omega \subset \mathbb{R}^2$, the interpolation operators $\mathfrak{I}^{(i)} : H^2(\Omega) \to \operatorname{span} \Psi^{(i)}$, $i = 1, 3$ fulfil*

$$\|v - \mathfrak{I}^{(1)} v\|_{L_2(\Omega)} \leq c\, h^2\, |v|_{H^2(\Omega)} \quad \text{for } v \in H^2(\Omega),$$

and

$$\|v - \mathfrak{I}^{(3)} v\|_{L_2(\Omega)} \leq c\, h^3\, |v|_{H^3(\Omega)} \quad \text{for } v \in H^3(\Omega),$$

where $h = \max\{h_K : K \in \mathcal{K}_h\}$ and the constant c only depends on the maximal aspect ratio σ of the mesh.

Proof. Using the same ideas as in the proof of Theorem 12 yields for $i = 1, 3$

$$\|v - \mathfrak{I}^{(i)} v\|_{L_2(K)} \leq c h_K \|\widehat{v} - \widehat{\mathfrak{I}}^{(i)} \widehat{v}\|_{L_2(\widehat{K})} \leq c h_K \|\widehat{v} - \widehat{\mathfrak{I}}^{(i)} \widehat{v}\|_{H^1(\widehat{K})}.$$

According to (2.9), we obtain for $v \in H^2(\Omega)$

$$\|v - \mathfrak{I}^{(1)} v\|_{L_2(K)} \leq c h_K |\widehat{v}|_{H^2(\widehat{K})} \leq c h_K^2 |v|_{H^2(K)},$$

and for $v \in H^3(\Omega)$

$$\|v - \mathfrak{I}^{(3)} v\|_{L_2(K)} \leq c h_K |\widehat{v}|_{H^3(\widehat{K})} \leq c h_K^3 |v|_{H^3(K)}.$$

Summing up the square of these terms finishes the proof. □

As mentioned in the beginning of this section, error estimates for interpolation operators carry over to approximation errors of the finite element method. Let u be the solution of the model problem obtained by the variational formulation (1.4) and u_h its Galerkin approximation gained by (1.5). Céa's lemma together with the last theorem yield

Theorem 13. *Let $\mathcal{K}_h$ be a regular mesh of a bounded polygonal domain $\Omega \subset \mathbb{R}^2$. Then, it is*

$$\|u - u_h\|_{H^1(\Omega)} \leq c\, h\, |u|_{H^2(\Omega)} \quad \text{for } u \in H^2(\Omega)$$

in case of the lower order method, i.e. $V_h = \operatorname{span}\{\Psi^{(1)} \setminus \Psi_D\}$, and

$$\|u - u_h\|_{H^1(\Omega)} \leq c\, h^2\, |u|_{H^3(\Omega)} \quad \text{for } u \in H^3(\Omega)$$

in case of higher order trial functions, i.e. $V_h = \operatorname{span}\{\Psi^{(3)} \setminus \Psi_D\}$. Here, we have $h = \max\{h_K : K \in \mathcal{K}_h\}$, and the constant c only depends on the maximal aspect ratio σ of the mesh.

Remark 4. For the estimates in the theorem, we have implicitly assumed that there are no errors in the evaluation of the bilinear form and the right hand side of the Galerkin formulation. Additionally, this means that we use $u_D = u_{Dh}$ for the extension of the Dirichlet datum of the boundary value problem. Therefore, it is $u - u_h = u_0 - u_{0h}$ and $u - \mathfrak{I}^{(i)}u = u_0 - \mathfrak{I}^{(i)}u_0$, $i = 1, 3$. The case of approximate data f, g_D, g_N in the discrete problem can be treated in the usual way, where the Strang lemma is used instead of Céa's lemma, see [18, 69].

The change of the norm in which the interpolation error is measured gives an additional power of h. This behaviour is not natural for the finite element convergence. To prove a corresponding result, the class of problems has to be restricted such that the adjoint variational formulation admits a sufficiently regular solution. The technique goes back to Aubin and Nitsche, see [3, 55].

Theorem 14. *Let $\mathcal{K}_h$ be a regular mesh of a bounded polygonal domain $\Omega \subset \mathbb{R}^2$. Under the condition that for any $g \in L_2(\Omega)$ there is a unique solution of*

$$\text{Find } w \in V: \quad a_\Omega(v, w) = (g, v), \quad \forall v \in V,$$

with $w \in H^2(\Omega)$ such that

$$|w|_{H^2(\Omega)} \le C \, \|g\|_{L_2(\Omega)},$$

it is

$$\|u - u_h\|_{L_2(\Omega)} \le c\, h^2 \, |u|_{H^2(\Omega)} \quad \text{for } u \in H^2(\Omega)$$

in case of the lower order method, i.e. $V_h = \operatorname{span}\{\Psi^{(1)} \setminus \Psi_D\}$, and

$$\|u - u_h\|_{L_2(\Omega)} \le c\, h^3 \, |u|_{H^3(\Omega)} \quad \text{for } u \in H^3(\Omega)$$

in case of higher order trial functions, i.e. $V_h = \operatorname{span}\{\Psi^{(3)} \setminus \Psi_D\}$. Here, we have $h = \max\{h_K : K \in \mathcal{K}_h\}$, and the constant c only depends on the maximal aspect ratio σ of the mesh.

Proof. Since $u - u_h \in V \subset L_2(\Omega)$ and due to the preliminaries of the theorem, there is a unique function $w \in H^2(\Omega)$ such that

$$a_\Omega(v, w) = (u - u_h, v) \quad \text{for } v \in V$$

and

$$|w|_{H^2(\Omega)} \le C \, \|u - u_h\|_{L_2(\Omega)}.$$

The Galerkin orthogonality (1.6) and the continuity of the bilinear form yield for arbitrary $v_h \in V_h$

$$\begin{aligned} \|u - u_h\|^2_{L_2(\Omega)} &= (u - u_h, u - u_h) = a_\Omega(u - u_h, w) \\ &= a_\Omega(u - u_h, w - v_h) \le M \, \|u - u_h\|_{H^1(\Omega)} \|w - v_h\|_{H^1(\Omega)}. \end{aligned}$$

The two terms on the right hand side are estimated separately. For the second one, we choose $v_h = \mathfrak{I}^{(1)} w \in V_h$ and obtain with Theorem 12

$$\|w - \mathfrak{I}^{(1)} w\|_{H^1(\Omega)} \leq ch|w|_{H^2(\Omega)} \leq ch\|u - u_h\|_{L_2(\Omega)}.$$

The first term $\|u-u_h\|_{H^1(\Omega)}$, which is the approximation error of the finite element method in the H^1-norm, is treated by Theorem 13. Finally, we obtain

$$\|u - u_h\|^2_{L_2(\Omega)} \leq cMh^k \, |u|_{H^k(\Omega)} \|u - u_h\|_{L_2(\Omega)}$$

for $k = 2, 3$. Dividing by $\|u - u_h\|_{L_2(\Omega)}$ yields the desired estimates. □

Remark 5. At this point, it is clear how to generalize the definition of trial functions to arbitrary order $n \in \mathbb{N}$ with $n > 2$. The key idea is found in the proof of Lemma 5. The trial space V_h has to contain the polynomial spaces $\mathcal{P}^n(K)$ for $K \in \mathcal{K}_h$. Therefore, we have to enrich V_h with additional edge bubble functions which are harmonic inside of each $K \in \mathcal{K}_h$ and interpolate polynomials of order up to n exactly on the boundaries of the elements. Furthermore, we have to introduce element bubble functions which vanish on ∂K and fulfil Poisson problems inside of K. For the Poisson problems the right hand sides are chosen such that they form a basis of the space $\mathcal{P}^{n-2}(K)$ for each element $K \in \mathcal{K}_h$.

2.4 Diffusion coefficient

All examples in Section 2.1 and 2.2 have been Poisson problems with material coefficient $a(\cdot) \equiv 1$. Since the numerical scheme presented in [20] can handle piecewise constant coefficients, there is no error with respect to the coefficient. In the general case, a piecewise constant approximation $a^h(\cdot)$ of $a(\cdot)$ is needed.

In Example 5, we recognize that this coarse approximation of the material coefficient seems to be enough in case of the lower order method, whereas the convergence of the higher order method slows down due to this approximation error.

Example 5. The function $u(x) = |x - x^*|$, $x \in \mathbb{R}^2$ with $x^* = (-0.1, 0.2)^\top$ fulfils

$$\begin{aligned} -\operatorname{div}\left(\frac{1}{|x - x^*|}\nabla u\right) &= 0 \quad \text{in } \Omega = (0,1)^2, \\ u &= g_D \quad \text{on } \Gamma \end{aligned} \tag{2.10}$$

as well as

$$\begin{aligned} -\Delta u &= f \quad \text{in } \Omega = (0,1)^2, \\ u &= g_D \quad \text{on } \Gamma \end{aligned} \tag{2.11}$$

with $g_D = \gamma_0 u$ and $f(x) = -|x - x^*|^{-1}$. The convergence is shown in Figure 2.8 for the finite element method on a sequence of uniform refined meshes.

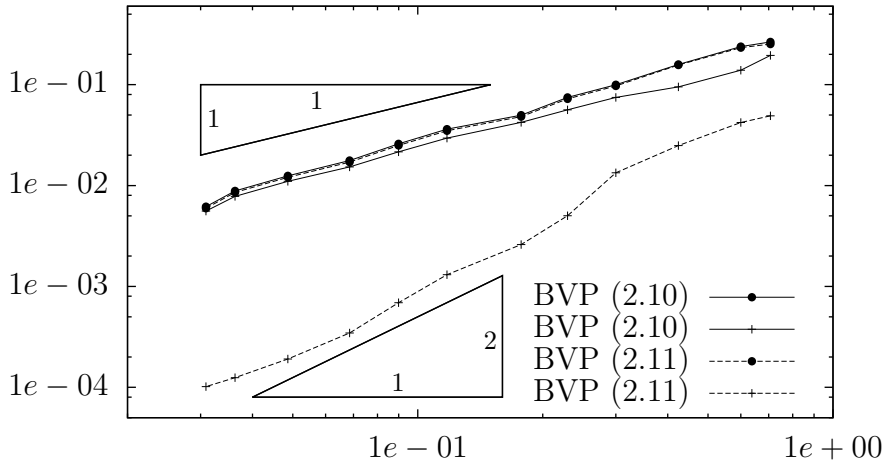

Figure 2.8: Absolute error with respect to h in the H^1-norm for problem (2.10) and (2.11) in Example 5 with $\Psi = \Psi^{(1)} \setminus \Psi_D$ ($\bullet$) and $\Psi = \Psi^{(3)} \setminus \Psi_D$ ($+$), respectively, and triangles with slope one and two

To analyse the impact of the approximation error of the material coefficient, the first Strang lemma [69] is used. Replacing the exact material coefficient in the bilinear form $a_\Omega(\cdot,\cdot)$ by an approximated one can be seen as an approximation $a^h_\Omega(\cdot,\cdot)$ of the bilinear form. We restrict ourselves to approximations $a^h(\cdot)$ of the material coefficient which fulfil

$$0 < a_{\min} \leq a^h(x) \leq a_{\max} \quad \text{for } x \in \Omega \text{ and } h > 0. \tag{2.12}$$

Therefore, the bilinear form $a^h_\Omega(\cdot,\cdot)$ is uniformly coercive as well as bounded on V_h for $h > 0$, and the variational formulation has a unique solution. The following formulation of the Strang lemma is taken from [18].

Lemma 9. *Consider a family of discrete problems whose associated approximate bilinear forms $a^h_\Omega : V_h \times V_h \to \mathbb{R}$ are uniformly V_h-elliptic. Then there exists a constant C independent of the space V_h such that*

$$\|u - u_h\|_{H^1(\Omega)} \leq C \inf_{v_h \in V_h} \left\{ \|u - v_h\|_{H^1(\Omega)} + \sup_{w_h \in V_h} \frac{|a_\Omega(v_h, w_h) - a^h_\Omega(v_h, w_h)|}{\|w_h\|_{H^1(\Omega)}} \right\}.$$

Obviously, the approximation error in the finite element method is estimated by a constant times the sum of two terms. One which gives the best approximation error and one which measures the error coming from the inexact bilinear form. Choosing $v_h = \mathfrak{I}^{(3)} u$ in the lemma yields

$$\|u - u_h\|_{H^1(\Omega)} \leq C \|u - \mathfrak{I}^{(3)} u\|_{H^1(\Omega)} + \sup_{w_h \in V_h} \frac{|a_\Omega(\mathfrak{I}^{(3)} u, w_h) - a^h_\Omega(\mathfrak{I}^{(3)} u, w_h)|}{\|w_h\|_{H^1(\Omega)}}.$$

In Figure 2.9, we see that for Example 5 the interpolation error converges with second order. This coincides with the theory of Section 2.3 which gives us quadratic

convergence for the interpolation of a function $u \in H^3(\Omega)$ in the Sobolev norm. Hence, the approximation quality of the bilinear form is responsible for the reduced rate of convergence for the finite element method. To improve the approximation of the bilinear form, we propose to use a globally continuous approximation $a^h = \mathfrak{I}^{(1)}a$ of the coefficient function. As already discussed, the trial functions $\psi_z \in \Psi^{(1)}$ and thus the interpolation $\mathfrak{I}^{(1)}a$ reach their minimal and maximal values on the boundary of the elements $K \in \mathcal{K}_h$. Since these functions are piecewise linear on the boundaries ∂K, the extremal values are even obtained in the nodes of the mesh. Consequently, condition (2.12) holds because of

$$a_{\min} \leq \min_{z\in\mathcal{N}_h} a(z) = \min_{z\in\mathcal{N}_h} a^h(z) \leq a^h(x) \leq \max_{z\in\mathcal{N}_h} a^h(z) = \max_{z\in\mathcal{N}_h} a(z) \leq a_{\max}$$

for $x \in \Omega$. Due to this choice of a^h, the numerical realization described in Section 2.1 does not work any more. This problem is discussed in the next section.

The following example shows the optimal convergence for a problem with varying material properties.

Example 6. We solve again the first problem mentioned in Example 5 and use the approximation $a^h = \mathfrak{I}^{(1)}a$ for the material coefficient instead of a piecewise constant one. In Figure 2.9, we recognize the improved rate of convergence due to the better approximation of the material coefficient, and we see the convergence of the interpolation error $\|u - \mathfrak{I}^{(3)}u\|_{H^1(\Omega)}$.

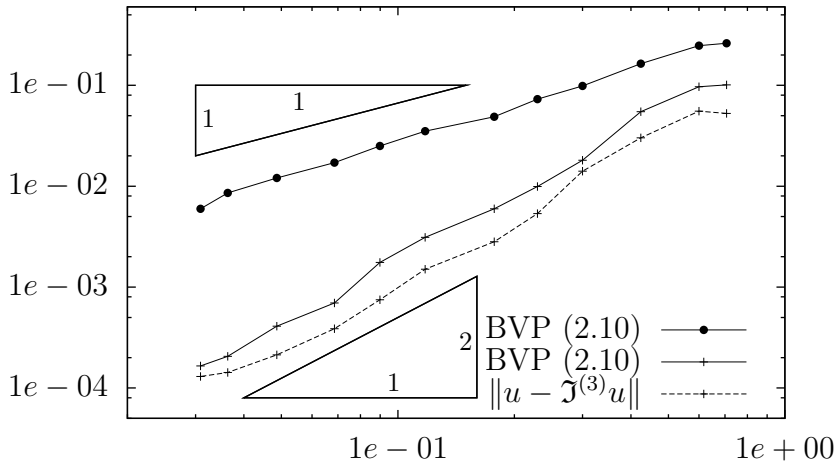

Figure 2.9: Absolute error with respect to h in the H^1-norm for improved approximation of $a_\Omega(\cdot,\cdot)$ in Example 6 with $\Psi = \Psi^{(1)} \setminus \Psi_D$ ($\bullet$) and $\Psi = \Psi^{(3)} \setminus \Psi_D$ ($+$), respectively, and interpolation error $\|u - \mathfrak{I}^{(3)}u\|_{H^1(\Omega)}$ as well as triangles with slope one and two

2.5 Numerical realization

In the previous sections, we have seen the discrete Galerkin formulation and the corresponding approximations of solutions of different boundary value problems. In the case of piecewise constant material coefficients, the set up of the finite element matrix has been address at the end of Section 2.1. Nevertheless, the globally continuous approximation of the material coefficient, which is essential for the higher order method, introduces new difficulties while compiling the stiffness matrix.

For the sake of completeness, the discrete formulation is reviewed. We seek the approximate solution of the mixed boundary value problem (1.1) in the form $u_h = u_{0h} + u_{Dh}$, where u_{Dh} is an extension of the discretized Dirichlet datum. This extension is chosen to be

$$u_{Dh} = \sum_{\psi \in \Psi_D} \beta_\psi \psi \quad \text{with} \quad \Psi_D = \{\psi_z, \psi_E : z \in \mathcal{N}_{h,D}, E \in \mathcal{E}_{h,D}\},$$

where the coefficients β_ψ are obtained by interpolation of g_D. For the unknown part u_{0h} of the approximation, we take the ansatz

$$u_{0h} = \sum_{\psi \in \Psi} \beta_\psi \psi \quad \text{with} \quad \Psi = \Psi^{(3)} \setminus \Psi_D.$$

Here, the same symbol β_ψ is used for the coefficients of u_{0h} and u_{Dh}, but there should be no confusion since $\Psi \cap \Psi_D = \varnothing$. The Galerkin formulation yields the system of liner equations

$$\sum_{\psi \in \Psi} \beta_\psi \, a_\Omega(\psi, \phi) = (f, \phi) + (g_N, \phi)_{\Gamma_N} - \sum_{\psi \in \Psi_D} \beta_\psi \, a_\Omega(\psi, \phi) \quad \text{for } \phi \in \Psi.$$

The system matrix is symmetric and positive definite due to the ellipticity of the bilinear form. Additionally, we obtain a sparse matrix since the involved trial functions have only local support. Therefore, an appropriate iterative solver, like a cg-method, can be used to approximate the solution of the system of linear equations.

As we have recognized earlier, the main topic is to evaluate the bilinear form $a_\Omega(\cdot, \cdot)$ applied to trial functions in the set up of the system. The boundary integral $(g_N, \phi)_{\Gamma_N}$ and the volume integral (f, ϕ) are handled with numerical quadrature. Here, we can split the Neumann boundary into edges where the trial functions are quadratic polynomials. The volume integral over Ω can be decomposed into integrals over elements and we use numerical integration over each polygonal region. For this purpose, there are different integration schemes available like [54] or a simple summation over quadratures on triangles. The evaluation of trial functions in quadrature nodes within an element is done using the representation formula (1.16).

In the following, we make use of Green's formulae which involve the linear trace operators γ_0^K and γ_1^K as we have seen in Section 1.6. In the case of trial

functions $\psi \in \Psi^{(3)}$, we have $\gamma_0^K \psi = \psi$ on ∂K since $\psi \in C^2(K) \cap C^0(\overline{K})$. Therefore, we omit the trace operator γ_0^K in boundary integrals if no confusion occurs. Due to the regularity of the trial functions, namely $\psi \in H^2(K)$, we have additionally

$$(\gamma_1^K \psi)(x) = n_K(x) \cdot (\gamma_0^K \nabla \psi)(x) \quad \text{for } x \in \partial K,$$

where $n_K(x)$ denotes the outer normal vector of the domain K at x.

As proposed in Section 2.4, the material coefficient is approximated by the interpolant $\mathfrak{I}^{(1)} a$, that means

$$a^h(x) = \sum_{\lambda \in \Psi^{(1)}} \alpha_\lambda \lambda(x) \quad \text{with} \quad \alpha_{\lambda_z} = a(z),\ z \in \mathcal{N}_h.$$

Remember $\Delta \lambda = 0$ in all $K \in \mathcal{K}_h$ and let $\psi, \phi \in \Psi$, then

$$\nabla \psi \cdot \nabla \phi = \frac{1}{2}\big(\Delta(\psi\phi) - \psi \Delta \phi - \phi \Delta \psi\big)$$

together with Green's second identity yield

$$\begin{aligned} a_\Omega(\psi,\phi) \approx a_\Omega^h(\psi,\phi) &= \int_\Omega a^h \nabla\psi \cdot \nabla\phi = \sum_{K \in \mathcal{K}_h, \lambda \in \Psi^{(1)}} \alpha_\lambda \int_K \lambda \nabla\psi \cdot \nabla\phi \\ &= \sum_{K \in \mathcal{K}_h, \lambda \in \Psi^{(1)}} \frac{\alpha_\lambda}{2} \Big\{ \int_K (\lambda \Delta(\psi\phi) - \psi\phi\Delta\lambda) - \int_K \lambda\psi\Delta\phi - \int_K \lambda\phi\Delta\psi \Big\} \\ &= \sum_{K \in \mathcal{K}_h, \lambda \in \Psi^{(1)}} \frac{\alpha_\lambda}{2} \Big\{ \int_{\partial K} \big(\lambda\phi\,\gamma_1^K\psi + \lambda\psi\,\gamma_1^K\phi - \psi\phi\,\gamma_1^K\lambda\big) - \int_K (\lambda\psi\Delta\phi + \lambda\phi\Delta\psi) \Big\}. \end{aligned}$$

At first glance, this representation for the bilinear form looks more complicated than the standard one. But it turns out that it has some advantages. Depending on the sort of trial and test functions many terms vanish. For example, let $\psi, \phi \in \Psi^{(2)}$ then the volume integral is zero since ψ and ϕ are harmonic. In particular, the only case when the volume integral does not vanish is that ψ or ϕ is an element bubble function and the Laplacian of this function is minus one. Hence, we have to evaluate integrals like

$$\int_K \lambda\psi \quad \text{with } \lambda \in \Psi^{(1)} \text{ and } \psi \in \Psi^{(3)} \text{ for } K \in \mathcal{K}_h.$$

In the implementation, this integration is done with the help of numerical quadrature using the representation formula for λ and ψ, see below.

The boundary integral contains three terms which are similar to each other. Obviously, it is sufficient to study

$$\int_{\partial K} \lambda\phi\,\gamma_1^K\psi \quad \text{for } \lambda, \phi, \psi \in \Psi^{(3)}. \tag{2.13}$$

Here, the conormal derivative as well as the traces of the trial and test functions are involved. In the following, the boundary integral formulation is used to handle this kind of integrals.

Let $K \in \mathcal{K}_h$. First, we consider $\psi \in \Psi^{(2)}$ that means ψ fulfils the boundary value problem

$$\begin{aligned} -\Delta\psi &= 0 \quad \text{in } K, \\ \psi &= g \quad \text{on } \partial K \end{aligned} \tag{2.14}$$

with some piecewise quadratic function g on ∂K. In Section 1.6, we have seen how to approximate the Neumann datum from given Dirichlet datum. This has been done by the use of a variational formulation. In the current notation, we have

$$\Phi_N = \{\tau_E^0, \tau_E^1 : E \in \mathcal{E}(K)\},$$

where $\tau_E^0, \tau_E^1 : \partial K \to \mathbb{R}$ with

$$\tau_E^0 = \begin{cases} 1, & \text{on } E \\ 0, & \text{else} \end{cases} \qquad \text{and} \qquad \tau_E^1 = \begin{cases} 1, & \text{at } z_e \\ \text{linear}, & \text{on } E \\ 0, & \text{else} \end{cases}$$

for $E = \overline{z_b z_e}$. The set Φ_N forms a basis of the space of piecewise linear functions which is used to approximate $H^{-1/2}(\partial K)$ and thus the Neumann trace of ψ. We recognize that the space of piecewise quadratic and globally continuous functions on ∂K is spanned by

$$\Phi_D = \{\gamma_0^K \psi_z, \gamma_0^K \psi_E : z \in \mathcal{N}(K), E \in \mathcal{E}(K)\}.$$

Obviously, the bases Φ_D as well as Φ_N coincide with the one proposed in Section 1.6 for higher order boundary element methods in two dimensions. For the discretization of the boundary ∂K, we use the naturally given decomposition by the polygonal structure. So, the boundary element method is applied on a coarse mesh with only a few elements.

We come back to the boundary value problem (2.14) for ψ. The Dirichlet datum $\gamma_0^K \psi = g \in \operatorname{span} \Phi_D$ is given and the Neumann datum $\gamma_1^K \psi$ is approximated by $t_h \in \operatorname{span} \Phi_N$. With the representations

$$t_h = \sum_{\tau \in \Phi_N} t_\tau \tau \qquad \text{and} \qquad g = \sum_{\varphi \in \Phi_D} g_\varphi \varphi,$$

we obtain the relationship between the Dirichlet and Neumann datum as a system of linear equations

$$\mathbf{V}_{K,h} \underline{t}_h = \left(\tfrac{1}{2}\mathbf{M}_{K,h} + \mathbf{K}_{K,h}\right) \underline{g},$$

where the underline refers to the coefficient vector, e.g. $\underline{t}_h = (t_\tau)_{\tau \in \Phi_N}$. The matrices are defined as

$$\mathbf{V}_{K,h} = \Big((\mathbf{V}_K \tau, \vartheta)_{L_2(\partial K)} \Big)_{\vartheta \in \Phi_N, \tau \in \Phi_N}$$

and

$$\mathbf{M}_{K,h} = \Big((\varphi, \vartheta)_{L_2(\partial K)} \Big)_{\vartheta \in \Phi_N, \varphi \in \Phi_D}, \quad \mathbf{K}_{K,h} = \Big((\mathbf{K}_K \varphi, \vartheta)_{L_2(\partial K)} \Big)_{\vartheta \in \Phi_N, \varphi \in \Phi_D}.$$

When the boundary element matrices are computed, we can get the approximation of the Neumann trace of each harmonic trial function ψ with respect to the element $K \in \mathcal{K}_h$ by multiplying $\mathbf{V}_{K,h}^{-1} \left(\frac{1}{2} \mathbf{M}_{K,h} + \mathbf{K}_{K,h} \right)$ with the coefficients $\underline{g}$ of its Dirichlet trace, where $g = \gamma_0^K \psi \in \operatorname{span} \Phi_D$. Consequently, this matrix is computed once per element and stored. The evaluation of the trial function in the interior of an element is approximated by inserting the exact Dirichlet trace and the approximated Neumann trace into the representation formula (1.12). Afterwards, the integrals therein are computed analytically.

For the approximation of the integral (2.13), we use a similar trick as in the case of piecewise constant coefficients in Section 2.1. Let

$$\Phi_{Ex} = \{ \gamma_0^K(\psi_{z_b} \psi_{z_e}), \gamma_0^K(\psi_{z_b} \psi_{z_b}), \gamma_0^K(\psi_{z_b} \psi_E), \gamma_0^K(\psi_{z_e} \psi_E), \gamma_0^K(\psi_E \psi_E) : E \in \mathcal{E}(K) \}$$

and choose an arbitrary function $q_h \in \operatorname{span} \Phi_{Ex}$ with

$$q_h = \sum_{\chi \in \Phi_{Ex}} q_\chi \chi.$$

Taking advantage of the symmetric representation of the Steklov-Poincaré operator and its approximation

$$\widetilde{\mathbf{S}}_K g = \mathbf{D}_K g + \left(\tfrac{1}{2} \mathbf{I} + \mathbf{K}'_K \right) t_h,$$

it is

$$\begin{aligned}
\int_{\partial K} q_h \, \gamma_1^K \psi &\approx \int_{\partial K} q_h \, \widetilde{\mathbf{S}}_K g = \left(q_h, \mathbf{D}_K g + \left(\tfrac{1}{2} \mathbf{I} + \mathbf{K}'_K \right) t_h \right)_{L_2(\partial K)} \\
&= (\mathbf{D}_K g, q_h)_{L_2(\partial K)} + \tfrac{1}{2} (q_h, t_h)_{L_2(\partial K)} + (\mathbf{K}_K q_h, t_h)_{L_2(\partial K)} \\
&= \underline{q}_h^\top \mathbf{D}_{K,h}^{Ex} \underline{g} + \underline{q}_h^\top \left(\tfrac{1}{2} \left(\mathbf{M}_{K,h}^{Ex} \right)^\top + \left(\mathbf{K}_{K,h}^{Ex} \right)^\top \right) \underline{t}_h \\
&= \underline{q}_h^\top \mathbf{D}_{K,h}^{Ex} \underline{g} + \underline{q}_h^\top \left(\tfrac{1}{2} \left(\mathbf{M}_{K,h}^{Ex} \right)^\top + \left(\mathbf{K}_{K,h}^{Ex} \right)^\top \right) \mathbf{V}_{K,h}^{-1} \left(\tfrac{1}{2} \mathbf{M}_{K,h} + \mathbf{K}_{K,h} \right) \underline{g} \\
&= \underline{q}_h^\top \mathbf{S}_{K,h}^{Ex} \underline{g},
\end{aligned}$$

where

$$\mathbf{S}_{K,h}^{Ex} = \mathbf{D}_{K,h}^{Ex} + \left(\tfrac{1}{2} \left(\mathbf{M}_{K,h}^{Ex} \right)^\top + \left(\mathbf{K}_{K,h}^{Ex} \right)^\top \right) \mathbf{V}_{K,h}^{-1} \left(\tfrac{1}{2} \mathbf{M}_{K,h} + \mathbf{K}_{K,h} \right)$$

with

$$\mathbf{D}_{K,h}^{Ex} = \Big((\mathbf{D}_K \varphi, \chi)_{L_2(\partial K)} \Big)_{\chi \in \Phi_{Ex}, \varphi \in \Phi_D}$$

and

$$\mathbf{M}_{K,h}^{Ex} = \Big((\chi, \tau)_{L_2(\partial K)} \Big)_{\tau \in \Phi_N, \chi \in \Phi_{Ex}}, \quad \mathbf{K}_{K,h}^{Ex} = \Big((\mathbf{K}_K \chi, \tau)_{L_2(\partial K)} \Big)_{\tau \in \Phi_N, \chi \in \Phi_{Ex}}.$$

Since $q_h = \lambda\phi \in \Phi_{Ex}$ for the integral (2.13) and $g \in \Phi_D$ for $\psi \in \Psi^{(2)}$, the coefficient vectors $\underline{q}_h$ and $\underline{g}$ contain only zeros and a single one. Therefore, the approximation of integral (2.13) coincides with an entry of the matrix $\mathbf{S}^{Ex}_{K,h}$.

In the case of $\psi \in \Psi^{(3)} \setminus \Psi^{(2)}$, the trial function fulfils for one $K \in \mathcal{K}_h$ the boundary value problem

$$\begin{aligned} -\Delta\psi &= 1 \quad \text{in } K \\ \psi &= 0 \quad \text{on } \partial K \end{aligned} \tag{2.15}$$

which is reduced to the previous situation. For this reason, we write $\psi = \psi_h + \psi_p$ with $\psi_p(x) = -\frac{1}{4}|x - z_K|^2$. Then, (2.15) yields

$$\begin{aligned} -\Delta\psi_h &= 0 \quad \text{in } K \\ \psi_h &= g \quad \text{on } \partial K \end{aligned}$$

with $g = -\gamma_0^K\psi_p \in \operatorname{span}\Phi_D$. This problem can be treated as described earlier. The integral (2.13) splits into two parts

$$\int_{\partial K} q_h\,\gamma_1^K\psi = \int_{\partial K} q_h\,\gamma_1^K\psi_h + \int_{\partial K} q_h\,\gamma_1^K\psi_p \approx \underline{q}_h^\top \mathbf{S}^{Ex}_{K,h}\underline{g} + \int_{\partial K} q_h\,\gamma_1^K\psi_p.$$

In contrast to the previous case, $\underline{g}$ is now a full vector but $\underline{q}_h$ still contains a single one. The first term of the approximation turns into a scalar product of $\underline{g}$ and a row of $\mathbf{S}^{Ex}_{K,h}$. Due to the construction of ψ_p, the conormal derivative $\gamma_1^K\psi_p$ is constant on each edge $E \in \mathcal{E}(K)$. This fact can easily be seen using the parametrisation $x(s) = z_b + s(z_e - z_b) \in E = \overline{z_b z_e}$ for $0 \le s \le 1$ in

$$\gamma_1^K\psi_p(x) = -\tfrac{1}{2}(x - z_K)\cdot n_K = -\tfrac{1}{2}(z_b - z_K)\cdot n_K - \tfrac{1}{2}s\underbrace{(z_e - z_b)\cdot n_K}_{=0}.$$

On $E \in \mathcal{E}(K)$, the function q_h is a given polynomial of degree less or equal than four. Therefore, the boundary integral in the second term of the approximation can be computed analytically.

For the evaluation of an element bubble function ψ_K inside of $K \in \mathcal{K}_h$, we evaluate ψ_h according to above and ψ_p separately.

The final step in the set up of the finite element matrix is to compute all these boundary integral matrices to construct $\mathbf{S}^{Ex}_{K,h}$. The mass matrices $\mathbf{M}_{K,h}$ and $\mathbf{M}^{Ex}_{K,h}$ can be computed analytically, whereas numerical integration is used to compile the others. In the realisation, we utilise an advanced adaptive integration scheme, which is based on local subdivision of edges and shifting of Gaussian points [66] according to the singularities of the integral kernels. By the use of this quadrature, integrals of the form

$$(\mathbf{V}_K\nu, \mu)_{L_2(\partial K)} \quad \text{and} \quad (\mathbf{K}_K\nu, \mu)_{L_2(\partial K)} \tag{2.16}$$

for

$$\nu \in \left\{\tau_E^0, \left(\tau_E^1\right)^j : E \in \mathcal{E}(K), j = 1, \ldots, 4\right\} \quad \text{and} \quad \mu \in \left\{\tau_E^0, \tau_E^1 : E \in \mathcal{E}(K)\right\}$$

are computed. Due to the local support of ν and μ on the boundary ∂K, the quadrature of (2.16) has a computational complexity of $\mathcal{O}(1)$. Building linear combinations of these integrals, we can construct the matrices $\mathbf{K}_{K,h}^{Ex}$, $\mathbf{K}_{K,h}$ and $\mathbf{V}_{K,h}$. Even the entries of $\mathbf{D}_{K,h}^{Ex}$ can be written as linear combinations of (2.16), see [68]. Therefore, the local computations of the boundary element matrices have a complexity of $\mathcal{O}(|\mathcal{E}(K)|^2)$, where $|\mathcal{E}(K)|$ denotes the number of edges in $K \in \mathcal{K}_h$. So, the most costly part in the set up of the local stiffness matrices $\mathbf{S}_{K,h}^{Ex}$ is the inversion of $\mathbf{V}_{K,h}$ which has a complexity of $\mathcal{O}(|\mathcal{E}(K)|^3)$. For this task, we use an efficient LAPACK routine.

In total, the computations of the local boundary integral matrices and thus the local stiffness matrices can be done in a preprocessing step and they are highly parallelizable since matrices from different elements are independent. In the theoretical considerations of the previous sections, we have allowed $|\mathcal{E}(K)|$ to be unbounded. Nevertheless, for the numerical application it is suitable to asume a regular and stable mesh according to Definitions 2 and 3. For such meshes, the number of nodes and thus the number of edges per element is uniformly bounded according to Lemma 4. Therefore, the local complexity in the computations of the boundary element matrices is bounded. In practical applications, the elements usually have only a few edges and consequently all appearing matrices are small. In this scenario the local complexity is negligible compared to the overall complexity of the global finite element computations.

Chapter 3

Adaptive BEM-based FEM

In all considerations and experiments till now, we have worked with a sequence of uniform refined meshes. We always started with an initial mesh and refined all elements equally. For this reason, the mesh size $h = \max\{h_K : K \in \mathcal{K}_h\}$ decreased continuously and we have studied convergence with respect to h. In many practical applications, however, the problems do not meet the requirements of the convergence theorems proven in Chapter 2. The solution may contain singularities due to complicated geometries of the domains or jumping material coefficients as we have seen in Section 1.4. In such cases, it is advisable to adapt the meshes to the problem. This can be done in a preprocessing step while generating the initial mesh or fully automatic in an adaptive refinement strategy during the computations.

In this chapter, we focus on an adaptive finite element method which is based on a posteriori error estimates. The well known residual error estimate is introduced, and we prove its reliability on general polygonal meshes which are regular and stable. The techniques for the proofs are mainly based on [74]. However, the challenging part is to deal with the non-simplicial elements. Triangles and quadrangles in classical meshes can always be mapped onto a reference element and the estimates can be performed there. Since this is not possible for arbitrary polygonal elements, we have to take special care of the constants appearing in the estimates. Especially, the Poincaré constant has to be mentioned at this point. These constants have to be uniformly bounded over the whole mesh and even over the whole sequence of meshes in the limiting case. Additionally, we have to overcome some technical difficulties where the isosceles triangles from Lemma 3 come into play.

Finally, numerical examples show optimal rates of convergence in the energy norm with respect to the degrees of freedom for the adaptive finite element strategy which applies the residual error estimator on polygonal meshes. Additionally, we discuss the impact of the nodes inserted during the refinement strategy which would appear as conditional degrees of freedom, often called hanging nodes, in a classical finite element realization.

3.1 General ideas in the adaptive FEM

The error introduced by the BEM-based finite element method has been examined in Chapter 2. We have shown estimates of the type

$$\|u - u_h\|_{H^1(\Omega)} \leq c h^{k-1} |u|_{H^k(\Omega)} \quad \text{for } k = 2, 3 \tag{3.1}$$

with the exact solution $u \in H^k(\Omega)$ of the model problem and its approximation $u_h \in V_h$ on some mesh $\mathcal{K}_h$. Such estimates are called a priori error estimates since the right hand side is given in advance without the knowledge of the approximation u_h. They are suitable for convergence statements in the case of smooth solutions and if the element diameters decreases uniformly. But their use is limited in some situations. What to do if the solution does not meet the smoothness assumption and we have $u \notin H^k(\Omega)$. This may happen for non-convex domains or jumping coefficients, see Section 1.4. Additionally, the estimate says nothing about the approximation quality within some subset of the domain. It is even impossible to compute the upper bound of the error in (3.1) since the exact solution is unknown.

Due to these reasons, an estimate of the form

$$\|u - u_h\| \leq c\, \eta \quad \text{for} \quad \eta^2 = \sum_{K \in \mathcal{K}_h} \eta_K^2$$

with $\eta = \eta(u_h)$ is desirable for practical considerations. Here, $\|\cdot\|$ denotes some norm and η is a computable error estimator, which depends on the current approximation u_h. Therefore, the inequality is called a posteriori error estimate. The values η_K, which are assigned to the elements $K \in \mathcal{K}_h$, serve as error indicator over the corresponding elements. With the help of such an estimator, we can judge the actual accuracy of the approximation. Furthermore, we can rate the approximation quality over the elements with the indicators η_K and we may adapt the mesh according to this information.

The preceding considerations lead to an adaptive strategy, the adaptive finite element method which is abbreviated to AFEM. This scheme can be sketched as

$$\mathit{SOLVE} \rightarrow \mathit{ESIMATE} \rightarrow \mathit{MARK} \rightarrow \mathit{REFINE} \rightarrow \mathit{SOLVE} \rightarrow \cdots .$$

First, we solve the discrete boundary value problem on a given mesh and compute the error estimator η and the error indicators η_K for all elements. If the desired accuracy is reached according to η, we are done. If not, we mark some elements for refinement. These elements are chosen on the basis of the error indicators η_K. Next, the marked elements are refined, and thus we obtain a new mesh which is adapted to the problem. So, we can solve the boundary value problem on the refined mesh and continue this procedure until the desired accuracy is achieved.

Since we adapt the mesh successively to the exact solution of the boundary value problem, the hope is that we obtain optimal rates of convergence even in the case of $u \notin H^2(\Omega)$. Due to local refinements of the mesh, it makes no sense

to measure the convergence with respect to the mesh size h. Instead of h, we use the number of degrees of freedom (DoF) in the system of linear equations. In the following, we discuss the steps of the AFEM in more detail.

For triangular meshes and piecewise linear trial functions, the first convergence proof for the adaptive finite element method applied to the Poisson problem can be found in [26]. Here, the mesh has to fulfil some fineness assumption. In [52], this condition is removed and the notion of data oscillation is introduced. A general convergence result for conforming adaptive finite elements, which is valid for several error estimates and for a class of problems, has been published seven years later in [53]. The first convergence rates are proven in [12], where an additional coarsening step is introduced and the refinement is done in such a way that a new node lies inside each marked element of the previous mesh. In [17], the authors show a decay rate of the energy error plus data oscillation in terms of the number of degrees of freedom without the additional assumptions on coarsening and refining.

Whereas the cited theory is done for triangular meshes, we introduce an adaptive finite element method on regular and stable polygonal meshes. In the *SOLVE* step, we approximate the solution of the boundary value problem on the current mesh $\mathcal{K}_h$. This is done as described in Chapter 2. First, we restrict ourselves to the case of a piecewise constant material coefficient such that

$$a(x) = a_K \quad \text{for } x \in K \text{ and } K \in \mathcal{K}_h$$

for the initial mesh and consequently for all meshes in the refinement process. In the discrete Galerkin formulation, the lower order trial space is used, i.e.

$$V_h = \operatorname{span} \Psi \quad \text{with} \quad \Psi = \Psi^{(1)} \setminus \Psi_D.$$

Here, $\Psi^{(1)}$ is the set of lower order basis functions and Ψ_D contains all of them which belong to the Dirichlet boundary. Afterwards, we discuss how to incorporate approximation errors in the data and we allow the higher order trial space in the BEM-based FEM, i.e. $\Psi = \Psi^{(3)} \setminus \Psi_D$. Solving the discrete problem, we obtain an approximation $u_h \in V_h$ on the current mesh.

The *ESTIMATE* part is for the computation of the a posteriori error estimator η and local error indicators η_K. There is a great variety of estimators in the literature. The most classical one is the residual error estimate which goes back to [5]. This estimator measures the jumps of the conormal derivative of the approximation u_h over the element boundaries. Other estimators are obtained by solving local Dirichlet [6] or Neumann [8] problems on element patches. The engineering community came up with an error indicator that uses the difference between ∇u_h and its continuous approximation, see [78]. The equilibrated residual error estimator [13] is obtained by post processing of the approximation and belongs to the more general class of functional analytic error estimates [62]. Finally, we mention the hierarchical [24] and the goal oriented [7] error estimates. For a comparison of all these strategies see for example [16].

In the adaptive finite element method in this chapter, we use a residual error estimate and prove its reliability on regular and stable meshes. Since the exact solution of the boundary value problem may fulfil $u \notin H^2(\Omega)$, we cannot apply pointwise interpolation operators from Section 2.3. Therefore, we have to use a quasi-interpolation operator in forthcoming proofs.

After the computation of the estimator and the local error indicators, we have to *MARK* several elements for refinement. There are different strategies in the literature for this task. The most classical one is the maximum strategy which has been proposed already in [6]. Here, all elements $K \in \mathcal{K}_h$ are marked which fulfil

$$\eta_K \geq \theta \, \eta_{\max}$$

for a given parameter $0 \leq \theta \leq 1$ and $\eta_{\max} = \max\{\eta_K : K \in \mathcal{K}_h\}$. So, the elements with the largest error indicators are chosen for refinement. For large values of θ, the strategy becomes more selective, whereas for small θ, we obtain almost a uniform refinement. A similar idea is used by the modified equidistribution strategy. For a given parameter $0 \leq \theta \leq 1$ and the global error estimator η, all elements $K \in \mathcal{K}_h$ are marked which satisfy

$$\eta_K \geq \theta \, \frac{\eta}{\sqrt{|\mathcal{K}_h|}} \, .$$

In this strategy one tries to reach a state where the error is distributed equally over all elements. The parameter θ controls again the selectivity. Finally, we mention Dörfler's strategy, see [26]. Here, a set of elements $\mathcal{K}_M \subset \mathcal{K}_h$ is marked such that

$$\Big(\sum_{K \in \mathcal{K}_M} \eta_K^2 \Big)^{1/2} \geq (1-\theta) \, \eta,$$

where $0 \leq \theta < 1$ is again a given parameter and η the global estimator. It is advantageous to choose the set $\mathcal{K}_M$ as small as possible. This can be achieved by sorting the elements $K \in \mathcal{K}_h$ according to the value of their error indicators η_K. Since every sorting algorithm is computationally expensive, Dörfler proposed in [26] the following procedure with given parameter $0 < \nu < 1$, which is chosen to be small.

```
sum = 0.0
μ = 1.0
while (sum < (1-θ)² η²) do
   μ = μ - ν
   for all K ∈ 𝒦_h
      if (K is not marked)
         if (η_K > μ η_max)
            mark K
            sum = sum + η_K²
```

Dörfler's marking strategy was one of the key points in the proofs of convergence and convergence rates of AFEM in the literature mentioned above. Since this

strategy is so successful, we use it in the realization of the adaptive method in this chapter.

As the name of the last step *REFINE* already indicates, this is the time where the marked elements are refined. Usually, this step is more complicated for standard methods working on triangular or quadrangular meshes because of the strict admissibility conditions on the mesh. In such cases, it has to be guaranteed that no hanging nodes appear. Therefore, the mesh has to be completed in the sense that neighbouring elements are refined until all hanging nodes disappear. In the literature, one can find several strategies like red-green refinement or newest vertex bisection with completion algorithms, see [12, 74]. Another possibility to handle hanging nodes is to treat them as conditional degrees of freedom, i.e. to fix the value of the finite element functions in these points to be a suitable interpolation of their neighbouring regular nodes. Nevertheless, the first idea with completion spreads the local refinement into a neighbourhood and the second one produces artificial nodes. Both scenarios are somehow unpleasant for the numerical realization. Due to the use of the BEM-based finite element method, we are in the fortune situation to cope with arbitrary polygonal meshes. Therefore, we do not have to worry about hanging nodes because they are incorporated as ordinary nodes in the strategy and thus contribute to the approximation accuracy. This behaviour is discussed more precisely in Section 3.4. The refinement only affects the marked elements and is done as described in Section 1.5. During the refinement process, we just have to enforce the regularity and stability of the sequence of meshes.

The overall algorithm of the adaptive finite element method is finally realized according to the following concept, where $\varepsilon > 0$ is some given tolerance for the error estimate.

$\mathcal{K}_h \leftarrow$ `initial grid`
`solve for` u_h `on` $\mathcal{K}_h$
`compute` $\eta_K \ \forall K \in \mathcal{K}_h$ `and then` η
while `(`η `>` ε`)` **do**
    `mark a set of elements (Dörfler's strategy)`
    $\mathcal{K}_h \leftarrow$ `refine grid`
    `solve for` u_h `on` $\mathcal{K}_h$
    `compute` $\eta_K \ \forall K \in \mathcal{K}_h$ `and then` η

3.2 Quasi-interpolation operator

Before we present the quasi-interpolation operator, we review the neighbourhoods of nodes, edges and elements. These open sets are defined in Section 1.5 as element patches by

$$\overline{\omega}_z = \bigcup_{z \in \mathcal{N}(K')} \overline{K'}, \qquad \overline{\omega}_E = \bigcup_{E \in \mathcal{E}(K')} \overline{K'}, \qquad \overline{\omega}_K = \bigcup_{\overline{K} \cap \overline{K'} \neq \varnothing} \overline{K'}$$

for $z \in \mathcal{N}_h$, $E \in \mathcal{E}_h$ and $K \in \mathcal{K}_h$. Additionally, the L_2-projection $Q_z : L_2(\omega_z) \to \mathbb{R}$ into the space of constants is needed. For $v \in H^1_D(\Omega)$, we define the quasi-interpolation operator $\mathfrak{I}_h : H^1_D(\Omega) \to V_h$ by

$$\mathfrak{I}_h v = \sum_{z \in \mathcal{N}_h \setminus \mathcal{N}_{h,D}} (Q_z v)\psi_z.$$

The definition is very similar to the one of Clément [19]. The major difference is the use of non-polynomial trial functions on polygonal meshes. In contrast to the interpolation operators in Section 2.3, we use the L_2-projection over patches instead of point evaluations to determine the coefficients in the linear combination of trial functions. This modification is necessary since point evaluations are not well defined for functions $v \in H^1_D(\Omega)$. Our main interest in this section is to prove approximation properties of $\mathfrak{I}_h$ which are stated in Proposition 2 below. If no confusion arises, we write v for both the function and the trace of the function on an edge.

Proposition 2. *Let $\mathcal{K}_h$ be a regular and stable mesh and let $v \in H^1_D(\Omega)$, $E \in \mathcal{E}_h$ and $K \in \mathcal{K}_h$. Then, it holds*

$$\|v - \mathfrak{I}_h v\|_{L_2(K)} \leq c h_K |v|_{H^1(\omega_K)},$$
$$\|v - \mathfrak{I}_h v\|_{L_2(E)} \leq c h_E^{1/2} |v|_{H^1(\omega_E)},$$

where the constant $c > 0$ depends only on the regularity and stability parameters σ and c_1, see Definitions 2 and 3.

In view of the proof, let $\mathcal{K}_h$ be a regular and stable mesh and denote by c a generic constant that solely depends on the parameters σ and c_1 from Definitions 2 and 3. We show an approximation estimate for the L_2-projection on patches. The important fact is here that the constant appearing in the estimate only depends on the regularity and stability parameters of the mesh and not on the shape of the patches.

Lemma 10. *There exists a constant $c = c(\sigma)$ such that for every $z \in \mathcal{N}_h$ and $v \in H^1(\omega_z)$, it is*

$$\|v - Q_z v\|_{L_2(\omega_z)} \leq c h_{\omega_z} |v|_{H^1(\omega_z)},$$

where h_{ω_z} denotes the diameter of ω_z. If $K \in \mathcal{K}_h$ with $K \subset \omega_z$, it follows

$$\|v - Q_z v\|_{L_2(\omega_z)} \leq c h_K |v|_{H^1(\omega_z)},$$

where c depends on both the regularity and stability parameters.

Proof. It is known that the first inequality holds with the Poincaré constant

$$C_P(\omega_z) = \sup_{v \in H^1(\omega_z)} \frac{\|v - Q_z v\|_{L_2(\omega_z)}}{h_{\omega_z} |v|_{H^1(\omega_z)}} < \infty,$$

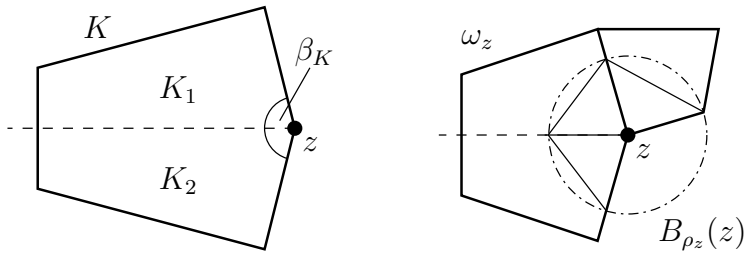

Figure 3.1: Element K which is split along the bisector of the angle β_K (left), patch ω_z with admissible decomposition $\{\omega_i\}_{i=1}^3$ and triangulation (right)

see for example [73]. This constant depends only on the shape of the patch ω_z. Therefore, we have to show that the Poincaré constant $C_P(\omega_z)$ can be bounded independently of $z \in \mathcal{N}_h$ from above in terms of the regularity parameter σ. We make use of Lemma 3 which guaranties that all angles inside the polygonal elements are bounded from below by α_0 and this constant depends only on σ. For convex domains ω, Payne and Weinberger [56] have shown $C_P(\omega) \leq 1/\pi$. In general, the patches ω_z are not convex, but they are star shaped with respect to z.

We distinguish two cases. First, we assume $\omega_z = K$ which is the trivial case. Since the element K is convex, we have $C_P(\omega_z) \leq 1/\pi \leq c$. If ω_z contains more than one element, we use Proposition 2.10 (Decomposition) of [73]. As preliminary of this proposition, an admissible decomposition $\{\omega_i\}_{i=1}^n$ of ω_z with pairwise disjoint domains ω_i and

$$\overline{\omega}_z = \bigcup_{i=1}^{n} \overline{\omega}_i$$

is needed. Admissible means in this context, that there exist triangles $\{T_i\}_{i=1}^n$ such that $T_i \subset \omega_i$ and for every pair i, j of different indices, there is a sequence $i = k_0, \ldots, k_\ell = j$ of indices such that for every m the triangles $T_{k_{m-1}}$ and T_{k_m} share a complete side.

Let us construct a decomposition $\{\omega_i\}_{i=1}^n$ of ω_z which is admissible. For any $z \in \mathcal{N}_h$, it is

$$\overline{\omega}_z = \bigcup_{z \in \mathcal{N}(K)} \overline{K}.$$

The angle between two neighbouring sides in a polygon K, a triangle T_i and a domain ω_i at the node z are labelled β_K, β_{T_i} and β_{ω_i}, respectively, see Figure 3.1. The set $\{\omega_i\}_{i=1}^n$ is defined as follows. It contains all elements $K \in \mathcal{K}_h$ with $z \in \mathcal{N}(K)$ which satisfy $\beta_K \leq \pi/2$. Additionally, if $\beta_K > \pi/2$ the set contains the two segments K_1 and K_2 which are obtained by splitting K along the bisector of the angle β_K, see again Figure 3.1. Due to the convexity of K, the segments K_1 and K_2 are also convex. We have constructed a decomposition $\{\omega_i\}_{i=1}^n$ of ω_z into convex subsets ω_i which satisfy

$$\alpha_1 \leq \beta_{\omega_i} \leq \pi/2 \quad \text{for} \quad i = 1, \ldots, n$$

with

$$\alpha_1 = \min\{\alpha_0, \pi/4\}.$$

According to Corollary 1, it is

$$n \leq 2|\{K \in \mathcal{K}_h : z \in K\}| \leq c.$$

In the next step, we intersect the boundary of the circle $B_{\rho_z}(z)$ with radius

$$\rho_z = \min\left\{\inf_{x\in\partial\omega_z\setminus\Gamma} |z-x|, \min\{|z-x| : x \in \mathcal{N}_{h,D} \cup \mathcal{N}_{h,N}, x \in \partial\omega_z\}\right\}$$

centred in z with the edges of ω_i, $i = 1, \ldots, n$ adjacent to z. The radius ρ_z is chosen in such a way that $\omega_i \cap B_{\rho_z}(z)$ for $i = 1, \ldots, n$ is a circular sector. Afterwards, we connect the points of intersection so that we obtain a coarse triangulation $\{T_i\}_{i=1}^n$ of $\omega_z \cap B_{\rho_z}(z)$ with $T_i \subset \omega_i$ for $i = 1, \ldots, n$, see Figure 3.1. According to the construction, every T_i is an isosceles triangle with angle $\beta_{T_i} = \beta_{\omega_i}$ at z which is enclosed by two sides of length ρ_z. Consequently, we have

$$|T_i| = \frac{1}{2}\rho_z^2 \sin\beta_{T_i} \geq \frac{1}{2}\rho_z^2 \sin\alpha_1 \quad \text{for } i = 1, \ldots, n$$

and the diameter h_{T_i} of T_i fulfils

$$h_{T_i} = \max\left\{\rho_z, 2\rho_z \sin\frac{\beta_{T_i}}{2}\right\} \leq 2\rho_z.$$

Obviously, the decomposition $\{\omega_i\}_{i=1}^n$ of ω_z is admissible. Thus, we can apply Proposition 2.10 (Decomposition) of [73] which yields

$$C_P(\omega_z) \leq \max_{1\leq i\leq n}\left\{8(n-1)\left(1 - \min_{1\leq j\leq n}\frac{|\omega_j|}{|\omega_z|}\right)\left(C_P^2(T_i) + 2C_P(T_i)\right)\frac{|\omega_z|\,h_{T_i}^2}{|T_i|\,h_{\omega_z}^2}\right\}^{1/2}$$

for the Poincaré constant. Because of $|\omega_z| \leq h_{\omega_z}^2$, we obtain

$$\frac{|\omega_z|\,h_{T_i}^2}{|T_i|\,h_{\omega_z}^2} \leq \frac{h_{T_i}^2}{|T_i|} \leq \frac{4\rho_z^2}{\frac{1}{2}\rho_z^2\sin\alpha_1} \leq \frac{8}{\sin\alpha_1} \leq c.$$

Since the constant in Corollary 1 as well as α_0 and thus α_1 solely depend on the regularity parameter σ, we can bound $C_P(\omega_z)$ independently of $z \in \mathcal{N}_h$ in terms of σ, i.e. $C_P(\omega_z) < c$ where $c = c(\sigma)$.

Finally, the second inequality in the lemma follows directly from the first one and the application of Lemma 4 which produces the additional dependence of the constant c on the stability parameter c_1. □

Lemma 11. *Let $v \in H^1(K)$ and $E \in \mathcal{E}(K)$, then it is*

$$\|v\|_{L_2(E)} \leq c\left\{h_E^{-1/2}\|v\|_{L_2(T_E)} + h_E^{1/2}|v|_{H^1(T_E)}\right\}$$

with the isosceles triangle $T_E \subset K$ from Lemma 3.

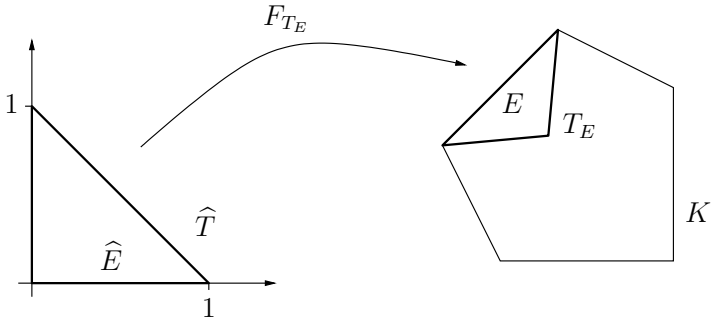

Figure 3.2: Affine transformation of the reference triangle $\widehat{T}$ to $T_E \subset K$

Proof. Let

$$\widehat{T} = \{x \in \mathbb{R}^2 : 0 \le x_1, x_2 \le 1,\ x_1 + x_2 \le 1\}$$

be the reference triangle with horizontal edge $\widehat{E}$. According to the trace theorem, see Theorem 3, there exists a constant $\widehat{c}_{LT}$ such that

$$\|\widehat{v}\|_{L_2(\widehat{E})} \le \widehat{c}_{LT}\, \|\widehat{v}\|_{H^1(\widehat{T})}$$

for $\widehat{v} \in H^1(\widehat{T})$. Let $K \in \mathcal{K}_h$ be an arbitrary element with edge E and let $v \in H^1(K)$. Owing to Lemma 3, there is a isosceles triangle $T_E \subset K$ with longest side E. We choose the affine transformation $F_{T_E} : \widehat{T} \to T_E$ in such a way, that $\widehat{E}$ is mapped onto E, see Figure 3.2. We set $\widehat{v} = v \circ F_{T_E} \in H^1(\widehat{T})$. For this transformation, it is known [18] that

$$|\widehat{v}|_{H^m(\widehat{T})} \le C\|DF_{T_E}\|_2^m |\det DF_{T_E}|^{-1/2} |v|_{H^m(T_E)} \quad \text{for } v \in H^m(T_E),$$

where C only depends on m and the spatial dimension which is equal to two here. Moreover, we have

$$\|DF_{T_E}\|_2 \le (2+\sqrt{2})h_E \quad \text{and} \quad |\det DF_{T_E}| = 2|T_E| = \frac{1}{2}\tan(\alpha_0)h_E^2.$$

Using this transformation, we get

$$\begin{aligned}
\|v\|_{L_2(E)} &= h_E^{1/2}\|\widehat{v}\|_{L_2(\widehat{E})} \le \widehat{c}_{LT} h_E^{1/2}\|\widehat{v}\|_{H^1(\widehat{T})} \\
&= \widehat{c}_{LT} h_E^{1/2}\left\{\|\widehat{v}\|_{L_2(\widehat{T})}^2 + |\widehat{v}|_{H^1(\widehat{T})}^2\right\}^{1/2} \le \widehat{c}_{LT} h_E^{1/2}\left\{\|\widehat{v}\|_{L_2(\widehat{T})} + |\widehat{v}|_{H^1(\widehat{T})}\right\} \\
&\le c h_E^{1/2}\big\{|\det DF_{T_E}|^{-1/2}\|v\|_{L_2(T_E)} + |\det DF_{T_E}|^{-1/2}\|DF_{T_E}^{-1}\|_2 |v|_{H^1(T_E)}\big\} \\
&\le c\left\{h_E^{-1/2}\|v\|_{L_2(T)} + h_E^{1/2}|v|_{H^1(T_E)}\right\}.
\end{aligned}$$

□

Finally, we prove Proposition 2 with the help of the stated lemmata.

Proof (Proposition 2). For $K \in \mathcal{K}_h$, we have

$$\sum_{z \in \mathcal{N}(K)} \psi_z = 1 \quad \text{on } \overline{K}$$

and $\|\psi_z\|_{L_\infty(\overline{K})} = 1$ for $z \in \mathcal{N}(K)$. To prove the first estimate in the proposition, we distinguish two cases. Let $K \in \mathcal{K}_h$ and let all nodes $z \in \mathcal{N}(K)$ of the element K be located in the interior of Ω or in the interior of the boundary Γ_N. Applying Lemma 10, we obtain

$$\begin{aligned} \|v - \mathfrak{I}_h v\|_{L_2(K)} &\leq \sum_{z \in \mathcal{N}(K)} \|\psi_z (v - Q_z v)\|_{L_2(K)} \\ &\leq \sum_{z \in \mathcal{N}(K)} \|v - Q_z v\|_{L_2(\omega_z)} \\ &\leq \sum_{z \in \mathcal{N}(K)} c h_K |v|_{H^1(\omega_z)} \\ &\leq c h_K |v|_{H^1(\omega_K)}. \end{aligned}$$

The last estimate is valid because of the fact that the number of nodes in $\mathcal{N}(K)$ is uniformly bounded with respect to $K \in \mathcal{K}_h$ according to Lemma 4.

In the case that at least one node of the element K is on the boundary Γ_D, we write

$$\begin{aligned} v - \mathfrak{I}_h v &= \sum_{z \in \mathcal{N}(K)} \psi_z v - \sum_{z \in \mathcal{N}(K) \setminus \mathcal{N}_{h,D}} \psi_z Q_z v \\ &= \sum_{z \in \mathcal{N}(K)} \psi_z (v - Q_z v) + \sum_{z \in \mathcal{N}(K) \cap \mathcal{N}_{h,D}} \psi_z Q_z v \end{aligned}$$

and obtain

$$\|v - \mathfrak{I}_h v\|_{L_2(K)} \leq \sum_{z \in \mathcal{N}(K)} \|\psi_z (v - Q_z v)\|_{L_2(K)} + \sum_{z \in \mathcal{N}(K) \cap \mathcal{N}_{h,D}} \|\psi_z Q_z v\|_{L_2(K)}.$$

The first sum has already been estimated, so let us have a look at the term in the second sum. For $z \in \mathcal{N}(K) \cap \mathcal{N}_{h,D}$, we have

$$\|\psi_z Q_z v\|_{L_2(K)} \leq |Q_z v| \, \|\psi_z\|_{L_\infty(K)} \, |K|^{1/2} \leq h_K |Q_z v|.$$

Since $z \in \Gamma_D$, there is an element K' and an edge $E' \in \mathcal{E}(K')$ such that $z \in \mathcal{N}(E')$ and $E' \in \mathcal{E}_{h,D}$. Furthermore, there is an isosceles triangle $T_{E'}$ with $T_{E'} \subset K'$ according to Lemma 3. Since v vanishes on E', we obtain with Lemma 11 and with the stability condition $h_{E'}^{-1} \leq c_1 h_{K'}^{-1}$ from Definition 3

$$\begin{aligned} |Q_z v| &= h_{E'}^{-1/2} \|Q_z v\|_{L_2(E')} = h_{E'}^{-1/2} \|v - Q_z v\|_{L_2(E')} \\ &\leq c h_{E'}^{-1/2} \left\{ h_{E'}^{-1/2} \|v - Q_z v\|_{L_2(T_{E'})} + h_{E'}^{1/2} |v - Q_z v|_{H^1(T_{E'})} \right\} \\ &\leq c \left\{ h_{K'}^{-1} \|v - Q_z v\|_{L_2(\omega_z)} + |v|_{H^1(\omega_z)} \right\}. \end{aligned}$$

Using Lemma 10 and putting all estimates together proves the first statement of Proposition 2.

To prove the second estimate in the proposition, we proceed in a similar manner. Let $E \in \mathcal{E}_h$, we have

$$\sum_{z \in \mathcal{N}(E)} \psi_z = 1 \quad \text{on } E$$

and $\|\psi_z\|_{L_\infty(E)} = 1$ for $z \in \mathcal{N}(E)$. First, let $E \in \mathcal{E}_h$ be such that all nodes z of the edge E are located in the interior of Ω or in the interior of the boundary Γ_N. Applying Lemmata 10 and 11 as well as $h_{K_E} h_E^{-1/2} \leq c_1 h_E^{1/2}$, where $K_E \in \mathcal{K}_h$ is an element with edge E, we obtain

$$\begin{aligned}
\|v - \mathfrak{I}_h v\|_{L_2(E)} &\leq \sum_{z \in \mathcal{N}(E)} \|\psi_z (v - Q_z v)\|_{L_2(E)} \\
&\leq \sum_{z \in \mathcal{N}(E)} \|v - Q_z v\|_{L_2(E)} \\
&\leq \sum_{z \in \mathcal{N}(E)} c \left\{ h_E^{-1/2} \|v - Q_z v\|_{L_2(T_E)} + h_E^{1/2} |v - Q_z v|_{H^1(T_E)} \right\} \\
&\leq \sum_{z \in \mathcal{N}(E)} c \left\{ h_E^{-1/2} \|v - Q_z v\|_{L_2(\omega_z)} + h_E^{1/2} |v|_{H^1(\omega_z)} \right\} \\
&\leq \sum_{z \in \mathcal{N}(E)} c h_E^{1/2} |v|_{H^1(\omega_z)} \\
&\leq c h_E^{1/2} |v|_{H^1(\omega_E)},
\end{aligned}$$

where T_E is the isosceles triangle of E with $T_E \subset K_E$.

If at least one node of E is on Γ_D, we have

$$\|v - \mathfrak{I}_h v\|_{L_2(E)} \leq \sum_{z \in \mathcal{N}(E)} \|\psi_z (v - Q_z v)\|_{L_2(E)} + \sum_{z \in \mathcal{N}(E) \cap \mathcal{N}_{h,D}} \|\psi_z Q_z v\|_{L_2(E)}.$$

The first sum has already been estimated, so let us have a look at the term in the second sum. For $z \in \mathcal{N}(E) \cap \mathcal{N}_{h,D}$, we have

$$\|\psi_z Q_z v\|_{L_2(E)} = |Q_z v| \, \|\psi_z\|_{L_2(E)} = \frac{1}{\sqrt{3}} h_E^{1/2} |Q_z v|.$$

Since $z \in \Gamma_D$, there is an element K' and an edge $E' \in \mathcal{E}(K')$ such that $z \in \mathcal{N}(E')$ and $E' \in \mathcal{E}_{h,D}$. Furthermore, there is an isosceles triangle $T_{E'}$ with $T_{E'} \subset K'$ according to Lemma 3. Since v vanishes on E', we obtain with Lemma 11 and with the stability condition $h_{E'}^{-1} \leq c_1 h_{K'}^{-1}$

$$\begin{aligned}
|Q_z v| &= h_{E'}^{-1/2} \|Q_z v\|_{L_2(E')} = h_{E'}^{-1/2} \|v - Q_z v\|_{L_2(E')} \\
&\leq c h_{E'}^{-1/2} \left\{ h_{E'}^{-1/2} \|v - Q_z v\|_{L_2(T_{E'})} + h_{E'}^{1/2} |v - Q_z v|_{H^1(T_{E'})} \right\} \\
&\leq c \left\{ h_{K'}^{-1} \|v - Q_z v\|_{L_2(\omega_z)} + |v|_{H^1(\omega_z)} \right\}.
\end{aligned}$$

Using Lemma 10 and putting all estimates together yields the second statement of Proposition 2 and concludes the proof. □

3.3 Residual error estimate

In this section, we formulate the main result for the residual error estimator and prove its reliability. This estimator bounds the difference of the exact solution and the Galerkin approximation in the energy norm $\|\cdot\|_E$ defined in Remark 2. Among others, the residual error estimator measures the jumps of the conormal derivatives over the element edges. Such a jump over an internal edge $E \in \mathcal{E}_{h,\Omega}$ is defined by

$$[\![u_h]\!]_E = n_K \cdot \gamma_0^K(a\nabla u_h) + n_{K'} \cdot \gamma_0^{K'}(a\nabla u_h),$$

where $K, K' \in \mathcal{K}_h$ are the neighbouring elements of E with $E \in \mathcal{E}(K) \cap \mathcal{E}(K')$. In the case of a piecewise constant material coefficient $a(\cdot)$, this definition is equivalent to

$$[\![u_h]\!]_E = a_K \gamma_1^K u_h + a_{K'} \gamma_1^{K'} u_h,$$

due to the local regularity of the finite element approximation $u_h \in V_h$ which fulfils $u_h \in H^2(K)$ for $K \in \mathcal{K}_h$. We assume that the Dirichlet boundary datum g_D is approximated exactly, i.e. $g_{Dh} = g_D$. Consequently, we obtain $u - u_h \in H^1_D(\Omega)$ since it is possible to set $u_{Dh} = u_D$.

In the first formulation of the residual error estimate we additionally assume a piecewise constant material coefficient $a(\cdot)$ such that the Galerkin orthogonality (1.6) can be exploited as in the proof of Lemma 2. Furthermore, we restrict ourselves to

$$V_h = \operatorname{span}\Psi \quad \text{with} \quad \Psi = \Psi^{(1)} \setminus \Psi_D.$$

Theorem 15. *Let $\mathcal{K}_h$ be a regular and stable mesh. Then the residual error estimate is reliable, i.e.*

$$\|u - u_h\|_E \leq \frac{c}{\sqrt{a_{\min}}}\, \eta_R$$

with

$$\eta_R^2 = \sum_{K \in \mathcal{K}_h} \eta_K^2$$

and

$$\eta_K^2 = h_K^2 \|f\|^2_{L_2(K)} + \sum_{E \in \mathcal{E}(K)} h_E \|R_E\|^2_{L_2(E)},$$

where

$$R_E = \begin{cases} 0 & \text{for } E \in \mathcal{E}_{h,D}, \\ g_N - a_K \gamma_1^K u_h & \text{for } E \in \mathcal{E}_{h,N} \text{ with } E \in \mathcal{E}(K), \\ -\frac{1}{2}[\![u_h]\!]_E & \text{for } E \in \mathcal{E}_{h,\Omega}, \end{cases}$$

and the constant $c > 0$ depends only on the regularity and stability parameters σ and c_1, see Definitions 2 and 3.

Proof. In the first step, we define the functional $\mathcal{R}$ on $V = H^1_D(\Omega)$ by

$$\mathcal{R}(v) = a_\Omega(u - u_h, v) = \int_\Omega a\nabla(u - u_h) \cdot \nabla v.$$

It is easy to see that $\mathcal{R}$ is linear and continuous on V and thus it belongs to the dual V' of V. By the use of Green's first identity (1.11) and splitting the integral, we obtain

$$\begin{aligned}\mathcal{R}(v) &= \int_\Omega fv + \int_{\Gamma_N} g_N v - \sum_{K\in\mathcal{K}_h} \int_K a_K \nabla u_h \cdot \nabla v \\ &= \sum_{K\in\mathcal{K}_h} \int_K fv + \sum_{E\in\mathcal{E}_{h,N}} \int_E g_N v - \sum_{K\in\mathcal{K}_h} \int_{\partial K} a_K \gamma_1^K u_h \, v\end{aligned}$$

since the approximation u_h is harmonic on each element. If we rearrange the sums and take into account that we integrate over each edge in the interior of Ω two times, we obtain

$$\begin{aligned}\mathcal{R}(v) &= \sum_{K\in\mathcal{K}_h} \Big\{ \int_K fv + \sum_{E\in\mathcal{E}(K)\cap\mathcal{E}_{h,N}} \int_E (g_N - a_K\gamma_1^K u_h)v \\ &\qquad -\frac{1}{2} \sum_{E\in\mathcal{E}(K)\cap\mathcal{E}_{h,\Omega}} \int_E [\![u_h]\!]_E \, v \Big\} \\ &= \sum_{K\in\mathcal{K}_h} \Big\{ \int_K fv + \sum_{E\in\mathcal{E}(K)} \int_E R_E v \Big\}.\end{aligned}$$

According to the Riesz representation theorem, see Theorem 5, and Remark 2 on page 14, it is

$$\|u - u_h\|_E = \sup_{0\neq v\in V} \frac{|\mathcal{R}(v)|}{\|v\|_E}. \tag{3.2}$$

Next, we estimate $|\mathcal{R}(v)|$. For this reason, the Galerkin orthogonality

$$a_\Omega(u - u_h, v_h) = 0 \quad \text{for } v_h \in V_h$$

is utilized which has been used already in the proof of Lemma 2. Additionally, we use the triangular inequality as well as the Cauchy-Schwarz inequality and obtain

$$\begin{aligned}|\mathcal{R}(v)| &= |\mathcal{R}(v - \mathfrak{I}_h v)| \\ &\le \sum_{K\in\mathcal{K}_h} \Big\{ \Big| \int_K f(v - \mathfrak{I}_h v) \Big| + \sum_{E\in\mathcal{E}(K)} \Big| \int_E R_E(v - \mathfrak{I}_h v) \Big| \Big\} \\ &\le \sum_{K\in\mathcal{K}_h} \Big\{ \|f\|_{L_2(K)} \|v - \mathfrak{I}_h v\|_{L_2(K)} + \sum_{E\in\mathcal{E}(K)} \|R_E\|_{L_2(E)} \|v - \mathfrak{I}_h v\|_{L_2(E)} \Big\}.\end{aligned}$$

To estimate $|\mathcal{R}(v)|$ even further, we remember $|\mathcal{E}(K)| = |\mathcal{N}(K)| \leq c$ and the fact that each element is covered by a finite number of patches, see Lemma 4. The Cauchy-Schwarz inequality and Proposition 2 with the estimates for the interpolation error of the operator $\mathfrak{I}_h$ yield

$$\begin{aligned}
|\mathcal{R}(v)| &\leq c \sum_{K\in\mathcal{K}_h} \left\{ \|f\|_{L_2(K)}\, h_K |v|_{H^1(\omega_K)} + \sum_{E\in\mathcal{E}(K)} \|R_E\|_{L_2(E)}\, h_E^{1/2} |v|_{H^1(\omega_E)} \right\} \\
&\leq c \sum_{K\in\mathcal{K}_h} \left\{ h_K \|f\|_{L_2(K)} + \Big(\sum_{E\in\mathcal{E}(K)} h_E \|R_E\|^2_{L_2(E)} \Big)^{1/2} \right\} |v|_{H^1(\omega_K)} \\
&\leq c \sum_{K\in\mathcal{K}_h} \left\{ h_K^2 \|f\|^2_{L_2(K)} + \sum_{E\in\mathcal{E}(K)} h_E \|R_E\|^2_{L_2(E)} \right\}^{1/2} |v|_{H^1(\omega_K)} \\
&\leq c \Big(\sum_{K\in\mathcal{K}_h} \eta_K^2 \Big)^{1/2} |v|_{H^1(\Omega)}.
\end{aligned}$$

Because of

$$|v|_{H^1(\Omega)} \leq \left| \sqrt{\frac{a}{a_{\min}}}\, v \right|_{H^1(\Omega)} = \frac{1}{\sqrt{a_{\min}}} \|v\|_E, \tag{3.3}$$

we have

$$|\mathcal{R}(v)| \leq \frac{c}{\sqrt{a_{\min}}}\, \eta_R \, \|v\|_E.$$

Inserting the last estimate into (3.2) concludes the proof. □

Remark 6. The constant in front of the residual error estimator in the last theorem depends on $a_{\min}$. It is more desirable to have an error estimate with a constant independent of the actual problem. Such estimates are called robust. Under certain assumptions, like for example a quasi-monotone material coefficient $a \in L_\infty(\Omega)$, it is possible to derive estimates which fulfil this criterion, see [27, 58].

For the previous theorem, we have assumed that the material coefficient $a(\cdot)$ is piecewise constant on the initial mesh, but this is not the case in general. Therefore, we have to approximate it by a piecewise constant function or in the advanced setting by the interpolant $\mathfrak{I}^{(1)}a$. In Section 2.4, we have mentioned that such an approximation $a^h(\cdot)$ of $a(\cdot)$ yields an approximated bilinear form

$$a^h_\Omega(u,v) = \int_\Omega a^h \nabla u \cdot \nabla v.$$

In the same way, there is sometimes a need to replace the exact Neumann datum g_N and the right hand side f in the model problem (1.1) by some approximations g_{Nh} and f_h, respectively. This leads to an approximated right hand side

$$\ell_h(v) = (f_h, v) + (g_{Nh}, v)_{\Gamma_N} - a^h_\Omega(u_{Dh}, v)$$

in the discrete variational formulation of the problem. Lets set

$$u_D + V = \{v = v_0 + u_D \in H^1(\Omega) : v_0 \in V\}.$$

Since we assume $u_D = u_{Dh}$, the discrete Galerkin solution fulfils $u_h \in u_D + V_h$ as well as

$$a_\Omega^h(u_h, v_h) = (f_h, v_h) + (g_{Nh}, v_h)_{\Gamma_N} \quad \text{for } v_h \in V_h, \tag{3.4}$$

where we allow the case of higher order trial functions, i.e.

$$V_h = \operatorname{span} \Psi \quad \text{with} \quad \Psi = \Psi^{(3)} \setminus \Psi_D.$$

On the other hand, the exact solution of the problem fulfils $u \in u_D + V$ and

$$a_\Omega(u, v) = (f, v) + (g_N, v)_{\Gamma_N} \quad \text{for } v \in V. \tag{3.5}$$

Obviously, there is no Galerkin orthogonality any more and we cannot exploit this property in the proof of the reliability of the residual error estimate. For this reason, we have to rewrite the functional $\mathcal{R}$ such that it incorporates the approximation errors of the data. Due to (3.5) and by adding and subtracting the approximations f_h as well as g_{Nh}, we obtain

$$\begin{aligned}
\mathcal{R}(v) &= a_\Omega(u - u_h, v) \\
&= (f, v) + (g_N, v)_{\Gamma_N} - a_\Omega(u_h, v) \\
&= (f - f_h, v) + (g_N - g_{Nh}, v)_{\Gamma_N} - a_\Omega(u_h, v) \\
&\quad + (f_h, v) + (g_{Nh}, v)_{\Gamma_N}.
\end{aligned}$$

Subtracting the right hand side of (3.4) and adding its left hand side yields

$$\begin{aligned}
\mathcal{R}(v) &= (f - f_h, v) + (g_N - g_{Nh}, v)_{\Gamma_N} - a_\Omega(u_h, v) \\
&\quad + (f_h, v - v_h) + (g_{Nh}, v - v_h)_{\Gamma_N} + a_\Omega^h(u_h, v_h).
\end{aligned}$$

Next, we add and subtract $a_\Omega^h(u_h, v)$ and obtain

$$\begin{aligned}
\mathcal{R}(v) &= (f - f_h, v) + (g_N - g_{Nh}, v)_{\Gamma_N} - \int_\Omega (a - a^h) \nabla u_h \cdot \nabla v \\
&\quad + (f_h, v - v_h) + (g_{Nh}, v - v_h)_{\Gamma_N} - a_\Omega^h(u_h, v - v_h).
\end{aligned}$$

Splitting the integrals gives

$$\begin{aligned}
\mathcal{R}(v) = \sum_{K \in \mathcal{K}_h} \Bigg\{ & \int_K (f - f_h) v + \sum_{E \in \mathcal{E}(K) \cap \mathcal{E}_{h,N}} \int_E (g_N - g_{Nh}) v - \int_K (a - a^h) \nabla u_h \cdot \nabla v \\
& + \int_K f_h (v - v_h) + \sum_{E \in \mathcal{E}(K) \cap \mathcal{E}_{h,N}} \int_E g_{Nh} (v - v_h) \\
& - \int_K a^h \nabla u_h \cdot \nabla (v - v_h) \Bigg\}.
\end{aligned}$$

The use of the local identity

$$\int_K a^h\nabla u_h\cdot(v-v_h) = \int_{\partial K} n_K\cdot\gamma_0^K(a^h\nabla u_h)\,\gamma_0^K(v-v_h) - \int_K \operatorname{div}(a^h\nabla u_h)(v-v_h)$$

yields

$$\begin{aligned}\mathcal{R}(v) \;=\; \sum_{K\in\mathcal{K}_h}\Big\{ &\int_K (f-f_h)v + \sum_{E\in\mathcal{E}(K)\cap\mathcal{E}_{h,N}}\int_E (g_N-g_{Nh})v - \int_K (a-a^h)\nabla u_h\cdot\nabla v\\ &+\int_K \big(f_h+\operatorname{div}(a^h\nabla u_h)\big)(v-v_h)\\ &+\sum_{E\in\mathcal{E}(K)\cap\mathcal{E}_{h,N}}\int_E \big(g_{Nh}-n_K\cdot\gamma_0^K(a^h\nabla u_h)\big)(v-v_h)\\ &-\sum_{E\in\mathcal{E}(K)\cap\mathcal{E}_{h,\Omega}}\int_E n_K\cdot\gamma_0^K(a^h\nabla u_h)\,(v-v_h)\Big\}.\end{aligned}$$

If we rearrange the sums and use the abbreviations

$$\widetilde{R}_K = f_h + \operatorname{div}(a^h\nabla u_h)$$

and

$$\widetilde{R}_E = \begin{cases} 0 & \text{for } E\in\mathcal{E}_{h,D},\\ g_{Nh}-n_K\cdot\gamma_0^K(a^h\nabla u_h) & \text{for } E\in\mathcal{E}_{h,N} \text{ with } E\in\mathcal{E}(K),\\ -\frac{1}{2}[\![u_h]\!]_{E,h} & \text{for } E\in\mathcal{E}_{h,\Omega},\end{cases}$$

where

$$[\![u_h]\!]_{E,h} = n_K\cdot\gamma_0^K(a^h\nabla u_h) + n_{K'}\cdot\gamma_0^{K'}(a^h\nabla u_h),$$

we obtain

$$\begin{aligned}\mathcal{R}(v) \;=\; \sum_{K\in\mathcal{K}_h}\Big\{ &\int_K (f-f_h)v + \sum_{E\in\mathcal{E}(K)\cap\mathcal{E}_{h,N}}\int_E (g_N-g_{Nh})v - \int_K (a-a^h)\nabla u_h\cdot\nabla v\\ &+\int_K \widetilde{R}_K(v-v_h) + \sum_{E\in\mathcal{E}(K)}\int_E \widetilde{R}_E(v-v_h)\Big\}.\end{aligned}$$

Next, we choose $v_h = \mathfrak{I}_h v$ and estimate $|\mathcal{R}(v)|$ with the same techniques as in the proof of Theorem 15. For the last two terms, we recognize directly

$$\left|\int_K \widetilde{R}_K(v-v_h) + \sum_{E\in\mathcal{E}(K)}\int_E \widetilde{R}_E(v-v_h)\right| \;\le\; c\,\widetilde{\eta}_K\,|v|_{H^1(\omega_K)},$$

where

$$\widetilde{\eta}_K^2 = h_K^2\|\widetilde{R}_K\|_{L_2(K)}^2 + \sum_{E\in\mathcal{E}(K)} h_E\|\widetilde{R}_E\|_{L_2(E)}^2.$$

Multiple applications of the Cauchy-Schwarz inequality and Theorem 3, which gives $\|v\|_{L_2(E)} \leq c_{LT}\|v\|_{H^1(K)}$ for $E \in \mathcal{E}(K)$, yield for the first terms

$$\begin{aligned}
&\left| \int_K (f - f_h)v + \sum_{E\in\mathcal{E}(K)\cap\mathcal{E}_{h,N}} \int_E (g_N - g_{Nh})v - \int_K (a - a^h)\nabla u_h \cdot \nabla v \right| \\
&\quad \leq \|f - f_h\|_{L_2(K)}\|v\|_{L_2(K)} + \sum_{E\in\mathcal{E}(K)\cap\mathcal{E}_{h,N}} \|g_N - g_{Nh}\|_{L_2(E)}\|v\|_{L_2(E)} \\
&\qquad + \|(a - a^h)\nabla u_h\|_{L_2(K)}\|\nabla v\|_{L_2(K)} \\
&\quad \leq c\left(\|f - f_h\|_{L_2(K)} + \sum_{E\in\mathcal{E}(K)\cap\mathcal{E}_{h,N}} \|g_N - g_{Nh}\|_{L_2(E)} \right. \\
&\qquad \left. + \|(a - a^h)\nabla u_h\|_{L_2(K)} \right) \|v\|_{H^1(K)} \\
&\quad \leq c\,\widetilde{\delta}_K\,\|v\|_{H^1(K)},
\end{aligned}$$

where

$$\widetilde{\delta}_K^2 = \|f - f_h\|_{L_2(K)}^2 + \sum_{E\in\mathcal{E}(K)\cap\mathcal{E}_{h,N}} \|g_N - g_{Nh}\|_{L_2(E)}^2 + \|(a - a^h)\nabla u_h\|_{L_2(K)}^2.$$

In total, it is

$$\begin{aligned}
|\mathcal{R}(v)| &\leq c \sum_{K\in\mathcal{K}_h} \left\{ \widetilde{\eta}_K\,|v|_{H^1(\omega_K)} + \widetilde{\delta}_K\,\|v\|_{H^1(K)} \right\} \\
&\leq c \sum_{K\in\mathcal{K}_h} \left\{ \widetilde{\eta}_K^2 + \widetilde{\delta}_K^2 \right\}^{1/2} \|v\|_{H^1(\omega_K)} \\
&\leq c \left(\sum_{K\in\mathcal{K}_h} \left\{ \widetilde{\eta}_K^2 + \widetilde{\delta}_K^2 \right\} \right)^{1/2} \|v\|_{H^1(\Omega)}.
\end{aligned}$$

Since the norm $\|\cdot\|_{H^1(\Omega)}$ and the semi-norm $|\cdot|_{H^1(\Omega)}$ are equivalent on V, we obtain with (3.3)

$$|\mathcal{R}(v)| \leq \frac{c}{\sqrt{a_{\min}}} \left(\sum_{K\in\mathcal{K}_h} \left\{ \widetilde{\eta}_K^2 + \widetilde{\delta}_K^2 \right\} \right)^{1/2} \|v\|_E.$$

Inserting this estimate into (3.2) proves the following result.

Theorem 16. *Let $\mathcal{K}_h$ be a regular and stable mesh. Then the extended residual error estimate is reliable, i.e.*

$$\|u - u_h\|_E \leq \frac{c}{\sqrt{a_{\min}}}\,\widetilde{\eta}_R$$

with

$$\widetilde{\eta}_R^2 = \sum_{K\in\mathcal{K}_h} \left\{ \widetilde{\eta}_K^2 + \widetilde{\delta}_K^2 \right\},$$

where the error indicators for the finite element and data approximation, $\widetilde{\eta}_K$ and $\widetilde{\delta}_K$, are defined as above. The constant $c > 0$ depends only on the regularity and stability parameters σ and c_1, see Definitions 2 and 3.

So, in the case that we approximate the initial data f, g_N and the diffusion coefficient $a(\cdot)$ for the computations, the additional approximation errors enter the residual error estimate. Therefore, the accuracy of the data approximation influences the adaptive refinement. The term

$$\widetilde{\delta}_R = \Big(\sum_{K \in \mathcal{K}_h} \widetilde{\delta}_K^2 \Big)^{1/2}$$

is often used as global estimator for the data error.

3.4 Numerical examples

In this section, we have a look at different numerical examples to confirm our theoretical results and to show optimal rates of convergence for the adaptive BEM-based finite element method. But before, we have to discuss how to analyse the convergence.

If the solution of the model problem fulfils $u \in H^2(\Omega)$, we know from Section 2.3 that the BEM-based FEM converges quadratically in the mesh size h with respect to the L_2-norm on a sequence of regular meshes which are uniformly refined. We also know that the convergence is linear in this situation when the error is measured with respect to the H^1-norm or with respect to the equivalent energy norm $\|\cdot\|_E$ defined in Remark 2. As we have already mentioned, it makes no sense to analyse the convergence in the mesh size h in case of adaptive refinements. Therefore, we use the number of degrees of freedom (DoF) in the system of linear equations. Since the relation

$$\mathrm{DoF} = O(h^{-2})$$

holds for uniform triangular meshes, we say that the method has an optimal rate of convergence with respect to the L_2-norm if it converges linearly in the degrees of freedom. Accordingly, the method has an optimal rate of convergence with respect to the H^1-norm or with respect to the energy norm if it converges with the rate $1/2$ in the DoF. This terminology is also valid for a sequence of adaptive refined meshes.

Let $\Omega = (-1,1) \times (-1,1) \subset \mathbb{R}^2$ be split into two domains, $\Omega_1 = \Omega \setminus \overline{\Omega}_2$ and $\Omega_2 = (0,1) \times (0,1)$. We are interested in the boundary value problem

$$\begin{aligned} -\mathrm{div}\,(a \nabla u) &= 0 \quad \text{in } \Omega, \\ u &= g \quad \text{on } \Gamma = \Gamma_D, \end{aligned}$$

where the coefficient a is given by

$$a = \begin{cases} 1 & \text{in } \Omega_1, \\ k_2 & \text{in } \Omega_2. \end{cases}$$

Using polar coordinates (r, φ), we choose the boundary data as restriction of the global function

$$g(x) = r^\lambda \begin{cases} \cos(\lambda(\varphi - \pi/4)) & \text{for } x \in \mathbb{R}^2_+, \\ \beta \cos(\lambda(\pi - |\varphi - \pi/4|)) & \text{else,} \end{cases}$$

with

$$\lambda = \frac{4}{\pi} \arctan\left(\sqrt{\frac{3+k_2}{1+3k_2}}\right) \quad \text{and} \quad \beta = -k_2 \frac{\sin\left(\lambda \frac{\pi}{4}\right)}{\sin\left(\lambda \frac{3\pi}{4}\right)},$$

where $\mathbb{R}^2_+ = \{x = (x_1, x_2)^\top \in \mathbb{R}^2 : x_1, x_2 \geq 0\}$. This problem is constructed in such a way that $u = g$ is the exact solution in Ω. The parameter $k_2 > 0$ is responsible for the regularity of the solution. We have $u \in H^2(\Omega)$ if $k_2 < 1$, and otherwise u is singular in the sense that the gradient of u is not square integrable any more. Figure 3.3 displays approximations of the function g for two different values of k_2.

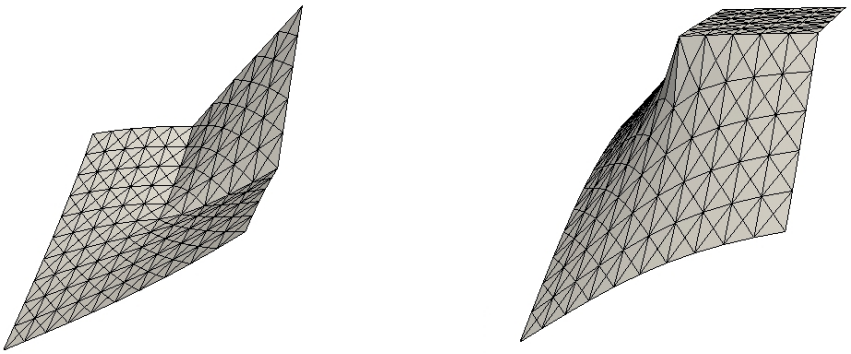

Figure 3.3: $k_2 = 0.01$ and therefore $g \in H^2(\Omega)$ (left), $k_2 = 100$ and so $g \notin H^2(\Omega)$ (right)

In the first numerical example, the convergence with respect to the DoF is shown for the BEM-based FEM on polygonal meshes. We choose $k_2 = 0.01$ so that $u \in H^2(\Omega)$ and we start with an initial polygonal mesh, see Figure 3.4. In every iteration step, we refine all elements such that we obtain a uniform refinement. In Figure 3.5, we sketch the approximation error $\|u - u_h\|_{L_2(\Omega)}$ with respect to the degrees of freedom in a logarithmic plot and recognize a graph with a slope of minus one which corresponds to linear convergence in the DoF. So, we obtain an optimal rate of convergence for the L_2-error by the proposed method on arbitrary polygonal meshes.

The rate of convergence with respect to the energy norm is analysed in the next numerical experiment. We perform the adaptive strategy with the error

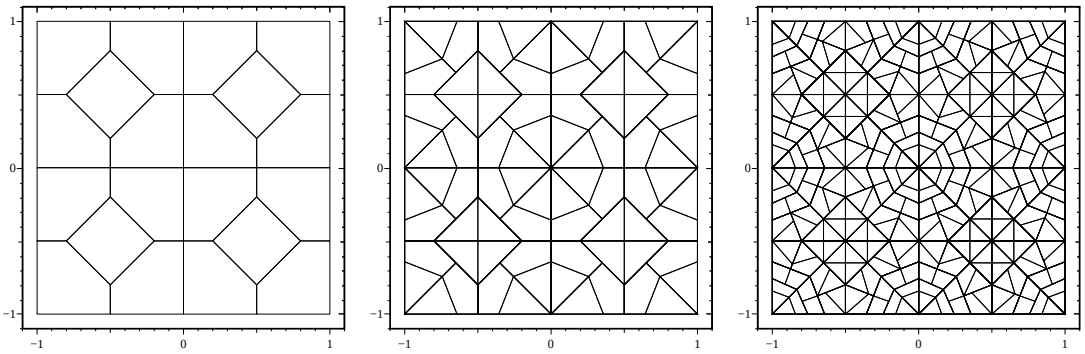

Figure 3.4: Initial mesh and uniform refinements

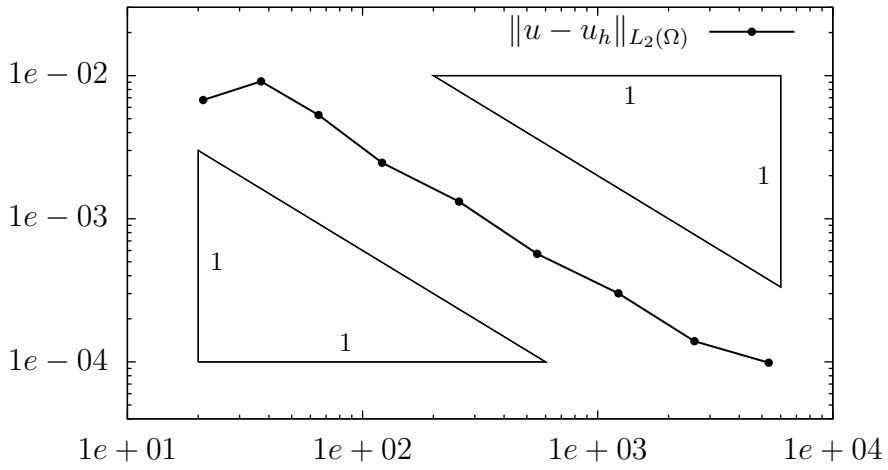

Figure 3.5: Convergence for smooth solution ($k_2 = 0.01$) with respect to DoF using uniform refinement, triangles with slope minus one

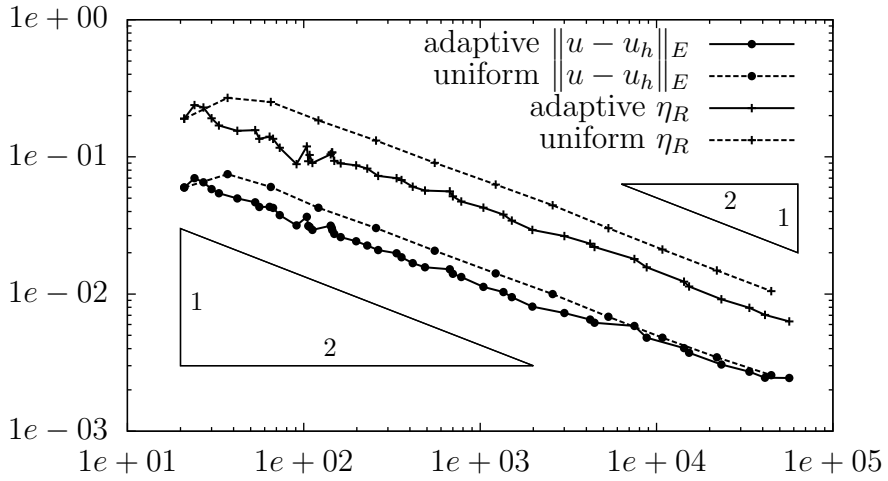

Figure 3.6: Convergence for smooth solution ($k_2 = 0.01$) with respect to DoF using adaptive and uniform refinement, triangles with slope minus one half

estimate η_R and with uniform refinement. In Figure 3.6, we observe optimal rates of convergence for the uniform as well as for the adaptive strategy with the proposed method. We also recognize that the error estimate η_R reproduces the behaviour of the error $\|u - u_h\|_E$ asymptotically very well.

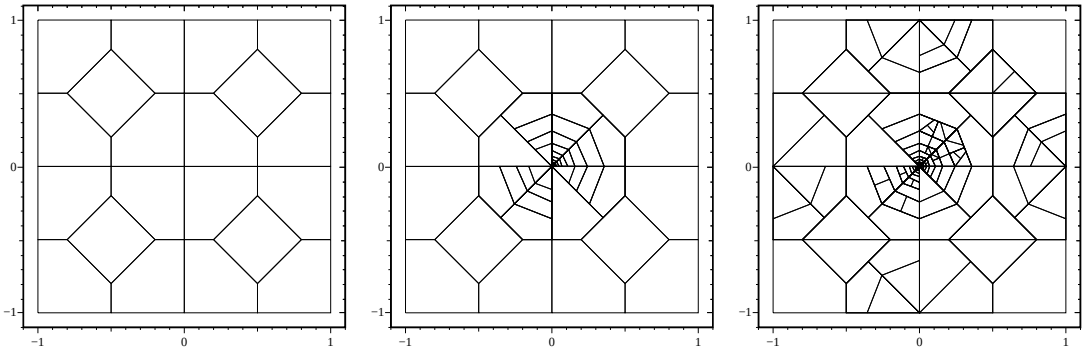

Figure 3.7: Initial mesh and adaptive refinements for $k_2 = 100$

If one considers boundary value problems with smooth solutions, it is very difficult for an adaptive strategy to perform better than a uniform one. Therefore, we choose the problem in such a way that it has a singular solution $u \notin H^2(\Omega)$. For $k_2 = 100$, we obtain the convergence results shown in Figure 3.8 for uniform and adaptive refinements, see Figures 3.4 and 3.7. Obviously, the error stays more or less constant at the beginning of the two strategies. This can be explained as follows. In our considerations, we have assumed that the boundary data is approximated exactly, but this assumption is not true here. The error in the Dirichlet datum dominates. Consequently, the method needs some refinement steps until the datum is approximated accurately enough to perform well. Nevertheless, we see that the rate of convergence for the uniform refinement slows down. In contrast, the adaptive method still converges optimal.

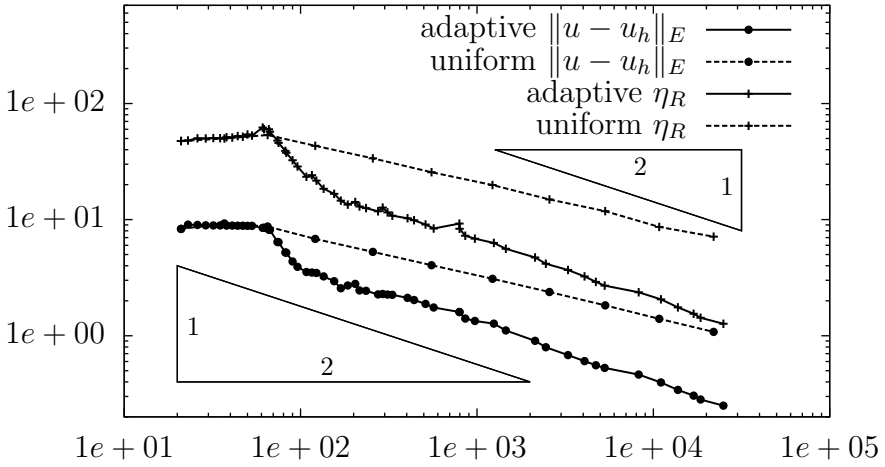

Figure 3.8: Convergence for singular solution ($k_2 = 100$) with respect to DoF using adaptive and uniform refinement, triangles with slope minus one half

Finally, a standard example is considered. We use again the polar coordinates (r, φ). Let $\Omega = \{x \in \mathbb{R}^2 : |r| < 1 \text{ and } 0 < \varphi < 3\pi/2\}$ and

$$g(x) = r^{2/3} \sin\left(\frac{2\varphi}{3}\right) \quad \text{for } x \in \mathbb{R}^2.$$

The problem reads

$$\begin{aligned} -\Delta u &= 0 \quad \text{in } \Omega, \\ u &= g \quad \text{on } \Gamma = \Gamma_D. \end{aligned}$$

It looks very simple but the solution $u = g$ is singular in the origin of the coordinate system. In Figure 3.9, the initial mesh and two adaptive refinements after five and ten steps are shown. The adaptive finite element method obviously recognizes the singularity and refines the mesh near the origin. Typically, one would expect that all elements near the origin should be refined in a similar manner. But in Figure 3.9, the triangle on the upper right of the origin is still not refined after five steps. Even after ten steps, there are large elements near the origin. This is a difference to standard finite element methods, where values at hanging nodes are prescribed by interpolation of values at classical nodes. In the proposed BEM-based FEM, there is no distinction between the nodes in the mesh. Consequently, a hanging node gives a degree of freedom and adds a trial function to the approximation space V_h. These trial functions also affect the approximation quality at neighbouring elements. In Figure 3.10, we see that the error over the upper right triangle of the origin is reduced by introducing hanging nodes without refining the element.

The convergence analysis for this example shows the same results as in the previous example. The uniform method does not converge optimal any more but the adaptive strategy has still an optimal rate of convergence, see Figure 3.11.

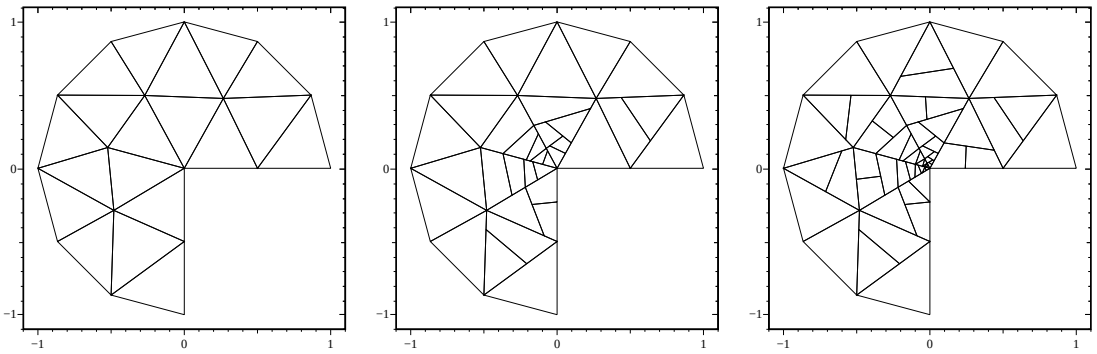

Figure 3.9: Initial mesh (left), adaptive refined mesh after five steps (middle), adaptive refined mesh after ten steps (right)

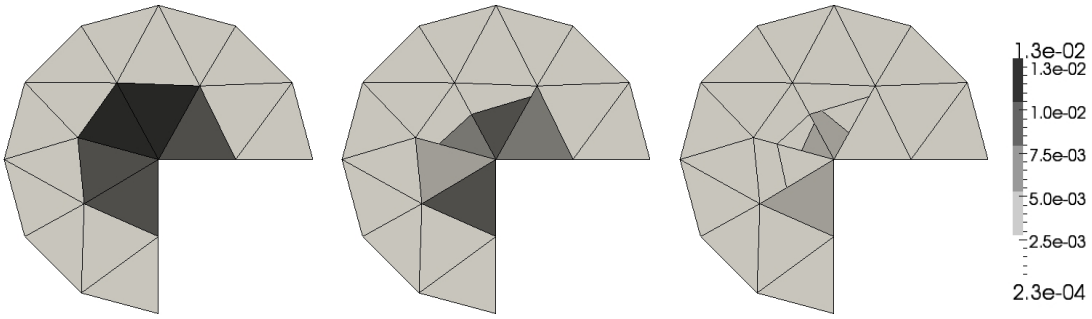

Figure 3.10: Error distribution $\|u - u_h\|_E^2$ for the first three meshes

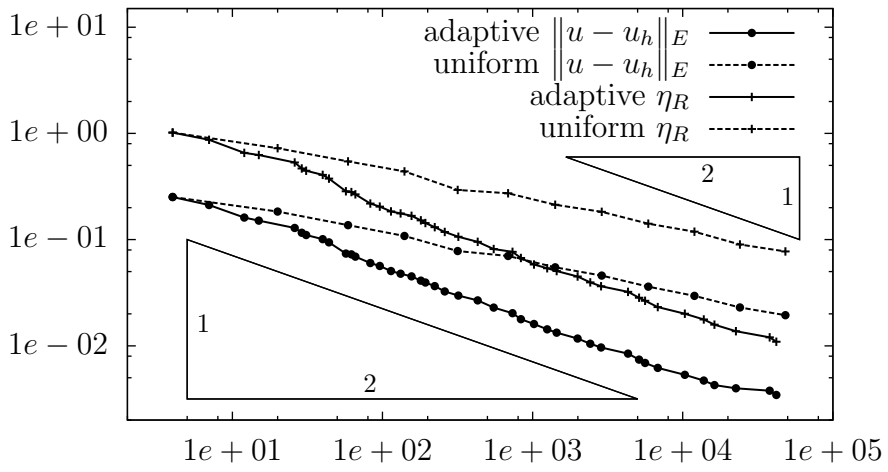

Figure 3.11: Convergence for singular solution on arc with respect to DoF, triangles with slope minus one half

Chapter 4

BEM-based FEM in 3D

The two dimensional version of the BEM-based finite element method is understood quite well. In the previous chapters, we have seen several developments of the method, and in the literature further topics are discussed, see [21, 39, 40, 41]. Already in [20], the authors have proposed a generalization to three space dimensions and this strategy is used in the cited literature. The idea is to allow only polyhedral elements with triangulated surfaces. In this situation, the definition of trial functions is straightforward as we discuss in the next section. Nevertheless, our aim is to introduce a new generalization of the lower order trial functions of the BEM-based finite element method in the three dimensional case. Arbitrary convex polyhedral elements are allowed, and we discuss how to cope with the polygonal faces of the polyhedral elements. Additionally, this approach yields a new point of view for the definition of trial functions in the framework of the BEM-based FEM. This perspective could be advantageous for other boundary value problems like convection-diffusion or Helmholtz equations.

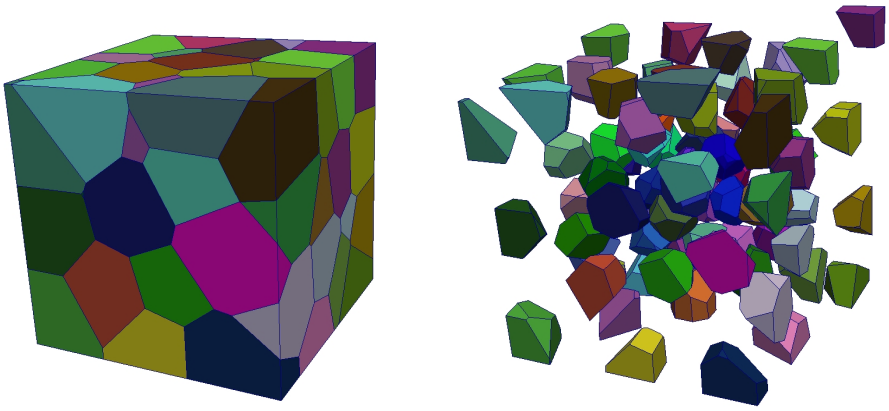

Figure 4.1: Polyhedral mesh of the unite cube

The use of polyhedral meshes might be even more favourable in three space dimensions than in the two dimensional case. While meshing complex geometries, simplicial elements can be restrictive and deteriorate the mesh quality. In

contrast, polyhedral cells are more flexible. An example of such a general mesh can be seen in Figure 4.1. Here, the unite cube is discretized with a Voronoi mesh according to [28].

4.1 Construction of trial functions

For the considerations in the three dimensional case, we keep the notations from previous chapters. $\mathcal{K}_h$ denotes the mesh which consists of convex polyhedral elements K. The convex faces of the polyhedra are labeled by F and the set of all faces is abbreviated to $\mathcal{F}_h$. This set is decomposed into $\mathcal{F}_h = \mathcal{F}_{h,\Omega} \cup \mathcal{F}_{h,D} \cup \mathcal{F}_{h,N}$, where the disjoint subsets contain all faces in the interior of Ω, on the Dirichlet boundary Γ_D and on the Neumann boundary Γ_N, respectively. As before, we have the set of nodes $\mathcal{N}_h$ and the set of edges $\mathcal{E}_h$. Additionally to $\mathcal{N}(K)$, $\mathcal{N}(E)$ and $\mathcal{E}(K)$, we introduce the sets $\mathcal{N}(F)$ for $F \in \mathcal{F}_h$ and $\mathcal{F}(K)$ for $K \in \mathcal{K}_h$. These sets contain the nodes which belong to the face F and the faces which belong to the element K, respectively.

Before we introduce the generalization of the lower order trial functions for the BEM-based FEM, the strategy from [20] is reviewed which has been used in the literature till now. Here, the authors assume that the surfaces of the elements are triangulated. In our notation, this means that all faces $F \in \mathcal{F}_h$ of the mesh are triangles. Due to this restriction, it is possible to define the lower oder trial functions in analogy with the two dimensional case. The nodal basis functions are given by the solution of local boundary value problems

$$\begin{gathered} -\Delta \psi_z = 0 \quad \text{in } K \quad \text{for all } K \in \mathcal{K}_h, \\ \psi_z(x) = \begin{cases} 1 & \text{for } x = z \\ 0 & \text{for } x \in \mathcal{N}_h \setminus \{z\} \end{cases}, \\ \psi_z \text{ is linear on each face of the mesh.} \end{gathered}$$

Here, the only difference to the two dimensional case is that the word 'edge' is replaced by the word 'face'. Since all faces are triangles, we are able to prescribe linear data on them such that ψ_z is continuous on the boundary of each element, i.e. $\psi_z \in C^0(\partial K)$ for $K \in \mathcal{K}_h$. This construction is not possible for general polygonal faces. Obviously, the triangulations of the element surfaces admit a boundary mesh $\mathcal{B}_h(K)$ of each $K \in \mathcal{K}_h$. This discretization of ∂K can be used directly in the three dimensional boundary element method discussed in Section 1.6. Following the same steps as in Section 2.1, we can set up the FEM system. For a piecewise constant material coefficient, the volume integral in the bilinear form of the variational formulation is reduced to integrals over the boundaries of the elements by the use of Green's first identity. Then, the product of the Dirichlet and Neumann trace has to be integrated. Finally, it turns out that the discretization of the symmetric Steklov-Poincaré operator multiplied by the constant coefficient serves as local stiffness matrix in the set up of the global finite element matrix.

Nevertheless, the restriction to polyhedra with triangular faces is not desirable. It is more convenient to work directly with polyhedral elements that have arbitrary polygonal faces. Of course, it is always possible to introduce triangulations of the surfaces, but this adds additional nodes to the mesh. Therefore, the number of degrees of freedom in the finite element computation is increased. These nodes might improve the accuracy of the approximation but they are artificial and spoil the idea of arbitrary polyhedral elements.

In the following, we give a generalization that copes with polygonal faces of polyhedral elements directly. For this reason, we go back to the two dimensional case and analyse the lower order trial functions again. We deal with a nodal trial function ψ_z. Thus, we set the value of the function equal to one at one node $z \in \mathcal{N}_h$ and equal to zero at every other node $x \in \mathcal{N}_h \setminus \{z\}$ of the mesh. Next, the datum in the nodes is used to extend the trial function linearly on the edges of the mesh. Finally, we use a harmonic extension of the data on the edges to get the functions inside the elements. Additionally, we observe that the linear extension of the nodal data to the edges is nothing else than a harmonic extension in the parameter space of the edge, i.e. we solve

$$\begin{aligned} -\psi_z'' &= 0 \quad \text{in } E \quad \text{for all } E \in \mathcal{E}_h, \\ \psi_z(x) &= \begin{cases} 1 & \text{for } x = z \\ 0 & \text{for } x \in \mathcal{N}_h \setminus \{z\} \end{cases}, \end{aligned}$$

where the derivatives are understood with respect to the linear parametrization of the edges. From this point of view, we start in the nodes, go to the edges and then into the elements. In each step, we extend the data from the previous step harmonically. Following these considerations, we are able to generalize the lower order trial functions to arbitrary dimension. The strategy is sketched in Figure 4.2. The values in the nodes are prescribed. Afterwards, we solve a Dirichlet problem for the Laplace equation on each edge in the corresponding parameter space. Then, we use the computed data as Dirichlet datum for the Laplace problem on each face, and finally we proceed with the Laplace problem on each

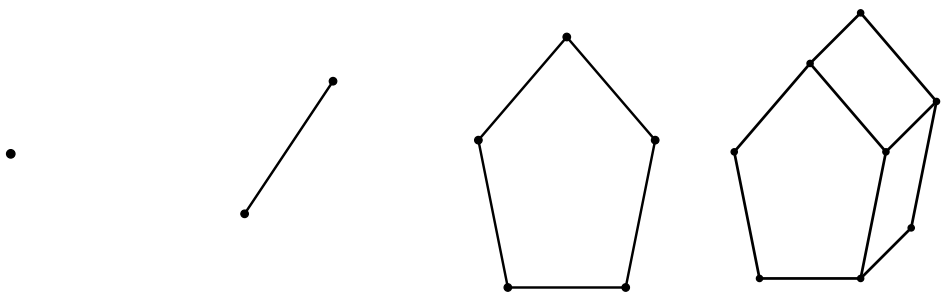

$\psi \in \{0, 1\}$ $\Delta_1 \psi = \psi'' = 0$ $\Delta_2 \psi = 0$ $\Delta_3 \psi = 0$

Figure 4.2: Stepwise construction of lower order trial functions

element, where the solutions on the faces are used as boundary values. Denoting the i-dimensional Laplace operator by Δ_i, we have for the trial function ψ_z, which belongs to $z \in \mathcal{N}_h$,

$$\begin{aligned} -\Delta_3 \psi_z &= 0 \quad \text{in } K \quad \text{for all } K \in \mathcal{K}_h, \\ -\Delta_2 \psi_z &= 0 \quad \text{in } F \quad \text{for all } F \in \mathcal{F}_h, \\ -\Delta_1 \psi_z &= 0 \quad \text{in } E \quad \text{for all } E \in \mathcal{E}_h, \\ \psi_z(x) &= \begin{cases} 1 & \text{for } x = z \\ 0 & \text{for } x \in \mathcal{N}_h \setminus \{z\} \end{cases}, \end{aligned}$$

where the Laplace operators have to be understood in the corresponding linear parameter spaces.

The trial functions restricted to one face are obviously the well known two dimensional trial functions from Section 2.1. Therefore, the trace of a trial function ψ_z on the boundary of K takes values between zero and one. Additionally, the Dirichlet datum on ∂K for the three dimensional Laplace problem is continuous. According to Theorem 6 of Section 1.4, we have

$$\psi_z \in C^0(\overline{K}) \cap C^2(K),$$

and ψ_z is even arbitrary smooth in the interior of K since it is harmonic. The maximum principle yields

$$0 < \psi_z < 1 \quad \text{in } K$$

for $z \in \mathcal{N}(K)$, and ψ_z has no local extrema inside of K unless it is constant. The only possibility for ψ_z to be constant over K is that $z \notin \mathcal{N}(K)$ and then we have $\psi_z \equiv 0$ on K. Consequently, the trial functions have local support. Due to the continuity of the trial functions over Ω, they belong to the Sobolev space $H^1(\Omega)$ and thus the later finite element computations yield conforming approximations. So, all desirable properties of the two dimensional case carry over to three dimensions.

At this point, we mention that for $K \in \mathcal{K}_h$ the functions ψ_z with $z \in \mathcal{N}(K)$ form barycentric coordinates, i.e. they satisfy (2.2) and (2.3) that are

$$\psi_z(x) \geq 0 \quad \text{on } \overline{K}$$

for $z \in \mathcal{N}(K)$ and

$$v = \sum_{z \in \mathcal{N}(K)} v(z) \psi_z$$

for any linear function v on $\overline{K}$. The first condition has been observed already and the second one follows in a similar way as in Section 2.1. A linear function restricted to an edge, face and an element fulfils the i-dimensional Laplace equation for $i = 1, 2, 3$, respectively. Since the right hand side of (2.3) also fulfils these equations and both sides coincide in the nodes $z \in \mathcal{N}(K)$, the equality follows because of the unique solvability of the Dirichlet problem for the Laplace

equation. More precisely, both sides of (2.3) coincides in the nodes and fulfil the Laplace equation on the edges, thus the equality holds on the edges. Since both sides are the same on the boundary of the faces and are harmonic on the faces, they are also equal in the interior of the faces. Finally, (2.3) holds on the whole element K because both sides fulfil the Laplace equation on the element and coincide on ∂K. A consequence of this property is that the pointwise interpolation with lower order trial functions is exact for linear polynomials and that the functions ψ_z for $z \in \mathcal{N}_h$ form a partition of unity over Ω. This statement has been proven in Lemma 5 for the two dimensional case.

The presented idea, how to generalize the lower order trial functions of the BEM-based finite element method for the model problem, can be transfered to other boundary value problems. In [21, 41], Helmholtz, Maxwell and convection-diffusion-reaction problems are considered. The trial functions are defined locally as solution of the underlying differential equation with constant material coefficients on each element, where piecewise linear data on the triangulation of the element boundary is prescribed. Instead of this boundary data, it might be advantageous to use the stepwise definition presented above and to work directly on the polygonal faces of the elements.

In the model problem, the underlying differential equation with piecewise constant coefficients and homogeneous right hand side reduces to the Laplace equation. In the general case of other boundary value problems, we obtain corresponding differential equations. These equations can be used to define the trial functions successively on the edges, faces and elements. Starting from the nodal values, boundary value problems are solved step by step in the corresponding parameter spaces of the edges, faces and elements. Here, the previously computed data is used as Dirichlet datum in the next step. Due to this construction the trial functions already capture some properties of the solution of the boundary value problem and therefore may improve the finite element computations. For example, this may enhance the stability in the convection-diffusion problem analysed in [41] even further.

4.2 Numerical considerations

The theoretical construction of the trial space in the three dimensional case has been discussed in the last section. Nevertheless, the numerical realization of these implicitly defined functions is still unclear. Whereas we have had to solve only local problems on the elements in the two dimensional setting, we now have to deal with problems on the faces as well as on the elements. When other partial differential equations are considered beside the model problem, we even have to solve boundary value problems on the edges. But for the current presentation, we restrict ourselves to the model problem and only mention necessary modifications for other problems.

As before, we make use of the boundary element method to approximate the nodal trial functions ψ_z in the interior of the elements. The approximation of ψ_z

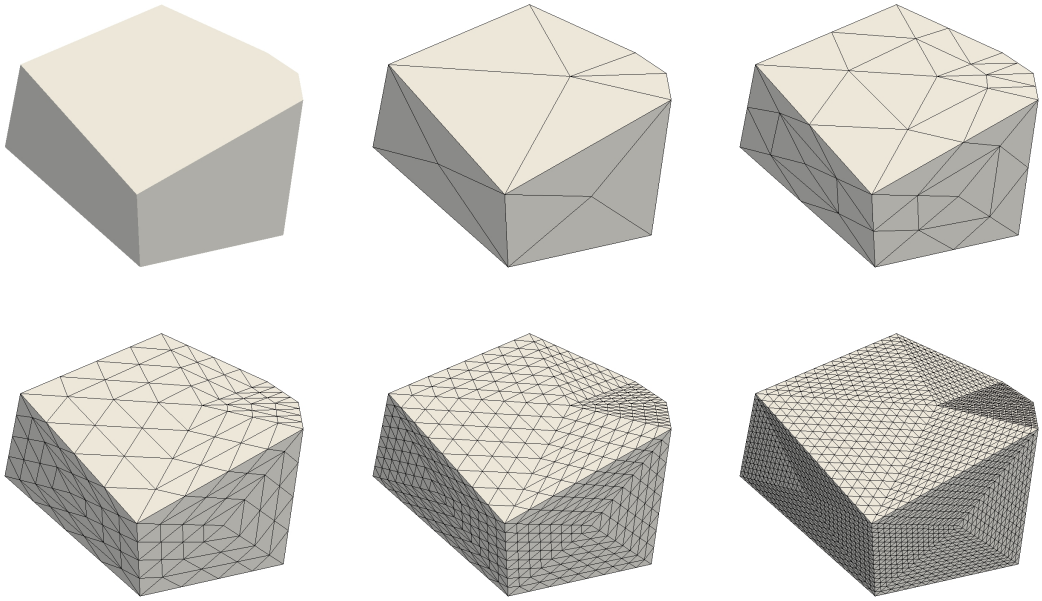

Figure 4.3: Polyhedral element and surface triangulations of level $l = 0, \ldots, 4$

on the surfaces of the elements can also be done with a two dimensional boundary element method in the parameter space of the faces. But it is more suitable to discretize the trial functions by a finite element method on the faces of the mesh. The advantage of this choice can be seen later.

For the realization of the two dimensional finite element method, triangulations of the faces are needed. For each $F \in \mathcal{F}_h$, we introduce a mesh $\mathcal{B}_h(F)$ of level l. The coarsest mesh with $l = 0$ is obtained by connecting the nodes $z \in \mathcal{N}(F)$ with the point

$$z_F = \frac{1}{|\mathcal{N}(F)|} \sum_{z \in \mathcal{N}(F)} z.$$

Afterwards, the meshes of level $l \geq 1$ are defined recursively by splitting each triangle of the previous level into four similar triangles. So, the midpoints of the sides of a triangle are connected successively, see Figure 4.3. The set of nodes in the triangular mesh is denoted by $\mathcal{M}_h(F)$. Obviously, we can combine the discretizations of the faces to a triangulation of the whole surface of an element $K \in \mathcal{K}_h$ by setting

$$\mathcal{B}_h(K) = \bigcup_{F \in \mathcal{F}(K)} \mathcal{B}_h(F) \quad \text{and} \quad \mathcal{M}_h(K) = \bigcup_{F \in \mathcal{F}(K)} \mathcal{M}_h(F).$$

Due to the construction, the surface mesh $\mathcal{B}_h(K)$ is conforming.

Now, we address the approximation of the trace of a trial function ψ_z, $z \in \mathcal{N}_h$ on a face $F \in \mathcal{F}_h$ with $z \in \mathcal{N}(F)$. For the finite element computations on the

face, we additionally need a trial space. Its basis $\Phi_D(F)$ and the trial functions φ_z for $z \in \mathcal{M}_h(F)$ are defined by

$$\varphi_z = \begin{cases} 1, & \text{at } z \\ \text{linear}, & \text{on } T \in \mathcal{B}_h(F) \\ 0, & \text{at } x \in \mathcal{M}_h(F) \setminus \{z\} \end{cases} \qquad \text{and} \quad \Phi_D(F) = \{\varphi_z : z \in \mathcal{M}_h(F)\}.$$

We approximate the trace of the trial function ψ_z by

$$g_z^F = \sum_{\varphi \in \Phi_D(F)} g_\varphi \varphi$$

where the coefficients g_φ which belong to $\varphi = \varphi_x$ with $x \in \partial F$ are fixed such that g_z^F coincides with the piecewise linear data of ψ_z on the edges of the face F. Consequently, we obtain the discrete Galerkin formulation

$$\text{Find } g_z^F : \quad \sum_{x \in \mathcal{M}_h(F)} g_{\varphi_x} \int_F \nabla \varphi_x \cdot \nabla \varphi_y = 0, \quad \forall y \in \mathcal{M}_h(F) : y \notin \partial F,$$

for the approximation of the trace of ψ_z on $F \in \mathcal{F}_h$, where $z \in \mathcal{N}(F)$. According to Section 1.3, this formulation admits a unique solution and the corresponding system of linear equations can be solved by a conjugate gradient method. Changing the level of the face discretization, the accuracy of the finite element approximation can be adapted.

To get an approximation g_z^K of the trace of ψ_z on the whole boundary of an element $K \in \mathcal{K}_h$, the Dirichlet problems on the faces $F \in \mathcal{F}(K)$ are solved successively. Afterwards, these approximations are combined to

$$g_z^K = \sum_{\varphi \in \Phi_D(K)} g_\varphi \varphi \quad \text{with} \quad \Phi_D(K) = \bigcup_{F \in \mathcal{F}(K)} \Phi_D(F).$$

So, we obtain a piecewise linear and globally continuous approximation of the Dirichlet trace $\gamma_0^K \psi_z$ over the surface triangulation $\mathcal{B}_h(K)$.

Next, we use the computed Dirichlet trace as boundary datum for the Laplace problem on the element to find an approximation of the trial function ψ_z in the interior of the element $K \in \mathcal{K}_h$. For this purpose the boundary element method is applied. At this point, it becomes clear why we have chosen a finite element discretization of the faces. The surface mesh $\mathcal{B}_h(K)$ and the trial functions on the boundary ∂K for the two dimensional finite element method fit into the theory of the boundary element method in Section 1.6. Following the ideas given there, we obtain an approximation t_z^K of the Neumann trace $\gamma_1^K \psi_z$ in the form

$$t_z^K = \sum_{\tau \in \Phi_N(K)} t_\tau \tau,$$

where for $T \in \mathcal{B}_h(K)$

$$\tau_T^0 = \begin{cases} 1, & \text{in } T \\ 0, & \text{else} \end{cases} \qquad \text{and} \qquad \Phi_N(K) = \{\tau_T^0 : T \in \mathcal{B}_h(K)\}.$$

Referring to the coefficient vectors of the approximations with an underline, we have

$$\underline{t}_z^K = \mathbf{V}_{K,h}^{-1}(\tfrac{1}{2}\mathbf{M}_{K,h} + \mathbf{K}_{K,h})\underline{g}_z^K \tag{4.1}$$

with the well known boundary element matrices of the single layer and the double layer potential as well as the mass matrix.

For each element $K \in \mathcal{K}_h$, the approximations of the Dirichlet and Neumann traces of the trial functions ψ_z with $z \in \mathcal{N}(K)$ are gathered in the matrices

$$D_K = \left(\underline{g}_z^K \right)_{z\in\mathcal{N}(K)} \qquad \text{and} \qquad N_K = \left(\underline{t}_z^K \right)_{z\in\mathcal{N}(K)}$$

such that each column corresponds to the datum of one ψ_z. The relation (4.1) turns into

$$N_K = \mathbf{V}_{K,h}^{-1}(\tfrac{1}{2}\mathbf{M}_{K,h} + \mathbf{K}_{K,h})D_K.$$

For a better understanding, we give the dimensions of the matrices.

$$\begin{aligned} \mathbf{V}_{K,h} &\in \mathbb{R}^{|\mathcal{B}_h(K)|\times|\mathcal{B}_h(K)|} & D_K &\in \mathbb{R}^{|\mathcal{M}_h(K)|\times|\mathcal{N}(K)|} \\ \mathbf{K}_{K,h} &\in \mathbb{R}^{|\mathcal{B}_h(K)|\times|\mathcal{M}_h(K)|} & N_K &\in \mathbb{R}^{|\mathcal{B}_h(K)|\times|\mathcal{N}(K)|} \\ \mathbf{M}_{K,h} &\in \mathbb{R}^{|\mathcal{B}_h(K)|\times|\mathcal{M}_h(K)|} \end{aligned}$$

In the global finite element computation, the number of degrees of freedom which correspond to the element K is $|\mathcal{N}(K)|$. For the local computations, we use $|\mathcal{B}_h(K)|$ degrees of freedom to approximate the Neumann trace of each trial function and the Dirichlet trace is represented by $|\mathcal{M}_h(K)|$ coefficients. Obviously, we have

$$|\mathcal{N}(K)| \le |\mathcal{M}_h(K)| \qquad \text{and} \qquad |\mathcal{F}(K)| \le |\mathcal{B}_h(K)|.$$

Since we know how to approximate the Dirichlet and Neumann data of the trial functions, the set up of the global finite element method can be addressed. We assume that the material coefficient is constant on each element such that

$$a(x) = a_K \quad \text{for } x \in K \text{ and } K \in \mathcal{K}_h,$$

or it is approximated by a piecewise constant function. The Galerkin formulation is treated in a similar way as in the two dimensional case of the lower order method in Section 2.1. We set

$$\Psi^{(1)} = \{\psi_z : z \in \mathcal{N}_h\} \quad \text{as well as} \quad \Psi_D = \{\psi_z : z \in \mathcal{N}_{h,D}\},$$

and we introduce the trial space

$$V_h = \operatorname{span}\Psi \quad \text{with} \quad \Psi = \Psi^{(1)} \setminus \Psi_D.$$

The discrete Galerkin formulation (1.5) for $u_h = u_{0h} + u_{Dh}$ with

$$u_{0h} = \sum_{\psi\in\Psi} \beta_\psi \psi \quad \text{and} \quad u_{Dh} = \sum_{\psi\in\Psi_D} \beta_\psi \psi$$

reads

$$\sum_{\psi\in\Psi} \beta_\psi \, a_\Omega(\psi,\phi) = (f,\phi) + (g_N,\phi)_{\Gamma_N} - \sum_{\psi\in\Psi_D} \beta_\psi \, a_\Omega(\psi,\phi) \quad \text{for } \phi \in \Psi,$$

where u_{Dh} is the discrete extension of the boundary data g_D in the model problem (1.1). As in Section 2.1, the main task is to study the bilinear form $a_\Omega(\cdot,\cdot)$ applied to trial functions out of $\Psi^{(1)}$. The integrals (f,ϕ) and $(g_N,\phi)_{\Gamma_N}$ are treated again with an appropriate numerical quadrature.

In analogy to the former case, we can derive element stiffness matrices which involve the symmetric discretizations of the local Steklov-Poincaré operators. Nevertheless, we present an alternative approach such that we do not have to set up the matrix $\mathbf{D}_{K,h}$ of the hypersingular integral operator. Let $\psi,\phi \in \Psi^{(1)}$, it is

$$a_\Omega(\psi,\phi) = \sum_{K\in\mathcal{K}_h} a_K \int\limits_K \nabla\psi\cdot\nabla\phi = \sum_{K\in\mathcal{K}_h} \frac{a_K}{2}\left(\int\limits_{\partial K} \gamma_1^K\psi\gamma_0^K\phi + \int\limits_{\partial K} \gamma_1^K\phi\gamma_0^K\psi \right)$$

according to Green's first identity (1.11) and since ψ as well as ϕ are harmonic on each element $K \in \mathcal{K}_h$. Obviously, there are $x,z \in \mathcal{N}_h$ such that $\psi = \psi_x$ and $\phi = \psi_z$ and if there is no $K \in \mathcal{K}_h$ with $x,z \in \mathcal{N}(K)$ we have $a_\Omega(\psi,\phi) = 0$. On the other hand, for each $K \in \mathcal{K}_h$ with $x,z \in \mathcal{N}(K)$ we get the approximations g_x^K, g_z^K for the Dirichlet traces and t_x^K, t_z^K for the Neumann traces of the trial functions ψ_x and ψ_z out of the matrices D_K and N_K, respectively. For the integrals in the representation above of the bilinear form, we choose the approximation

$$\int\limits_{\partial K} \gamma_1^K\psi_x\gamma_0^K\psi_z \approx \int\limits_{\partial K} t_x^K g_z^K = \sum_{\tau\in\Phi_N(K)} t_\tau \sum_{\varphi\in\Phi_D(K)} g_\varphi(\tau,\varphi)_{L_2(\partial K)} = \left(\underline{t}_x^K\right)^\top \mathbf{M}_{K,h}\, \underline{g}_z^K$$

with the mass matrix $\mathbf{M}_{K,h}$ defined as in Section 1.6. This yields the symmetric approximation

$$a_\Omega(\psi_x,\psi_z) \approx \sum_{K\in\mathcal{K}_h} \frac{a_K}{2}\left(\left(\underline{t}_x^K\right)^\top \mathbf{M}_{K,h}\, \underline{g}_z^K + \left(\underline{t}_z^K\right)^\top \mathbf{M}_{K,h}\, \underline{g}_x^K \right), \tag{4.2}$$

where the coefficient vectors are identical to zero if $x \notin \mathcal{N}(K)$ and $z \notin \mathcal{N}(K)$, respectively. Consequently, we use the local matrix

$$N_K^\top \mathbf{M}_{K,h}\, D_K \in \mathbb{R}^{|\mathcal{N}(K)|\times|\mathcal{N}(K)|}$$

for each $K \in \mathcal{K}_h$ to set up the global finite element matrix. Due to the symmetric approximation (4.2) of the bilinear form, we obtain a symmetric system matrix in the finite element method which is sparse and positive definite. Therefore, the conjugate gradient method is applied to get a solution of the system of linear equations.

In a post processing step, it might be interesting to evaluate the approximation u_h in some points. This is done with the help of the representation formula (1.16). Suppose, we want to evaluate u_h in a point $x \in K$ for same $K \in \mathcal{K}_h$.

Then, we obtain the approximation of the Dirichlet trace and the Neumann trace of u_h on the boundary of K as linear combinations of the columns in D_K and N_K, respectively. These approximations are inserted into the representation formula and the integrals therein can be computed analytically, see [68].

Finally, we summarize the steps which are needed to set up the system of linear equations in the presented finite element method. The trial functions are given by the values, one or zero, at the nodes of the mesh. In the case of the model problem, they are linear on the edges of the mesh. Otherwise, we choose the discretization level of the faces larger than one, i.e. $l > 1$. Therefore, we also obtain a discretization of the edges and the underlying boundary value problems can be solved on each edge to get the data of the trial functions on the edges. Afterwards, we solve the corresponding Dirichlet problem on every face $F \in \mathcal{F}_h$ for each node $z \in \mathcal{N}(F)$. Additionally, the boundary element matrices are set up for every element $K \in \mathcal{K}_h$. These computations can be done in parallel since there are no dependences between the calculations. The Dirichlet datum of the trial functions are gathered in the matrices D_K and the Neumann datum

$$N_K = \mathbf{V}_{K,h}^{-1}(\tfrac{1}{2}\mathbf{M}_{K,h} + \mathbf{K}_{K,h})D_K$$

is computed. After these preprocessing steps, the global finite element matrix is assembled with the help of the local matrices $N_K^\top \mathbf{M}_{K,h}\, D_K$ and the right hand side is set up.

4.3 Numerical experiments

All numerical examples in this section are formulated on the unite cube. As discretization, we utilize Voronoi meshes which are an example of polyhedral meshes. In Figure 4.4, the first meshes of the sequence for the convergence experiments are visualized. We see that the elements are non-trivial polyhedra with arbitrary polygonal faces. The meshes have been produced by generating random points according to [29] and constructing the corresponding Voronoi diagram in accordance with [28]. In the set up of the local boundary element matrices, we use a semi analytical integration scheme. The inner integral in the Galerkin matrices is evaluated analytically and the outer one is approximated by Gaussian quadrature. First of all, we give a simple example and visualize the approximation.

Example 7. The function $u(x) = -\frac{1}{6}\big((x_1-0.8)^2+(x_2-0.7)^2+(x_3-0.6)^2-3\big)$, $x \in \mathbb{R}^3$ fulfils

$$\begin{aligned} -\Delta u &= 1 \quad && \text{in } \Omega = (0,1)^3, \\ u &= g_D && \text{on } \Gamma \end{aligned}$$

with $g_D = \gamma_0 u$. We apply the proposed generalization of the BEM-based finite element method to three space dimension on the upper right mesh of Figure 4.4 with a discretization level $l = 1$ of the faces. In Figure 4.5, the approximation of the solution is visualized.

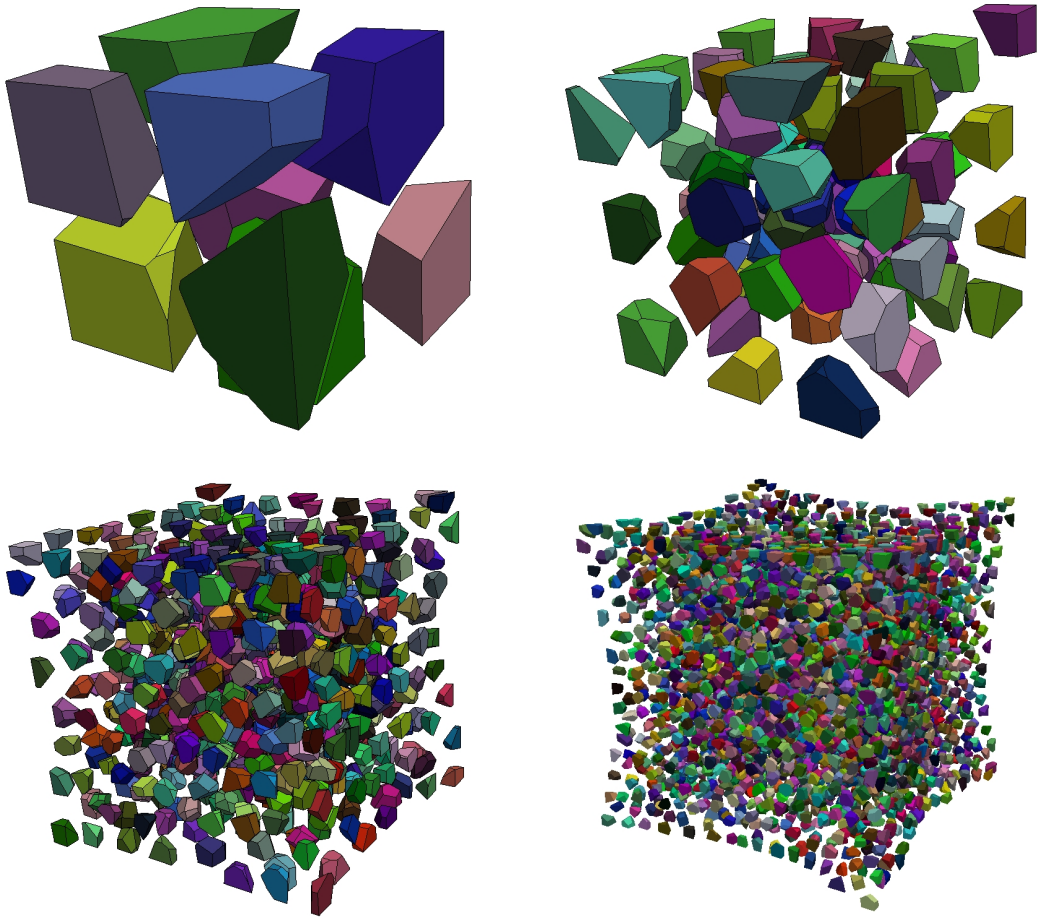

Figure 4.4: Sequence of Voronoi meshes

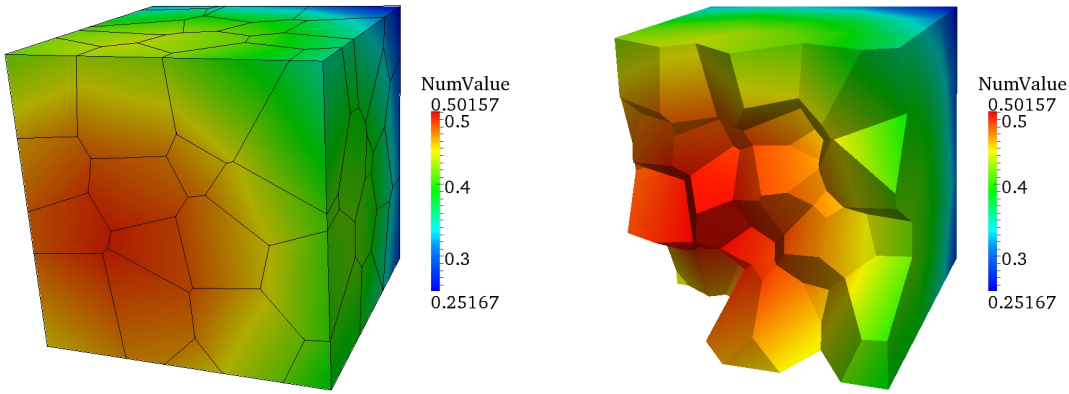

Figure 4.5: Approximation of the solution in Example 7 on the whole cube (left) and on a cut of the cube along element faces (right)

In Table 4.1, we sketch the number of elements $|\mathcal{K}_h|$ and the number of nodes $|\mathcal{N}_h|$ in the different Voronoi meshes. The proposed strategy approximates the solution by as many trial function as nodes are in the mesh. Therefore the number of degrees of freedom in the finite element method is $|\mathcal{N}_h|$ minus the number of nodes on the Dirichlet boundary Γ_D. The method proposed in [20] needs to triangulate the surfaces of the elements and the number of trial functions corresponds to the total number of nodes after the triangulation. In Table 4.1, this total number of nodes is listed in the case that the faces are triangulated with the level $l = 0, 1, 2$. We recognize that in this situation much more trial functions and thus degrees of freedom are required in the global computations. Roughly speaking, the number of nodes doubles if the coarsest discretization of the faces is used. If a finer triangulation is needed, the number of nodes and thus the number of degrees of freedom increase ten times for $l = 1$ and even more than forty times for $l = 2$. Since the diameter of the elements are equivalent in all four situations, the approximation errors of the finite element computations are of the same order. Therefore, the method proposed in this chapter is favourable because it has the smallest system matrix in the global finite element method. The dimension of this matrix is DoF $\times$ DoF, where DoF denotes the number of degrees of freedom which corresponds to $|\mathcal{N}_h|$ minus the nodes on the Dirichlet boundary Γ_D.

$\lvert\mathcal{K}_h\rvert$	$\lvert\mathcal{N}_h\rvert$	$l = 0$	$l = 1$	$l = 2$
9	46	98	424	1790
76	416	905	4170	18011
712	4186	9081	42446	184170
1316	7850	17013	79676	345903
5606	34427	74457	349663	1519143
26362	164915	356189	1675171	7280603

Table 4.1: Total number of nodes when working with triangulated surfaces

In the following, we investigate the influence of the face discretization. These triangulations of the faces are required to approximate the traces of the trial functions on the faces with the local two dimensional finite element methods and later in the boundary element computations. The finer the discretization is chosen the better is the approximation of the traces and thus the approximation of the trial functions. Even though the face discretization does not blow up the global system matrix, the computational effort for the local problems increases if the discretization level l is raised. In Table 4.2, we give the number of nodes $|\mathcal{N}_h|$ in the global mesh as well as the number of additional nodes coming from the triangulation of the faces. As one example, we pick the element K from Figure 4.3 and list the number of nodes $|\mathcal{M}_h(K)|$ and the number of triangles $|\mathcal{B}_h(K)|$ in the surface discretization of K for different levels l in Table 4.3. In the next example, we analyse the rates of convergence for different values of l.

$\lvert\mathcal{K}_h\rvert$	$\lvert\mathcal{N}_h\rvert$	$l=0$	$l=1$	$l=2$
9	46	52	378	1744
76	416	489	3754	17595
712	4186	4895	38260	179984
1316	7850	9163	71826	338053
5606	34427	40030	315236	1484716
26362	164915	191274	1510256	7115688

Table 4.2: Number of additional nodes coming from the face discretization

$\lvert\mathcal{N}(K)\rvert$	l	$\lvert\mathcal{M}_h(K)\rvert$	$\lvert\mathcal{B}_h(K)\rvert$
12	0	20	36
	1	74	144
	2	290	576
	3	1154	2304
	4	4610	9216

Table 4.3: Number of nodes $\lvert\mathcal{M}_h(K)\rvert$ and number of triangles $\lvert\mathcal{B}_h(K)\rvert$ in the surface discretization of the element in Figure 4.3 for different levels

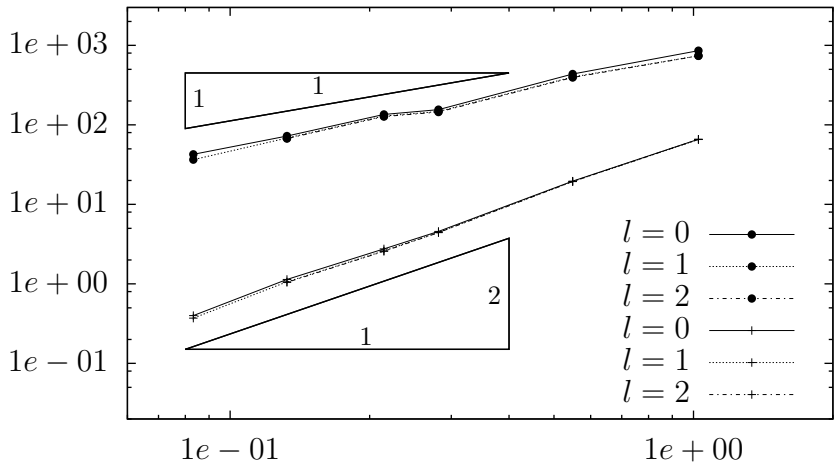

Figure 4.6: Absolute error in $\|\cdot\|_E$ ($\bullet$) and $\|\cdot\|_{L_2(\Omega)}$ ($+$) with respect to h for $l=0,1,2$ in Example 8 and triangles with slope one and two

Example 8. Consider the Dirichlet boundary value problem

$$\begin{aligned} -\Delta u &= 0 \quad \text{in } \Omega = (0,1)^3, \\ u &= g_D \quad \text{on } \Gamma \end{aligned}$$

with $g_D = \gamma_0 u$ such that

$$u(x) = e^{2\sqrt{2}\pi(x_1-0.3)} \cos(2\pi(x_2-0.3)\sin(2\pi(x_3-0.3), \quad x \in \mathbb{R}^3$$

is the exact solution. In Figure 4.6, the approximation errors $\|u-u_h\|_E$ and $\|u-u_h\|_{L_2(\Omega)}$ are given with respect to $h = \max\{h_K : K \in \mathcal{K}_h\}$ in a logarithmic plot for different discretization levels $l = 0, 1, 2$ of the faces.

This example has shown that the discretization level of the faces does not influence the rates of convergence. Therefore, the coarsest face discretization with $l = 0$ is sufficient to analyse the convergence rates in the forthcoming numerical experiments. Due to this choice, the local complexity in the two dimensional finite element method on the faces $F \in \mathcal{F}_h$ and the local boundary element methods on the elements $K \in \mathcal{K}_h$ is rather small. Furthermore, in Figure 4.6, we recognize linear convergence for the approximation error measured in the energy norm and quadratic convergence if the error is measured in the L_2-norm. This is the first numerical experiment in three space dimensions which confirms the rates of convergence for the BEM-based finite element method on Voronoi meshes with polyhedral elements and arbitrary polygonal faces.

Beside the Dirichlet problem for the Laplace equation, we also give examples for the Poisson problem and the case of a non-constant material parameter.

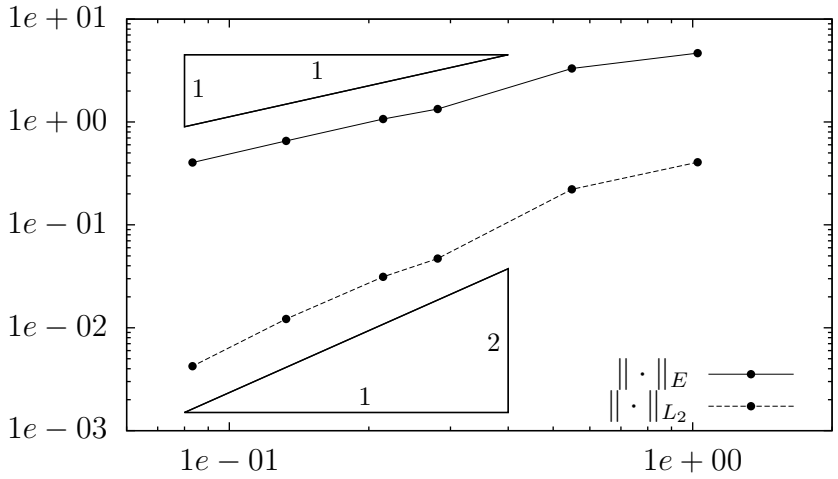

Figure 4.7: Absolute error with respect to h for Example 9 with $l = 0$ and triangles with slope one and two

Example 9. The function $u(x) = \cos(\pi x_1)\sin(2\pi x_2)\sin(3\pi x_3)$, $x \in \mathbb{R}^3$ fulfils the boundary value problem

$$\begin{aligned} -\Delta u &= f \quad \text{in } \Omega = (0,1)^3, \\ u &= g_D \quad \text{on } \Gamma \end{aligned}$$

with $f = 14\pi^2 u$ and $g_D = \gamma_0 u$ fixed. In Figure 4.7, the errors $\|u - u_h\|_E$ and $\|u - u_h\|_{L_2(\Omega)}$ are shown with respect to $h = \max\{h_K : K \in \mathcal{K}_h\}$ in logarithmic scale.

Example 10. We take the two functions already considered in Example 8 and 9 and label them by u_1 and u_2, respectively. They fulfil the boundary value problems

$$\begin{aligned} -\operatorname{div}\left((\tfrac{7}{2} - x_1 - x_2 - x_3)\nabla u_i\right) &= f_i \quad \text{in } \Omega = (0,1)^3, \\ u_i &= g_{iD} \quad \text{on } \Gamma \end{aligned}$$

for $i = 1, 2$, where f_i and g_{iD} have to be chosen appropriately. In Figure 4.8, the approximation errors $\|u_i - u_{ih}\|_E$ and $\|u_i - u_{ih}\|_{L_2(\Omega)}$ are shown with respect to $h = \max\{h_K : K \in \mathcal{K}_h\}$ in logarithmic scale for $i = 1, 2$.

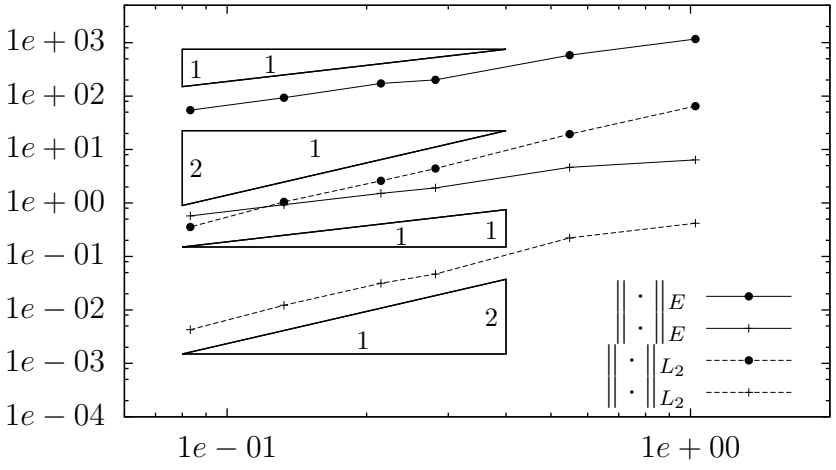

Figure 4.8: Absolute error $\|u_i - u_{ih}\|$ for $i = 1$ (•) and $i = 2$ (+) with respect to h for Example 10 and triangles with slope one and two

In the final two examples, we have also obtained optimal rates of convergence for the finite element approximation. So, the method yields linear convergence in the energy norm and quadratic convergence in the L_2-norm. This behaviour together with the flexibility of the polyhedral meshes and the conforming approximations makes the BEM-based finite element method an interesting and attractive strategy for ongoing research.

Conclusion

The presented finite element method with local Trefftz trial functions is a new strategy based on the idea in the recent publication [20]. We have given several novel developments that belong to the first extensions of the primal strategy. The introduced lower as well as higher order trial functions admit optimal rates of convergence on polygonal meshes. This approach, also called BEM-based FEM, yields conforming approximations on these arbitrary meshes. Thus, the developments fit into the current research topics in several areas. We just mention the discontinuous Petrov-Galerkin methods, the mimetic finite difference methods, multiscale finite element methods and the topic of generalized barycentric coordinates in computer graphics. In all these methods the use of polygonal meshes and the generalization to higher order approximation is discussed in the latest literature as for example [11, 23, 30, 35, 61].

According to the definition of the trial functions, the BEM-based FEM is a generalization of several well known strategies. If the lower order method is applied to a mesh containing only triangles or quadrangles the standard linear and bilinear trial functions of finite element methods are recovered. In the case that the mesh consists of one element with many nodes on the boundary, we end up with the boundary element method. And finally, a domain decomposition method is obtained if the convergence is analysed with respect to the refinement that solely adds nodes to the boundaries of the elements in the mesh. Thus, the coupling between these established methods and the BEM-based FEM is straightforward.

The investigated method has a high potential for future research. We already stated the idea how to generalize the strategy to arbitrary order of convergence. Here, it has been essential to cope with the restriction to piecewise constant material coefficients in the differential equation for what we proposed a novel approximation. Additionally, the reliability of the residual error estimate has been proven which is the first step to efficient adaptive strategies. In adaptive finite element methods the use of polygonal meshes is very attractive since local refinements produce no additional difficulties. The class of functional analytic error estimates [62] is promising for general meshes, but $H(\mathrm{div})$-conforming trial functions are needed for the flux variables. Such trial functions are the topic of ongoing research in the context of BEM-based FEM for mixed formulations of elliptic problems.

The developments extend to the three dimensional case. We have introduced trial functions on polyhedral elements with polygonal faces which gen-

eralize present ideas in the literature. Due to the stepwise construction, these functions already capture some properties of the solution of the underlying differential equation. Thus, their application to convection-diffusion or other boundary value problems is auspicious.

Bibliography

[1] A. Abdulle and A. Nonnenmacher. Adaptive finite element heterogeneous multiscale method for homogenization problems. *Comput. Methods Appl. Mech. Engrg.*, 200(37-40):2710–2726, 2011.

[2] R. A. Adams. *Sobolev Spaces*. Academic Press, 1975.

[3] J.-P. Aubin. Behavior of the error of the approximate solutions of boundary value problems for linear elliptic operators by Gelerkin's and finite difference methods. *Ann. Scuola Norm. Sup. Pisa (3)*, 21:599–637, 1967.

[4] I. Babuška and A. K. Aziz. On the angle condition in the finite element method. *SIAM J. Numer. Anal.*, 13(2):214–226, 1976.

[5] I. Babuška and W. C. Rheinboldt. A-posteriori error estimates for the finite element method. *Int. J. Numer. Methods Eng.*, 12(10):1597–1615, 1978.

[6] I. Babuška and W. C. Rheinboldt. Error estimates for adaptive finite element computations. *SIAM J. Numer. Anal.*, 15(4):736–754, 1978.

[7] W. Bangerth and R. Rannacher. *Adaptive finite element methods for differential equations*. Lectures in Mathematics ETH Zürich. Birkhäuser Verlag, Basel, 2003.

[8] R. E. Bank and A. Weiser. Some a posteriori error estimators for elliptic partial differential equations. *Math. Comp.*, 44(170):283–301, 1985.

[9] R. Becker, P. Hansbo, and M. G. Larson. Energy norm a posteriori error estimation for discontinuous Galerkin methods. *Comput. Meth. Appl. Mech. Eng.*, 192(5-6):723–733, 2003.

[10] L. Beirão da Veiga. A residual based error estimator for the mimetic finite difference method. *Numer. Math.*, 108(3):387–406, 2008.

[11] L. Beirão da Veiga, K. Lipnikov, and G. Manzini. Arbitrary-order nodal mimetic discretizations of elliptic problems on polygonal meshes. *SIAM J. Numer. Anal.*, 49(5):1737–1760, 2011.

[12] P. Binev, W. Dahmen, and R. DeVore. Adaptive finite element methods with convergence rates. *Numer. Math.*, 97(2):219–268, 2004.

[13] D. Braess and J. Schöberl. Equilibrated residual error estimator for edge elements. *Math. Comp.*, 77(262):651–672, 2008.

[14] F. Brezzi, K. Lipnikov, and M. Shashkov. Convergence of the mimetic finite difference method for diffusion problems on polyhedral meshes. *SIAM J. Numer. Anal.*, 43(5):1872–1896, 2005.

[15] V. I. Burenkov. *Sobolev spaces on domains*, volume 137. BG Teubner, 1998.

[16] C. Carstensen and C. Merdon. Estimator competition for Poisson problems. *J. Comput. Math.*, 28(3):309–330, 2010.

[17] J. M. Cascon, C. Kreuzer, R. H. Nochetto, and K. G. Siebert. Quasi-optimal convergence rate for an adaptive finite element method. *SIAM J. Numer. Anal.*, 46(5):2524–2550, 2008.

[18] P. G. Ciarlet. *The Finite Element Method for Elliptic Problems*. North-Holland, Amsterdam, 1978.

[19] Ph. Clément. Approximation by finite element functions using local regularization. *Rev. Française Automat. Informat. Recherche Opérationnelle Sér. RAIRO Analyse Numérique*, 9(R-2):77–84, 1975.

[20] D. Copeland, U. Langer, and D. Pusch. From the boundary element domain decomposition methods to local Trefftz finite element methods on polyhedral meshes. In *Domain decomposition methods in science and engineering XVIII*, volume 70 of *Lect. Notes Comput. Sci. Eng.*, pages 315–322. Springer, Berlin, 2009.

[21] D. M. Copeland. Boundary-element-based finite element methods for Helmholtz and Maxwell equations on general polyhedral meshes. *Int. J. Appl. Math. Comput. Sci*, 5(1):60–73, 2009.

[22] S. Dekel and D. Leviatan. The Bramble-Hilbert lemma for convex domains. *SIAM J. Math. Anal.*, 35(5):1203–1212, 2004.

[23] L. Demkowicz and J. Gopalakrishnan. Analysis of the DPG method for the Poisson equation. *SIAM J. Numer. Anal.*, 49(5):1788–1809, 2011.

[24] P. Deuflhard, P. Leinen, and H. Yserentant. Concepts of an adaptive hierarchical finite element code. *Impact Comput. Sci. Engrg*, 1:3–35, 1989.

[25] V. Dolejší, M. Feistauer, and V. Sobotíková. Analysis of the discontinuous Galerkin method for nonlinear convection-diffusion problems. *Comput. Methods Appl. Mech. Engrg.*, 194(25-26):2709–2733, 2005.

[26] W. Dörfler. A convergent adaptive algorithm for Poisson's equation. *SIAM J. Numer. Anal.*, 33(3):1106–1124, 1996.

[27] W. Dörfler and O. Wilderotter. An adaptive finite element method for a linear elliptic equation with variable coefficients. *ZAMM - Z. Angew. Math. Mech.*, 80(7):481–491, 2000.

[28] M. S. Ebeida and S. A. Mitchell. Uniform random voronoi meshes. In *Proceedings of the 20th International Meshing Roundtable*, pages 273–290. Springer Berlin Heidelberg, 2012.

[29] M. S. Ebeida, S. A. Mitchell, A. Patney, A. Davidson, and J. D. Owens. A simple algorithm for maximal Poisson-disk sampling in high dimensions. *Comput. Graph. Forum*, 31, 2012.

[30] Y. Efendiev, J. Galvis, and X.-H. Wu. Multiscale finite element methods for high-contrast problems using local spectral basis functions. *J. Comput. Phys.*, 230(4):937–955, 2011.

[31] Y. Efendiev and T. Y. Hou. *Multiscale Finite Element Methods – Theory and Applications*, volume 4 of *Surveys and Tutorials in the Applied Mathematical Sciences*. Springer, New York, 2009.

[32] M. Floater, K. Hormann, and G. Kós. A general construction of barycentric coordinates over convex polygons. *Adv. Comput. Math.*, 24:311–331, 2006.

[33] H. Gajewski, K. Gröger, and K. Zacharias. *Nichtlineare Operatorgleichungen und Operatordifferential-Gleichungen*. Akademie-Verlag, Berlin, 1974.

[34] D. Gilbarg and N. S. Trudinger. *Elliptic partial differential equations of second order*, volume 224. Springer Verlag, 1977.

[35] A. Gillette, A. Rand, and C. Bajaj. Error estimates for generalized barycentric interpolation. *Adv. Comput. Math.*, pages 1–23, 2011.

[36] P. Grisvard. *Elliptic problems in nonsmooth domains*. Monographs and studies in mathematics. Pitman Advanced Pub. Program, 1985.

[37] P. Grisvard. *Singularities in boundary value problems*, volume 22 of *Recherches en Mathématiques Appliquées [Research in Applied Mathematics]*. Masson, Paris, 1992.

[38] I. Herrera. Trefftz method: A general theory. *Numer. Meth. Part Differ. Equ.*, 16(6):561–580, 2000.

[39] C. Hofreither. L_2 error estimates for a nonstandard finite element method on polyhedral meshes. *J. Numer. Math.*, 19(1):27–39, 2011.

[40] C. Hofreither, U. Langer, and C. Pechstein. Analysis of a non-standard finite element method based on boundary integral operators. *Electron. Trans. Numer. Anal.*, 37:413–436, 2010.

[41] C. Hofreither, U. Langer, and C. Pechstein. A non-standard finite element method for convection-diffusion-reaction problems on polyhedral meshes. *AIP Conference Proceedings*, 1404(1):397–404, 2011.

[42] G. C. Hsiao and W. L. Wendland. Domain decomposition in boundary element methods. In *Fourth International Symposium on Domain Decomposition Methods for Partial Differential Equations (Moscow, 1990)*, pages 41–49. SIAM, Philadelphia, PA, 1991.

[43] P. Joshi, M. Meyer, T. DeRose, B. Green, and T. Sanocki. Harmonic coordinates for character articulation. *ACM Trans. Graph.*, 26(3):71.1–71.9, 2007.

[44] R. B. Kellogg. Higher order singularities for interface problems. In *The mathematical foundations of the finite element method with applications to partial differential equations (Proc. Sympos., Univ. Maryland, Baltimore, Md., 1972)*, pages 589–602. Academic Press, New York, 1972.

[45] R. B. Kellogg. On the Poisson equation with intersecting interfaces. *Applicable Anal.*, 4:101–129, 1974/75. Collection of articles dedicated to Nikolai Ivanovich Muskhelishvili.

[46] V. D. Kupradze and M. A. Aleksidze. An approximate method of solving certain boundary-value problems. *Soobšč. Akad. Nauk Gruzin. SSR*, 30:529–536, 1963.

[47] P. D. Lax and A. N. Milgram. Parabolic equations. In *Contributions to the theory of partial differential equations*, Annals of Mathematics Studies, no. 33, pages 167–190. Princeton Univ. Pr., 1954.

[48] R. Lazarov, S. Repin, and S. K. Tomar. Functional a posteriori error estimates for discontinuous Galerkin approximations of elliptic problems. *Numer. Meth. Part Differ. Equ.*, 25(4):952–971, 2009.

[49] S. Martin, P. Kaufmann, M. Botsch, M. Wicke, and M. Gross. Polyhedral finite elements using harmonic basis functions. *Comput. Graph. Forum*, 27(5):1521–1529, 2008.

[50] W. C. H. McLean. *Strongly elliptic systems and boundary integral equations.* Cambridge Univ Pr, 2000.

[51] N. G. Meyers and J. Serrin. $H = W$. *Proc. Nat. Acad. Sci. U.S.A.*, 51:1055–1056, 1964.

[52] P. Morin, R. H. Nochetto, and K. S. Siebert. Data oscillation and convergence of adaptive FEM. *SIAM J. Numer. Anal.*, 38(2):466–488, 2001.

[53] P. Morin, K. G. Siebert, and A. Veeser. A basic convergence result for conforming adaptive finite elements. *Math. Models Methods Appl. Sci.*, 18(5):707–737, 2008.

[54] S. E. Mousavi and N. Sukumar. Numerical integration of polynomials and discontinuous functions on irregular convex polygons and polyhedrons. *Comput. Mech.*, 47:535–554, 2011.

[55] J. Nitsche. Ein Kriterium für die Quasi-Optimalität des Ritzschen Verfahrens. *Numer. Math.*, 11:346–348, 1968.

[56] L. E. Payne and H. F. Weinberger. An optimal Poincaré inequality for convex domains. *Arch. Rational Mech. Anal.*, 5:286–292, 1960.

[57] M. Petzoldt. Regularity results for Laplace interface problems in two dimensions. *Z. Anal. Anwendungen*, 20(2):431–455, 2001.

[58] M. Petzoldt. A posteriori error estimators for elliptic equations with discontinuous coefficients. *Adv. Comput. Math.*, 16(1):47–75, 2002.

[59] L. Prandtl. Erich Trefftz. *ZAMM - Z. Angew. Math. Mech.*, 17(1):i–iv, 1937.

[60] Q.-H. Qin. *The Trefftz finite and boundary element method*. WIT Press, Southampton, 2000.

[61] A. Rand, A. Gillette, and C. Bajaj. Quadratic serendipity finite elements on polygons using generalized barycentric coordinates. Cornell University Library e-print, arXiv:1109.3259, 2011.

[62] S. Repin. *A posteriori estimates for partial differential equations*, volume 4 of *Radon Series on Computational and Applied Mathematics*. Walter de Gruyter GmbH & Co. KG, Berlin, 2008.

[63] S. Rjasanow and O. Steinbach. *The fast solution of boundary integral equations*. Mathematical and analytical techniques with applications to engineering. Springer, 2007.

[64] R. M. Rustamov. Boundary element formulation of harmonic coordinates. Technical report, Department of Mathematics and Computer Science, Drew University, Madison, New Jersey, USA, 2008.

[65] S. Sauter and C. Schwab. *Boundary Element Methods*. Springer, 2011.

[66] E. Schlemmer, J. Steffan, W. M. Rucker, and K. R. Richter. Accuracy improvement using a modified Gauss-quadrature for integral-methods in electromagnetics. *IEEE Trans. Magn.*, 28:1755–1758, 1992.

[67] Y.-S. Smyrlis. Applicability and applications of the method of fundamental solutions. *Math. Comp.*, 78(267):1399–1434, 2009.

[68] O. Steinbach. *Numerical approximation methods for elliptic boundary value problems: finite and boundary elements*. Springer, 2007.

[69] G. Strang. Variational crimes in the finite element method. In *The mathematical foundations of the finite element method with applications to partial differential equations (Proc. Sympos., Univ. Maryland, Baltimore, Md., 1972)*, pages 689–710. Academic Press, New York, 1972.

[70] N. Sukumar and A. Tabarraei. Conforming polygonal finite elements. *Internat. J. Numer. Methods Engrg.*, 61(12):2045–2066, 2004.

[71] A. Tabarraei and N. Sukumar. Application of polygonal finite elements in linear elasticity. *Int. J. Comput. Methods*, 3(4):503–520, 2006.

[72] E. Trefftz. Ein Gegenstück zum Ritzschen Verfahren. In *Proceedings of the 2nd International Congress of Technical Mechanics*, pages 131–137. Orell Fussli Verlag, 1926.

[73] A. Veeser and R. Verfürth. Poincaré constants for finite element stars. *IMA J. Numer. Anal.*, 32(1):30–47, 2012.

[74] R. Verfürth. *A review of a posteriori error estimation and adaptive mesh-refinement techniques*. Wiley-Teubner, 1996.

[75] R. Verfürth. A note on polynomial approximation in Sobolev spaces. *ESAIM-Math. Model. Numer. Anal.*, 33(4):715–719, 1999.

[76] E. L. Wachspress. *A Rational Finite Element Basis*. Academic Press, 1975.

[77] S. Weißer. Residual error estimate for BEM-based FEM on polygonal meshes. *Numer. Math.*, 118(4):765–788, 2011.

[78] O. C. Zienkiewicz and J. Z. Zhu. A simple error estimator and adaptive procedure for practical engineering analysis. *Int. J. Numer. Methods Eng.*, 24(2):337–357, 1987.